Ministry of Higher Education and Scientific Research
HASSIBA BENBOUALI UNIVERSITY OF CHLEF
Faculté des Sciences Exactes et Informatique
DEPARTMENT OF PHYSICS

THESIS

Presented for obtaining the degree of Doctor in Physics

Option: Theoretical physics

Submitted By:
FATEH MERABTINE

Titled:

Bose Gases In Deformed Algebra

Defended on 28/04/2025 before the jury composed of:

Rached Habib	Professor	University of Chlef	Presedent
Chaachoua Sameut Houria	Professor	University of Chlef	Examiner
Kouidri Smain	MCA	University of Saida	Examiner
Balaska Smain	Professor	Université of Oran1	Examiner
Hamil Bilel	MCA	University of Constantine1	Co-Supervisor
Hocine Ahmed	MCA	University of Chlef	Supervisor
Benarous Mohamed	Professor	University of Chlef	Inveted

University year: 2024-2025.

Hassiba Benbouali University of Chlef
Faculty of Exact Sciences and Informatics
Laboratory for Theoretical Physics and Material Physics

Doctora Thesis in Theoretical physics

Bose Gases In Deformed Algebra

Prepared By: Fateh Merabtine

Defended on 28/04/2025 before the jury composed of:

Mr. Rached Habib	Prof	University of Chlef	President
Mr. Balaska Smain	Prof	University of Oran 1	Examiner
Mme. Chachoua Sameut Houria	Prof	University of Chlef	Examiner
Mr. Kouidri Smain	MCA	University of Saida	Examiner
Mr. Hocine Ahmed	MCA	University of Chlef	Supervisor
Mr. Hamil Bilel	MCA	University of Constantine 1	Co - Supervisor
Mr. Benarous Mohamed	Prof	University of Chlef	Inveted

Chlef 2025.

Acknowledgments

First and foremost, I would like to express my profound gratitude to Allah Almighty for granting me the strength, knowledge, and opportunity to undertake this research study and complete it satisfactorily. Without His blessings, this achievement would not have been possible.

I would like to express my deepest appreciation to my supervisor, Dr. Ahmed Hocine, for their invaluable guidance, continuous support, and immense knowledge throughout my doctoral journey. Their patience, motivation, and extensive experience have been instrumental in shaping both my research and my development as a scholar.

I am particularly grateful to my co-supervisor, Dr. Bilel Hamil whose exceptional guidance and unwavering support have been crucial throughout this academic journey. Their meticulous attention to detail, constructive feedback, and profound expertise have significantly enhanced the quality of my research.

I extend my acknowledgements and gratitude to the discussion committee members, each by name, starting with the committee president, Pr. Rached Habib. My thanks also extend to, Pr. Balaska Smain, Pr. Chachoua Sameut Houria, and Dr. Kouidri Smain, each of whom served as discussants.

I would like to express my sincere gratitude to Pr. Benarous Mohamed for his invaluable guidance and for generously sharing his expertise throughout this research journey. His insights have been truly instrumental. I am equally indebted to Dr. Mohamed Madani, Head of the Physics Department at the University of Chlef, whose unwavering encouragement, thoughtful review of my work, and consistent support have been fundamental to the completion of this research.

I would like to extend my special thanks to Pr. Bekir Can Lütfüoğlu from Hradec Králové University for their significant contribution to our research papers and publications and also for his invetaition.

I am particularly indebted to Pr. Tolga Birkandan from Istanbul Technical University for hosting me and providing crucial assistance with the numerical calculations. Their expertise and support have been instrumental in advancing this research.

A heartfelt thank you goes to my colleague Miss. Zineb Taibi for her constant moral support and encouragement throughout this challenging journey. Her friendship and positive spirit have made this experience more meaningful.

Words cannot express how grateful I am to my family. To my parents, who have always believed in me and supported my dreams - your love and prayers have sustained me throughout. To my sisters, thank you for your endless encouragement and support. Your presence in my life has been a true blessing.

Finally, I would like to thank all those whose names I have not mentioned but who have contributed in various ways to the successful completion of this thesis. Your support, whether direct or indirect, has been greatly appreciated.

Dedication

To my mother and father,

To my sisters,

To my grandfather and grandmother,

To all my family.

Abstract

This thesis explores the impact of the Dunkl formalism, a mathematical framework incorporating a reflection term controlled by the Wigner parameter θ, on quantum statistical mechanics, particularly Bose-Einstein condensation (BEC) and related phenomena. It examines how Dunkl modification alters the properties of an ideal Bose gas, including statistical and thermodynamic behaviors, and modifies blackbody radiation, such as the Stefan-Boltzmann law. The research extends to BEC in harmonic and power-law traps, showing how θ influences critical temperatures, condensate fractions, and thermodynamic properties like specific heat capacity. Key findings highlight modified thermodynamic relations, invariant quantities under Dunkl transformation, and unique scaling behaviors, demonstrating the formalism's potential for advancing understanding of quantum systems and their applications. french

Résumé

Cette étude explore l'impact du formalisme de Dunkl, un cadre mathématique intégrant un terme de réflexion contrôlé par le paramètre de Wigner θ, sur la mécanique statistique quantique, en particulier la condensation de Bose-Einstein (BEC) et les phénomènes associés. Elle examine comment la modification de Dunkl altère les propriétés d'un gaz de Bose idéal, y compris les comportements statistiques et thermodynamiques, et modifie le rayonnement du corps noir, comme la loi de Stefan-Boltzmann. La recherche s'étend à la BEC dans des pièges harmoniques et à loi de puissance, montrant comment θ influence les températures critiques, les fractions de condensat et les propriétés thermodynamiques telles que la capacité thermique spécifique. Les résultats clés mettent en évidence des relations thermodynamiques modifiées, des quantités invariantes sous transformation de Dunkl, et des comportements d'échelle uniques, démontrant le potentiel de ce formalisme pour approfondir la compréhension des systèmes quantiques et leurs applications.

List of Figures

List of Tables

Contents

Introduction

Exactly a century ago, Albert Einstein made a groundbreaking prediction about a phenomenon occurring in a particular state of matter called the Bose-Einstein condensation (BEC) [1, 2]. This prediction was based on the quantum formulation developed by Satyendra Nath Bose [3], which Einstein communicated to him through a personal letter. Einstein postulated that beneath a critical temperature, a significant proportion of particles would undergo a distinctive quantum-statistical transformation, congregating in their minimal energy configurations. This theoretical prediction remained unconfirmed for several decades until its experimental realization in laboratory conditions. The inaugural demonstrations of this quantum phenomenon were conducted by Cornell and Wieman utilizing rubidium atoms [4]. Subsequently, Ketterle and his research team corroborated these findings through experiments with sodium atoms [5], further substantiating Einstein's prescient hypothesis regarding this unique phase transition. The scientific community recognized the profound impact of these investigations by conferring the 2001 Nobel Prize in Physics upon the researchers involved. Their pioneering work not only deepened our comprehension of quantum-level behaviors but also paved the way for the identification of previously unknown physical phenomena. This achievement marked a significant milestone in the field, underscoring the importance of their contributions to fundamental physics and opening new avenues for exploration in quantum science.

BEC represents a unique manifestation of quantum statistics, specifically observed in three-dimensional ensembles of integer-spin particles, known as bosons [6]. This phenomenon emerges when the thermal de Broglie wavelength, a quantum mechanical property intrinsic to the particles, exceeds the typical distance between individual particles in the system. Under these conditions, the quantum nature of the bosons becomes dominant, leading to the formation of a macroscopic quantum state with remarkable properties. In such a scenario, it becomes favorable for the particles to occupy a single ground state.

When the temperature drops below a critical point, the population of this ground state becomes macroscopic. Following its initial discovery, researchers have recognized BEC as the underlying mechanism in various physical phenomena. These manifestations include the frictionless flow observed in liquid helium, specific instances of superconductivity at elevated temperatures, theoretical condensates of Higgs particles, and the collective behavior of pion particles. This diverse range of examples illustrates the broad applicability and significance of BEC across different domains of physics. Subsequently, there has been a growing number of experimental and theoretical studies focused on the BEC. Researchers from various scientific fields have been actively investigating this intriguing quantum phenomenon. These studies aim to deepen our understanding of the underlying physics and explore the unique properties and potential applications of BEC [7–19].

The impact of external fields on BEC has been a subject of extensive research. Bagnato et al. explored the critical temperature and ground state occupation in a three-dimensional ideal Boson gas under a generalized power-law potential [20]. The effects of gravity on BE gas thermodynamics were examined by Gersch [22], while Widom provided theoretical support for condensation in a gravitationally confined ideal Bose liquid [23]. Baranov et al. analyzed two-dimensional BEC in a rectangular well with gravitational influences [24]. Rivas et al. calculated condensation temperatures for different trapping scenarios, including homogeneous gravitational fields [25]. Liu et al. employed a semiclassical approach to study one-dimensional non-interacting Bose gases in uniform gravitational fields [26], with Du et al. extending this work to higher dimensions [27]. Harmonic potential traps have also been thoroughly investigated. Kirsten et al. studied BEC of spin-0 particles in both isotropic and anisotropic harmonic traps [11]. Ketterle et al. investigated nonrelativistic BEC systems under isotropic harmonic potentials in one and three dimensions [5], complemented by Mullin's two-dimensional analysis [28]. Qi-Jun Zeng et al. examined harmonically trapped BEC in two and three dimensions using q-deformed boson theory [9, 10].

In the mid-20th century, a fundamental inquiry emerged in physics: Is it possible to extract commutation relations for physical quantities directly from classical equations of

motion? Wigner addressed this question in his seminal work [29], examining both a free particle system and a classical harmonic oscillator. His attempt to derive commutation relations from motion equations led to an unexpected outcome?the presence of an additional free constant. This result suggested that unique commutation relations were not attainable within the frameworks he investigated.

The discourse took a new turn in 1951 when Yang revisited the problem [30]. Shifting focus from classical to quantum systems, Yang applied more rigorous mathematical foundations, including refined definitions of Hilbert space and series expansions. His analysis of the quantum harmonic oscillator yielded a crucial insight: introducing a reflection operator to augment the momentum operator could eliminate the ambiguity in commutation relations that Wigner had encountered. This development marked a significant advancement in understanding the quantum-classical correspondence and the nature of fundamental physical relationships. Several decades after Yang's work, Dunkl made a significant mathematical contribution by introducing a novel derivative operator [31]. This operator, which could substitute the conventional partial derivative, shed new light on the interplay between differential-difference and reflection operators. Notably, when used to define a momentum operator, Dunkl's approach yields results reminiscent of Yang's earlier findings. The Dunkl derivative has since garnered substantial interest across both mathematical [32,33] and physical sciences [34–68]. Early physics applications centered on Calogero-Sutherland-Moser models [34,35]. Recent years have seen an expansion of Dunkl formalism into diverse physical systems. A key advantage of this approach is its ability to simultaneously generate odd and even wave function solutions due to the inherent reflection operator. This feature has driven numerous studies in the past decade. Genest et al. pioneered investigations into Dunkl-oscillator systems, examining isotropic [38] and anisotropic [39] cases in two dimensions, followed by algebraic analyses of isotropic systems [40] and three-dimensional anisotropic configurations [41]. The formalism's application expanded to relativistic physics with Sargolzaeipor et al.'s study of the Dunkl-Dirac oscillator [47], and Mota et al.'s two-dimensional solution [50]. More recent research has explored the Dunkl-Klein Gordon oscillator in multiple dimensions [54,55,61] and ex-

tended to the Duffin-Kemmer-Petiau oscillator [56], showcasing the formalism's versatility in quantum mechanical systems.

The applications of Dunkl formalism extend beyond traditional quantum mechanical systems. For example, Hamil et al. employed this approach to explore the thermal characteristics of magnetically influenced graphene layers [62], demonstrating its utility in condensed matter physics. In the realm of quantum mechanics, a Lie algebraic approach utilizing Dunkl formalism was applied to resolve nonrelativistic equations for position-dependent mass systems [63]. The evolution of Dunkl formalism continues, with recent literature proposing various generalizations of the Dunkl derivative [64–66]. These developments suggest ongoing efforts to expand the formalism's applicability and theoretical foundations. Furthermore, the framework has found relevance in advanced theoretical physics, as evidenced by its implementation in studies of noncommutative phase space [67]. This diverse range of applications underscores the versatility and growing importance of Dunkl formalism across multiple branches of physics.

This thesis presents a multifaceted investigation into the applications of Dunkl's algebraic structures within statistical and condensed matter physics. Following the introductory framework established in **Chapter 1**, the subsequent chapters unfold a series of interconnected studies that illuminate the versatility and significance of Dunkl formalism. **Chapter 2** offers a detailed examination of how Dunkl's algebra reframes our understanding of two fundamental concepts: the ideal Bose gas and blackbody radiation. This analysis reveals fresh perspectives on these well-established physical phenomena through the lens of Dunkl formalism. The focus shifts in **Chapter 3** to the exploration of Dunkl-Bose-Einstein condensation within harmonic trapping potentials. This chapter elucidates the profound effects of incorporating Dunkl symmetry into these quantum systems, unveiling new aspects of their behavior. **Chapter 4** broadens the scope by investigating the condensation dynamics of ideal Dunkl-Bose gases confined in power-law traps. This comprehensive study delineates how various trapping geometries influence condensate properties when viewed through the prism of Dunkl formalism. Collectively, these chapters aim to bridge the gap between abstract algebraic concepts and their concrete applications in

contemporary physical systems. By doing so, this thesis seeks to expand the boundaries of our comprehension regarding Dunkl's algebra and its far-reaching implications in modern physics.

Chapter 1

Wigner–Dunkl Quantum Mechanics

Quantum mechanics offers a robust mathematical framework for understanding and predicting the behavior of physical systems at the microscopic level. However, there are instances where the standard concepts require extension to address specific phenomena. For example, parity, a symmetry operation that involves spatial inversion, plays a crucial role in quantum mechanics, influencing the behavior and properties of quantum systems. In scenarios where traditional quantum mechanics falls short, such as when dealing with systems that exhibit non-commutative interactions, the Dunkl formalism provides a valuable extension. Dunkl algebra, with its non-commutative derivative operators, enables the study of quantum systems with interactions that are not adequately described by conventional methods.

In this chapter, we will explore the journey from classical mechanics to quantum mechanics and beyond [84, 85, 88]. We will start with the basics of classical mechanics, where we use tools like Poisson brackets to describe how physical systems move and change over time. From there, we will move to quantum mechanics, focusing on the Heisenberg picture, where we use operators for position and momentum that follow special rules called commutation relations. This will help us see how classical mechanics connects to quantum mechanics. Next, we will look at some special kinds of algebras called deformed algebras. These are mathematical tools that change the usual rules of quantum mechanics to create new ways of understanding physical systems. We will study two examples of these

deformed algebras: the Wigner algebra [29] and the Yang [30] algebra. These examples will show us how changing the rules can lead to new insights in physics. After that, we will introduce introduce the Dunkl algebra and its essential properties, including the Dunkl operator $\mathcal{D}$, which is defined by the combination of partial derivative with a linear combination of the difference-differential operator. Moreover, we examine its algebraic relations, non-commutative nature, Hermitian symmetry, and commutation relations with other operators. Additionally, we illustrate the application of Dunkl formalism in one-dimensional quantum mechanics, with a focus on Dunkl derivatives, and refer to the work of Chung and Hassanabadi [48], which applies Dunkl algebra to systems in a harmonic potential. By establishing a comprehensive foundation in Dunkl algebra, this chapter not only enriches our understanding of quantum mechanics but also sets the stage for exploring more complex systems such as the ideal Bose gas and BEC.

1.1 From Classical Mechanics to Quantum Mechanics

This section provides a comprehensive and detailed explanation of the transition from classical mechanics to quantum mechanics, focusing on the Heisenberg picture and the derivation of commutation relations. We begin with the classical Hamiltonian formalism and Poisson brackets, then proceed to the quantization process, and finally derive the Heisenberg equations of motion and the canonical commutation relations. The section aims to bridge the gap between classical and quantum mechanics, emphasizing the mathematical and physical foundations of this transition [84, 88].

1.1.1 Hamiltonian Formalism

In classical mechanics, the behavior of a system is defined through the Hamiltonian framework. The Hamiltonian $H(q, p)$, expressed in terms of the generalized coordinates q and

momenta p, represents the system's total energy:

$$H\left(p,q\right)=\frac{p^2}{2m}+V(q). \tag{1.1}$$

The change over time of an observable $A(p,q,t)$ is determined by Hamilton's equation:

$$\frac{dA}{dt}=\frac{\partial A}{\partial t}+\left\{A,H\right\}, \tag{1.2}$$

where $\{A,B\}$ is the Poisson bracket defined as:

$$\{A,B\}=\sum_i\left(\frac{\partial A}{\partial q_i}\frac{\partial B}{\partial p_i}-\frac{\partial A}{\partial p_i}\frac{\partial B}{\partial q_i}\right). \tag{1.3}$$

The Poisson brackets satisfy the following properties:

- Antisymmetry: $\{A,B\}=-\{B,A\}$.
- Linearity: $\{A,B+C\}=\{A,B\}+\{A,C\}$.
- Leibniz Rule: $\{A,BC\}=\{A,B\}C+B\{A,C\}$.
- Jacobi identity: $\{A,\{B,C\}\}+\{B,\{C,A\}\}+\{C,\{A,B\}\}=0$.

The time evolution of any function $f(q,p)$ is given by:

$$\frac{df}{dt}=\left\{f,H\right\}. \tag{1.4}$$

For the canonical variables q and p, the Poisson brackets are:

$$\{q_i,p_j\}=\delta_{ij},\qquad\qquad\{q_i,q_j\}=\{p_i,p_j\}=0, \tag{1.5}$$

where δ_{ij} is a Kronecker delta function defined by:

$$\delta_{ij}=\begin{cases}1 & \text{if}\quad i=j\\ 0 & \text{if}\quad i\neq j\end{cases}. \tag{1.6}$$

To find the classical equations of motion, start with the Hamiltonian $H(q,p)$ of a system. The changes over time of the coordinates q_i and momenta p_i are described by:

$$\frac{dq_i}{dt} = \{q_i, H\}, \qquad \frac{dp_i}{dt} = \{p_i, H\} \tag{1.7}$$

Using the definition of the Poisson bracket, we obtain the equation of motion as:

$$\begin{cases} \frac{dq_i}{dt} = \frac{\partial H}{\partial p_i}, \\ \\ \frac{dp_i}{dt} = -\frac{\partial H}{\partial q_i} \end{cases} . \tag{1.8}$$

These equations, known as Hamilton's equations of motion, explain how the system changes over time.

1.1.2 Quantization Procedure

The transition from classical to quantum mechanics involves replacing classical observables with operators and Poisson brackets with commutators. The correspondence principle states:

$$\{A, B\} \to \frac{1}{i\hbar}\left[\hat{A}, \hat{B}\right], \tag{1.9}$$

where $\left[\hat{A}, \hat{B}\right] = \hat{A}\hat{B} - \hat{B}\hat{A}$ is the commutator of the operators $\hat{A}$ and $\hat{B}$, and $\hbar$ is the reduced Planck constant.

For the canonical variables q and p, this leads to the canonical commutation relation:

$$[\hat{q}_i, \hat{p}_j] = i\hbar\delta_{ij}. \tag{1.10}$$

This relation is the cornerstone of quantum mechanics and ensures that position and momentum are conjugate variables with the Heisenberg uncertainty principle.

The classical Hamiltonian $H(q, p)$ is replaced by the Hamiltonian operator $\hat{H}(\hat{q}, \hat{p})$. For example, for a particle in a potential $V(\hat{q})$, the Hamiltonian operator is:

$$\hat{H} = \frac{\hat{p}^2}{2m} + V(\hat{q}) \tag{1.11}$$

1.1.3 Heisenberg Picture: Time Evolution of Operators

In the Heisenberg picture, the operators $\hat{q}(t)$ and $\hat{p}(t)$ evolve in time, while the state vectors remain constant. The time evolution of an operator $\hat{A}$ is given by the Heisenberg equation of motion:

$$\frac{d\hat{A}}{dt} = \frac{i}{\hbar}\left[\hat{H}, \hat{A}\right]. \tag{1.12}$$

For the position and momentum operators, this becomes:

$$\frac{d\hat{q}}{dt} = \frac{i}{\hbar}\left[\hat{H}, \hat{q}\right], \qquad \frac{d\hat{p}}{dt} = \frac{i}{\hbar}\left[\hat{H}, \hat{p}\right]. \tag{1.13}$$

By consider the Hamiltonian (1.11) we compute the commutators $\left[\hat{H}, \hat{q}\right]$ and $\left[\hat{H}, \hat{p}\right]$. Then, we recover the quantum analogs of Hamilton's equations:

$$\begin{cases} \frac{\hat{p}}{m} = \frac{i}{\hbar}\left[\hat{H}, \hat{q}\right], \\ -\frac{\partial V(\hat{q})}{\partial \hat{q}} = \frac{i}{\hbar}\left[\hat{H}, \hat{p}\right] \end{cases}. \tag{1.14}$$

These formulas stem from a fundamental rule in quantum mechanics: the Heisenberg-Born-Jordan commutation relationship (1.10). This foundational concept serves as the origin point from which the aforementioned equations.

The transition from classical to quantum mechanics is deeply rooted in the correspondence between Poisson brackets and commutators. The Heisenberg picture provides a natural framework for understanding this transition, preserving the structure of the equations of motion while incorporating quantum principles. The canonical commutation relations play a central role in this formulation, encoding the non-commutative nature of quantum observables Which we will prove is not the only relationship that can be relied upon in the next section.

1.2 Wigner's Concept: Extending Heisenberg's Algebra

To explore this problem from a fresh perspective, we consider an oscillator system characterized by a unit mass and a classical frequency of $\frac{1}{2\pi}$. The energy of this system can be described as:

$$\hat{H} = \frac{1}{2}\left[\hat{x}^2 + \hat{v}^2\right], \tag{1.15}$$

represented using the coordinates $\hat{x}$ and velocity $\hat{v}$ rather than coordinates and momenta and using units where $\hbar = m = 1$. The fundamental equations (1.14) transform to:

$$\begin{cases} \dot{\hat{x}} = i\left[\hat{H}, \hat{x}\right] = \hat{v}, \\ \\ \dot{\hat{x}} = -i\left[\hat{H}, \hat{v}\right] = \dot{\hat{v}}, \end{cases} \tag{1.16}$$

The simplest way to solve (1.15) and (1.16) follows the Born-Jordan approach. Assuming $\hat{H}$ is diagonal, with positive diagonal elements $E_0, E_1, E_2, \ldots$, equations (1.16) for matrix elements x_{nm} and v_{nm} are:

$$\begin{cases} i(E_n - E_m)x_{nm} = v_{nm} \\ \\ -i(E_n - E_m)v_{nm} = x_{nm} \end{cases}, \tag{1.17}$$

combining these results gives:

$$x_{nm} = (E_n - E_m)^2 x_{nm}. \tag{1.18}$$

The matrix element x_{nm} is only finite when $E_n - E_m = \pm 1$, From this, when x_{nm} becomes zero, the value v_{nm} also vanishes.

For an irreducible system, one can thus construct the energy spectrum as follows:

$$\begin{aligned} E_0 &= \text{ground state energy} \\ E_1 &= E_0 \pm 1 \\ E_2 &= E_1 \pm 1 = E_0 \pm 2 \\ E_3 &= E_2 \pm 1 = E_0 \pm 3 \\ &\vdots \end{aligned} \tag{1.19}$$

Consequently, the energy levels E_n connected by a finite matrix element of $\hat{x}$ or $\hat{v}$ form an arithmetic sequence:

$$E_n = E_0 + n. \tag{1.20}$$

Among the matrix elements x_{nm}, only those connecting adjacent energy levels $x_{n,n+1}$ and $x_{n+1,n}$ can be non-zero. A unitary diagonal matrix transformation can make $x_{n,n+1}$ real and positive. Due to the Hermitean property of x, $x_{n,n+1}$ and $x_{n+1,n}$ will then be real. The matrix elements of v will be purely imaginary:

$$\begin{cases} v_{n,n+1} = -ix_{n,n+1} = -ix_{n+1,n} \\ v_{n+1,n} = ix_{n+1,n} = -v_{n,n+1} \end{cases}, \tag{1.21}$$

follows from Eq. (1.17) and Eq. (1.20).

By use (1.21) and (1.20), the diagonal element corresponding to E_n being:

$$E_n = E_0 + n = x_{n,n+1}^2 + x_{n+1,n}^2, \tag{1.22}$$

hence the $x_{n,n+1}$ can be determined one after another:

$$\begin{aligned}
&n=0 \Longleftrightarrow x_{01}^2 = E_0 \\
&n=1 \Longleftrightarrow x_{01}^2 + x_{12}^2 = E_0 + 1 \Longleftrightarrow x_{12} = 1 \\
&n=2 \Longleftrightarrow x_{12}^2 + x_{23}^2 = E_0 + 2 \Longleftrightarrow x_{23} = (E_0+1)^{1/2} \\
&n=3 \Longleftrightarrow x_{23}^2 + x_{34}^2 = E_0 + 3 \Longleftrightarrow x_{34} = 2^{1/2} \\
&n=4 \Longleftrightarrow x_{34}^2 + x_{45}^2 = E_0 + 4 \Longleftrightarrow x_{45} = (E_0+2)^{1/2} \\
&\quad\vdots
\end{aligned} \tag{1.23}$$

In general, we can write:

$$x_{n,n+1} = \begin{cases} \sqrt{E_0 + \frac{n}{2}} & \text{for } n \text{ even} \\ \sqrt{\frac{1}{2} + \frac{n}{2}} & \text{for } n \text{ odd} \end{cases}.$$

The commutator of $\hat{x}$ and $\hat{v}$ is also automatically diagonal as a result of Eq. (1.21). Thus:

$$\begin{aligned}
[v,x]_{nn} &= \sum_l \left(v_{nl}x_{ln} - x_{nl}v_{ln}\right) \\
&= v_{n,n+1}x_{n+1,n} + v_{n,n-1}x_{n-1,n} - x_{n,n+1}v_{n+1,n} - x_{n,n-1}v_{n-1,n},
\end{aligned} \tag{1.24}$$

then we use Eq. (1.21) we obtine:

$$[v,x]_{nn} = -2i\left(x_{n,n+1}^2 - x_{n-1,n}^2\right). \tag{1.25}$$

Consequently:

$$\begin{aligned}
&n=0 \Longleftrightarrow [\hat{v},\hat{x}] = -2ix_{01}^2 = -2iE_0 \\
&n=1 \Longleftrightarrow [\hat{v},\hat{x}] = -2i\left(x_{12}^2 - x_{01}^2\right) = -2i\left(1-E_0\right) \\
&n=2 \Longleftrightarrow [\hat{v},\hat{x}] = -2i\left(x_{23}^2 - x_{12}^2\right) = -2iE_0 \\
&n=3 \Longleftrightarrow [\hat{v},\hat{x}] = -2i\left(x_{34}^2 - x_{23}^2\right) = 2i\left(1-E_0\right) \\
&n=4 \Longleftrightarrow [\hat{v},\hat{x}] = -2i\left(x_{45}^2 - x_{34}^2\right) = -2iE_0 \\
&\quad\vdots.
\end{aligned} \tag{1.26}$$

More general solution can be written as

$$\left([\hat{v},\hat{x}]+i\right)^2 = -\left(2E_0-1\right)^2. \tag{1.27}$$

Here, E_0 is a constant that characterizes the solution. The most common solution is $E_0 = 1/2$ leading to $[\hat{v},\hat{x}] = -i$.

1.2.1 Yang's Contribution

In 1951, Yang revisited the problem by shifting the focus from the classical harmonic oscillator to its quantum mechanical counterpart, utilizing more rigorous formulations of Hilbert spaces and series expansions [30]. His work yielded the key insight that incorporating a reflection operator into the momentum operator could resolve ambiguities inherent in the commutation relations.

Based on this approach, we define the Hamiltonian of the system as follows :

$$H = \frac{1}{2}\left(x^2+\dot{x}^2\right). \tag{1.28}$$

and then we easily get the equation of motion as

$$\ddot{x}+x = 0. \tag{1.29}$$

The problem is whether one can derive the commutation rules from the equation of motion taken over from the classical theory, together with the postulate that the energy is a time displacement operator:

$$\dot{f} = [f,H]. \tag{1.30}$$

As a result, the relationships established in the formulas (1.29) and (1.30) lead us to the conclusion

$$\dot{x} = \left[x,\frac{1}{2}\dot{x}^2\right] = \frac{1}{2}\left([x,\dot{x}]\,\dot{x}+\dot{x}\,[x,\dot{x}]\right), \tag{1.31}$$

Let us introduce the relation $[x,\dot{x}] = T+1$. Substituting this into our previous expression yields:

$$\{T,\dot{x}\} = 0. \tag{1.32}$$

In this context, $\{\cdot,\cdot\}$ represents the anticommutator operation. Combining the expressions from equations (1.28) and (1.29), we derive an analogous result:

$$\{T, x\} = 0. \tag{1.33}$$

Note that using equations (1.32) and (1.33), it can be shown:

$$\left[T, x^2\right] = \left[T, \dot{x}^2\right] = 0, \qquad \text{and} \qquad [T, H] = 0, \tag{1.34}$$

This result implies that T remains invariant throughout the system's evolution, with T^2 representing a fixed scalar value. When expressed in the position basis, equation (1.32) takes the form:

$$(x' + x'') \langle x' |T| x'' \rangle = 0. \tag{1.35}$$

Consequently, we can deduce that:

$$\langle x' |T| x'' \rangle = c(x')\delta (x' + x''), \tag{1.36}$$

where $c(x')$ is an arbitrary function of x', and the Hermitian property of T requires that $c(x') = c^*(-x')$. Expressing our formulation in terms of position eigenstates yields the following result:

$$T = c(x)R, \tag{1.37}$$

where R is the reflection operator defined by:

$$R |x\rangle = |-x\rangle . \tag{1.38}$$

From this representation of T, we obtain the explicit operational form of $\dot{x}$ as:

$$\dot{x} = -i\frac{d}{dx} + g(x) + i\frac{c(x)}{2x}R, \tag{1.39}$$

where $g(x)$ is real function. It can be shown that the term $g(x)$ can be removed by properly choosing the phase factor in the x-representation. Using a star to denote the operator in the new representation, we have:

$$\begin{aligned} \left(\frac{d}{dx}\right)^* &= e^{-iy}\frac{d}{dx}e^{iy} \\ &= \frac{d}{dx} + i\frac{dy}{dx}, \end{aligned} \tag{1.40}$$

and:

$$R^* = e^{-iy} R e^{iy} = e^{-2iy_-} R, \tag{1.41}$$

where y is a real function of x, and y_- is the odd part of y. If for y we choose $y = \int^x g(x)dx$, then Eq. (1.39) becomes:

$$\dot{x} = -i \left(\frac{d}{dx} \right)^* + i \frac{c'(x)}{2x} R^*, \qquad \text{where} \qquad c'(x) = c(x) e^{2iy_-}. \tag{1.42}$$

Dropping the stars and the dash, and with the help of (1.32), we can show that $c(x)$ is a numerical constant, thus :

$$\dot{x} = -i \frac{d}{dx} + i \frac{c}{2x} R. \tag{1.43}$$

For $c = 0$, we return to the usual cas $\dot{x} = -i \frac{d}{dx}$.

1.3 Relationships between Differential-Difference and Reflection Operators

As mentioned in the introduction, Dunkl [31] significantly advanced the discussion on the interplay between differential-difference and reflection operators by introducing a novel derivative operator that serves as an alternative to the traditional partial derivative. We will start by covering some fundamental aspects of reflections and the groups they form.

Consider a nonzero vector $\nu \in \mathbb{R}^N$. The reflection $\sigma_\nu \in O(N)$, where $O(N)$ is the orthogonal group, is defined by:

$$y\sigma_\nu = x - 2 \frac{\langle x, \nu \rangle}{|\nu|^2} \nu, \qquad \text{for } x \in \mathbb{R}^N, \tag{1.44}$$

where $\nu\sigma_\nu = -\nu$ and $x\sigma_\nu = x$, and $\langle x, \nu \rangle = \sum_{i=1}^N x_i \nu_i$. Any collection of such reflections generates a subgroup of $O(N)$, which under certain conditions is finite, forming what is known as a finite reflection group.

Assume G is a finite reflection group with a set $\{\sigma_j \mid 1 \leq j \leq m\}$ of reflections. Choose a set of vectors $\{\nu_j \mid 1 \leq j \leq m\} \subset \mathbb{R}^N$ such that $\sigma_j = \sigma_{\nu_j}$ for $1 \leq j \leq m$ and $|\sigma_j| = |\sigma_i|$ whenever $\sigma_j \propto \sigma_i$. Here, σ_j is conjugate to σ_i in G, implying $\nu_j\omega = \pm\sigma_j$ for some $\omega \in G$, since $\omega^{-1}\sigma_\nu\omega = \sigma_{\nu\omega}$ for $\nu \neq 0$.

Next, select positive parameters α_j for $1 \leq j \leq m$ such that $\alpha_j = \alpha_i$ when σ_j is conjugate to σ_i. Define the function $k(x) = \prod_{i=1}^{m} |\langle x, \nu_i\rangle|^{\alpha_i}$, which is invariant under the group G.

Let $S = \{x \in \mathbb{R}^N \mid |x| = 1\}$ be the unit sphere with the normalized rotation-invariant measure $d\omega$. Let ∇ denote the gradient vector and $\Delta = \sum_{j=1}^{N} \left(\frac{\partial}{\partial x_j}\right)^2$ be the Laplacian operator.

Based on these considerations, Dunkl defined the generalized formulas for the Laplacian and gradient as follows:

$$\Delta_K f(x) = \Delta f(x) + \sum_{i=1}^{m} \alpha_i \left[2\frac{\langle \nabla f(x), \nu_i\rangle}{\langle x, \nu_i\rangle} - |\nu_i|^2 \frac{f(x) - f(x\sigma_i)}{\langle x, \nu_i\rangle^2}\right], \tag{1.45}$$

and:

$$\nabla_K f(x) = \nabla f(x) + \sum_{i=1}^{m} \alpha_i \frac{f(x) - f(x\sigma_i)}{\langle x, \nu_i\rangle}\nu_i. \tag{1.46}$$

1.4 General overview of the Dunkl derivative

There are multiple ways to represent the deformed algebra in position space. Here we show the most commonly used version, which reads [31]:

$$\hat{\mathcal{D}}_j^\theta = \frac{\partial}{\partial x_j} + \frac{\theta_j}{x_j}\left(1 - \hat{R}_j\right). \tag{1.47}$$

Here, θ_j represents the Wigner (or deformation) parameter, and $\hat{R}_j$ denotes the reflection operators that satisfy the following actions

$$\hat{R}_j f(x_j) = f(-x_j), \qquad \hat{R}_i\hat{R}_j = \hat{R}_j\hat{R}_i, \qquad \hat{R}_j\frac{\partial}{\partial x_i} = -\delta_{ij}\frac{\partial}{\partial x_i}\hat{R}_j. \tag{1.48}$$

Here, we see that the reflection operator leads to two cases:

- For an even function, we have

$$\hat{R}_j f(x_j) = f(-x_j) \equiv +f(x_j), \tag{1.49}$$

- for an odd function, we get

$$\hat{R}_j f(x_j) = f(-x_j) \equiv -f(x_j). \tag{1.50}$$

Before diving into applications of quantum mechanics, it would be beneficial to call attention to some other characteristics of the Dunkl operator. Specifically, we should note the key role the Dunkl operator plays in analyzing certain integrable systems. Highlighting these additional facets of the Dunkl operator will provide helpful context and foundation before we shift our focus to applying quantum mechanics concepts and principles. Here are some mathematical properties of the Dunkl derivative:

1.4.1 Linearity

The Dunkl operator is linear, as it satisfies the following property

$$\hat{\mathcal{D}}_j \left(af(x_j) + bg(x_j)\right) = a\hat{\mathcal{D}}_j f(x_j) + b\hat{\mathcal{D}}_j g(x_j). \tag{1.51}$$

1.4.2 Leibniz rule

The Leibniz rule applies to the Dunkl derivative for any functions $f(x_j)$ and $g(x_j)$

$$\begin{aligned}\hat{\mathcal{D}}_j \left(f(x_j)g(x_j)\right) = &\left(\hat{\mathcal{D}}_j f(x_j)\right) g(x_j) + f(x_j)\left(\hat{\mathcal{D}}_j g(x_j)\right) \\ &- \frac{\theta_j}{x_j}\left[\left(1-\hat{R}_j\right) f(x_j)\right]\left[\left(1-\hat{R}_j\right) g(x_j)\right].\end{aligned} \tag{1.52}$$

If either $f(x_j)$ or $g(x_j)$ is even, the Leibniz formula reduces to the usual form

$$\hat{\mathcal{D}}_j \left(f(x_j)g(x_j)\right) = \left(\hat{\mathcal{D}}_j f(x_j)\right) g(x_j) + f(x_j)\left(\hat{\mathcal{D}}_j g(x_j)\right). \tag{1.53}$$

1.4.3 The square form

For any function $f(x_j)$, the square of the Dunkl derivative is given by

$$\hat{\mathcal{D}}_j^2 f(x_j) = \left[\frac{\partial}{\partial x_j} + \frac{\theta_j}{x_j}\left(1 - \hat{R}_j\right)\right]\left[\frac{\partial}{\partial x_j} + \frac{\theta_j}{x_j}\left(1 - \hat{R}_j\right)\right] f(x_j). \tag{1.54}$$

After some algebraic manipulation, we obtain the following form from equation (1.54)

$$\hat{\mathcal{D}}_j^2 = \frac{\partial^2}{\partial x_j^2} + \frac{\theta_j^2}{x_j^2}(1 - R_j) + \frac{2\theta_j}{x_j}\frac{\partial}{\partial x_j}. \tag{1.55}$$

1.4.4 The chain rule

It is well known that the Dunkl derivative does not obey the chain rule. We have

$$\hat{\mathcal{D}}_j f(u(x)) = \left[\frac{\partial}{\partial x_j} + \frac{\theta_j}{x_j}\left(1 - \hat{R}_j\right)\right](f(u(x))), \tag{1.56}$$

If we introduce the derivative $u(x)$ as $\frac{\partial}{\partial} f(u) = \frac{\partial u}{\partial x}\frac{\partial}{\partial u} f(u)$, a straightforward calculation yields

$$\hat{\mathcal{D}}_j f(u(x) = \frac{\partial u}{\partial x}\frac{\partial}{\partial u} f(u(x)) + \frac{\theta_j}{x_j}\left[f(u(x)) - \hat{R} f(u(x))\right]. \tag{1.57}$$

Example :

In this example, we calculate the Dunkl derivative of the function x^n. We have:

$$\hat{\mathcal{D}}_j x^n = \frac{\partial}{\partial x} x^n + \frac{\theta}{x}\left(1 - \hat{R}\right) x^n. \tag{1.58}$$

After some mannipulation , we can write

$$\hat{D}_j x^n = \left[n + \theta\left(1 - (-1)^n\right)\right] x^{n-1} \tag{1.59}$$

$$= [n]_\theta \, x^{n-1}, \tag{1.60}$$

where $[n]_\theta$ is θ-deformed number defined by

$$[n]_\theta = [n + \theta\,(1 - (-1)^n)]\,. \tag{1.61}$$

Here, it is possible to find a general form of the θ-deformed number. Indeed, by following the following identities:

$$\begin{cases} [0]_\theta = 0 \\ [1]_\theta = 1 + 2\theta \\ [2]_\theta = 2 \\ [3]_\theta = 3 + 2\theta \end{cases}, \tag{1.62}$$

We can deduce the following identity:

$$\begin{cases} [2k]_\theta = 2k \\ [2k+1]_\theta = 2k + 1 + 2\theta \end{cases}. \tag{1.63}$$

Hence, we can establish a condition on the parameter θ for equation (1.61) to be positive. The condition is as follows

$$\theta > -\frac{1}{2}. \tag{1.64}$$

Consequently, the Dunkl derivative behaves like ∂_x when acting on an even function, while it behaves like $\partial_x + \frac{2\theta}{x}$ when acting on an odd function. This property of the Dunkl derivative is significant in studying quantum systems with specific interactions, as it introduces a deformation parameter θ that affects the behavior of the derivative and leads to deformed numbers.

1.5 Integrating Dunkl Derivative into Quantum Mechanics

In Wigner-Dunkl quantum mechanics, the momentum operators are substituted with the Dunkl momentum

$$\frac{1}{i}\hat{\mathcal{D}}_j = \frac{1}{i}\left\{\frac{\partial}{\partial x} + \frac{\theta}{x}\left(1 - \hat{R}\right)\right\}, \tag{1.65}$$

where we consider $\hbar = 1$. To clarify further, we can extract the Wigner-Dunkl-Heisenberg commutator relation as follows:

$$\left[\hat{x}, \hat{\mathcal{D}}\right] = \left(1 + 2\theta\hat{R}\right). \tag{1.66}$$

In three dimensions, the commutation relation reads:

$$\left[\hat{x}_i, \hat{\mathcal{D}}_j\right] = \delta_{ij}\left(1 + 2\theta_{ij}\hat{R}_{ij}\right). \tag{1.67}$$

1.5.1 Dunkl − Schrödinger equation

The time-dependent Schrodinger equation for $\hbar = 1$ reads

$$i\frac{\partial}{\partial t}\Psi(x,t) = \hat{H}\Psi(x,t), \tag{1.68}$$

where

$$\hat{H} = \frac{\hat{p}^2}{2m} + V(x), \tag{1.69}$$

replacing $\hat{p}^2$ by equation Eq. (1.55), we find the time dependant Dunkl-Schrödinger equation

$$i\frac{\partial}{\partial t}\Psi(x,t) = -\frac{1}{2m}\left[\frac{\partial^2}{\partial x^2} + \frac{2\theta}{x}\left(1 - \hat{R}\right)\frac{\partial}{\partial x} - \frac{\theta}{x^2}\left(1 - \hat{R}\right) - V(x)\right]\Psi(x,t). \tag{1.70}$$

In the Hilbert space related to one-dimensional, the inner product of Wigner-Dunkl quantum mechanics is given by

$$\langle f|g\rangle = \int_{-\infty}^{+\infty} g^*(x)f(x)|x|^{2\theta}dx, \tag{1.71}$$

where $|x|^{2\theta}$ is the weight function. The expectation value of a physical operator $\mathcal{O}$ with respect to the state $\Psi(x,t)$ is defined by

$$\langle\mathcal{O}\rangle = \langle\Psi|\mathcal{O}\Psi\rangle = \int_{-\infty}^{+\infty} \Psi^*(x,t)\mathcal{O}\Psi(x,t)|x|^{2\theta}dx, \tag{1.72}$$

and $\mathcal{O}$ is a Hermicien operator if it obeys

$$\langle\mathcal{O}\Psi|\Psi\rangle = \langle\psi|\mathcal{O}\Psi\rangle\,. \tag{1.73}$$

For the weight function $|x|^{2\theta}$ we have following propositions:

- For an arbitrary even function $f(x)$ we have

$$\int_{-\infty}^{+\infty} |x|^{2\theta}\hat{\mathcal{D}}_x f(x)dx = 0. \tag{1.74}$$

- For the odd function $f(x)$ obeying $\lim_{x\longrightarrow\infty} x^{2\theta}f(x) = 0$ and $\theta > 0$, we have

$$\int_{-\infty}^{+\infty} |x|^{2\theta}\hat{\mathcal{D}}_x f(x)dx = 0. \tag{1.75}$$

From these ideas, one can easily find the projection relation in the Dunkl algebra

$$\int_{-\infty}^{\infty} |x|^{2\theta}|x><x|dx = 1. \tag{1.76}$$

1.6 Particle in a box

In this section, we will further explore the solution of the Dunkl-Schrödinger equation for a particle in a box. Let us consider a spinless particle with mass m confined in a one-dimensional potential given by

$$V(x) = \begin{cases} 0 & -L < x < L \\ \infty & other \end{cases}. \tag{1.77}$$

In the position representation, the time-independent Schrödinger equation for a particle in a box is given by

$$\frac{p^2}{2m}\psi(x) = E\psi(x). \tag{1.78}$$

where p is the momentum operator. In the Dunkl algebra, equation (1.78) becomes

$$-\frac{1}{2m}\left[\frac{\partial^2}{\partial x^2} + \frac{2\theta}{x}\frac{\partial}{\partial x} - \frac{\theta}{x^2}\left(1-\hat{R}\right)\right]\psi = E\psi. \tag{1.79}$$

Eq. (1.79) can be divided into two equations based on the parity of the solutions. Let us denote the even parity solution as ψ_+:

$$-\frac{1}{2m}\left[\partial^2 + \frac{2\theta}{x}\partial\right]\psi_+ = E\psi_+ \tag{1.80}$$

Using the method of function series, we assume the following form for ψ_+^λ:

$$\psi_+^\lambda = \sum_{n=0}^{\infty} a_n^+ x^{2n}|x|^\lambda. \tag{1.81}$$

By substituting equation (1.81) into equation (1.80) we can write

$$\begin{aligned} &-\frac{1}{2m}\left[\sum_{n=0}^{\infty}(2n+\lambda)(2n+\lambda-1)a_n^+ x^{2n-2}|x|^\lambda + \frac{2\theta}{x}\sum_{n=0}^{\infty}(2n+\lambda)a_n^+ x^{2n-1}|x|^\lambda\right] \\ &= E_+\sum_{n=0}^{\infty} a_n^+ x^{2n}|x|^\lambda. \end{aligned} \tag{1.82}$$

For $\lambda = 0$, the solution of Eq.(1.80)

$$\psi_+^{\lambda=0} = {}_0F_1\left(;\frac{1}{2}+\theta;-\frac{mE_+x^2}{2}\right). \tag{1.83}$$

For $x > 0$, we have $|x|^\lambda = x^\lambda$, Thus:

$$\begin{aligned} &-\frac{1}{2m}\left[\sum_{n=0}^{\infty}(2n+\lambda)(2n+\lambda-1)a_n^+x^{2n+\lambda-2}+2\theta\sum_{n=0}^{\infty}(2n+\lambda)a_n^+x^{2n+\lambda-2}\right] \\ &= E_+\sum_{n=0}^{\infty}a_n^+x^{2n+\lambda}, \end{aligned} \tag{1.84}$$

for $n = 0$ the previous equation is equivalent to the characteristic equation:

$$\lambda(\lambda-1+2\theta) = 0. \tag{1.85}$$

For the terms where $n > 0$, equating the coefficients of $x^{2n+\lambda}$ gives:

$$-\frac{1}{2m}[(2(n-1)+\lambda)(2(n-1)+\lambda-1)+2\theta(2(n-1)+\lambda)]a_{n-1}^+ = E_+a_n^+. \tag{1.86}$$

Shifting the index to $n+1$ and rearranging:

$$a_{n+1}^+ = -\frac{2mE_+}{(2n+2+\lambda)(2n+1+\lambda+2\theta)}a_n^+, \tag{1.87}$$

So, we can find the soulution of Eq. (1.80) as (See Appendix A):

$$\psi_+^{\lambda=0} = {}_0F_1\left(;\frac{1}{2}+\theta;-\frac{mE_+x^2}{2}\right). \tag{1.88}$$

For $\lambda = 1-2\theta$, the solution is given by:

$$\psi_+^{1-2\theta} = |x|^{1-2\theta}{}_0F_1\left(;\frac{3}{2}-\theta;-\frac{mE_+x^2}{2}\right). \tag{1.89}$$

In the case of $\theta = 0$, we find the even parity solution:

$$\psi_+ \longrightarrow \cos\left(\sqrt{2mE_+}x\right). \tag{1.90}$$

Thus, we discard the solution $\psi_+^{\lambda=1-2\theta}$ because it leads to

$$\frac{|x|}{\sqrt{2mE_+}}\sin\left(\sqrt{2mE_+}x\right), \tag{1.91}$$

in the limit $\theta \longrightarrow 0$. Equation (1.88) can be expressed in terms of the Bessel function as follows (See Appendix A):

$$J_n(x) = \frac{\left(\frac{1}{2}x\right)^n}{n!} {}_0F_1\left(n+1; -\frac{1}{4}x^2\right). \tag{1.92}$$

Then, $\psi_+^{\lambda=0}$ becomes

$$\psi_+^{\lambda=0} = N_+ x^{\frac{1}{2}-\theta} J_{\theta-\frac{1}{2}}(\sqrt{2mE_+}x), \tag{1.93}$$

where $N_+ = \frac{\left(\theta-\frac{1}{2}\right)!}{\left(\frac{1}{2}\sqrt{2mE_+}\right)^{\theta-\frac{1}{2}}}$ is a normalization constant. We still need to find the energy spectrum, which is determined by the boundary conditions $\psi_+(\pm L) = 0$:

$$\begin{cases} J_{\theta-\frac{1}{2}}\left(\sqrt{2mE_+}L\right) = 0 \\ \\ J_{\theta-\frac{1}{2}}\left(-\sqrt{2mE_+}L\right) = 0 \end{cases} \quad \Longleftrightarrow \sum_{n=0}^{\infty} \frac{\left(\sqrt{2mE_+}L\right)^n}{n!} = 0. \tag{1.94}$$

This last summation can be explicitly written as:

$$1 + \sqrt{2mE_+}L + \frac{\left(\sqrt{2mE_+}L\right)^2}{2!} + \frac{\left(\sqrt{2mE_+}L\right)^3}{3!} + ... + \alpha_{\theta-\frac{1}{2},n} = 0. \tag{1.95}$$

Finally, we get the energy level as

$$E_n^+ = \frac{1}{2mL^2}\alpha^2_{\theta-\frac{1}{2},n}, \qquad n = 1, 2, ... \tag{1.96}$$

where $\alpha_{\theta-\frac{1}{2},n}$ is a n-th zeros of $J_{\theta-\frac{1}{2}}$.

Next, let us consider the case of the odd functions, denoted by ψ_-, which satisfy the equation

$$-\frac{1}{2m}\left[\partial^2 + \frac{2\theta}{x}\partial - \frac{2\theta}{x^2}\right]\psi_- = E_-\psi_-. \tag{1.97}$$

We can transform the solution (1.81) for the odd case as follows:

$$\psi_{-}^{\lambda} = \sum_{n=0}^{\infty} a_n^{-} x^{2n+1} |x|^{\lambda}. \tag{1.98}$$

By substituting equation (1.98) into equation (1.97) and solving, we obtain the characteristic equation:

$$\lambda\left(\lambda + 2\theta + 1\right) = 0. \tag{1.99}$$

The recurrence relation for the odd case is given by:

$$a_n^{-} = -\frac{2mE_{-}}{\left(2n+\lambda\right)\left(2n+1+\lambda+2\theta\right)} a_{n-1}^{-}. \tag{1.100}$$

We now write all the terms as a function of a_0. We find for $\lambda = 0$

$$\psi_{-}^{\lambda=0} = x_0 F_1\left(;\frac{3}{2}+\theta;-\frac{mE_{-}x^2}{2}\right). \tag{1.101}$$

For $\lambda = 1 - 2\theta$ we have

$$\psi_{-}^{\lambda=-1-2\theta} = |x|^{-1-2\theta} x_0 F_1\left(;\frac{1}{2}-\theta;-\frac{mE_{-}x^2}{2}\right). \tag{1.102}$$

For the case of $\theta = 0$ we have the odd parity solution

$$\psi_{-} \longrightarrow \sin\left(\sqrt{2mE_{-}}x\right). \tag{1.103}$$

We discard the solution $\psi_{-}^{\lambda=-1-\theta}$ since it leads to

$$\frac{|x|}{x}\cos\left(\sqrt{2mE_{-}}x\right) \tag{1.104}$$

in the limit $\theta \longrightarrow 0$. In terms of the Bessel function, equation (1.101) can be written as

$$\psi_- = N_- x^{\frac{1}{2}-\theta} J_{\frac{1}{2}+\theta}\left(\sqrt{2mE_-}x\right), \tag{1.105}$$

where

$$N_- = \frac{\left(\theta-\frac{1}{2}\right)!}{\left(\frac{1}{2}\sqrt{2mE_-}\right)^{\theta-\frac{1}{2}}}, \tag{1.106}$$

is the normalization constant. The boundary condition $\psi_-(\pm L) = 0$ determines the energy levels for this case

$$\begin{cases} J_{\theta+\frac{1}{2}}\left(\sqrt{2mE_+}L\right) = 0 \\ \\ J_{\theta+\frac{1}{2}}\left(-\sqrt{2mE_+}L\right) = 0 \end{cases}. \tag{1.107}$$

Solving this condition leads to the relationship

$$\sum_{n=0}^{\infty} \frac{\left(\sqrt{2mE_-}L\right)^n}{n!} = 0. \tag{1.108}$$

After some manipulation, we obtain the energy levels as

$$E_n^- = \frac{1}{2mL^2}\alpha^2_{\theta+\frac{1}{2},n}, \qquad n = 1, 2, ... \tag{1.109}$$

where $\alpha_{\theta+\frac{1}{2},n}$ is a n-th zeros of $J_{\theta+\frac{1}{2}}$.

1.7 Harmonic Oscillator

In this section, we will discuss the energy eigenvalues and eigenstates of the harmonic oscillator in the presence of Dunkl derivations. We will use two methods: the direct method and the operator method.

Let us first consider the harmonic oscillator problem in one dimension with reflection symmetry. The Schrödinger equation is given by

$$\left[-\frac{1}{2m}\hat{\mathcal{D}}_x^2+\frac{1}{2}m\omega^2x^2\right]\psi=E\psi. \tag{1.110}$$

Applying the change of variable $\xi=\sqrt{m\omega}x$ and $\epsilon=\frac{2E}{\omega}$, we obtain the equation

$$-\hat{\mathcal{D}}_\xi^2\psi+\xi^2=\epsilon\psi. \tag{1.111}$$

To solve this equation, we can use the test function

$$\psi(\xi)=e^{-\frac{\xi^2}{2}}y(\xi). \tag{1.112}$$

By substituting equation (1.112) into equation (1.111), we obtain the following equation for $y(\xi)$

$$\hat{\mathcal{D}}_\xi^2y-\hat{\mathcal{D}}_\xi\left(\xi y\right)f_\xi\hat{\mathcal{D}}_\xi y+\epsilon y=0, \tag{1.113}$$

or equivalently

$$\hat{\mathcal{D}}_\xi^2y-2\xi\hat{\mathcal{D}}_\xi y+\left(\epsilon-1-2\theta\right)y=0. \tag{1.114}$$

This differential equation is the Hermit equation with reflection symmetry.

1.7.1 Even solution

We start with the even solution. Let us assume that the series expansion of $y(\xi)$ is given by

$$y = \sum_{n=0}^{\infty} a_n \xi^{2n}. \tag{1.115}$$

Applying the Dunkl derivative to ξ^{2n}, we find the following relationships

$$\begin{cases} \hat{\mathcal{D}}_\xi \xi^{2n} = [2n]_\theta \, \xi^{2n-1} \\ \\ \hat{\mathcal{D}}_\xi^2 \xi^{2n} = [2n]_\theta \, [2n-1]_\theta \, \xi^{2n-2} \end{cases} . \tag{1.116}$$

Substituting these relations into equation (1.115) and rearranging the terms, we obtain the following expression for the recurrence relation

$$\begin{aligned} (\epsilon_+ - 1 - 2\theta)\, a_0 \xi^0 + a_1 \, [2]_\theta \, [1]_\theta \, \xi^0 - 2a_1 \, [2]_\theta \, \xi^2 + (\epsilon_+ - 1 - 2\theta)\, a_1 \xi^2 \\ + a_2 \, [4]_\theta \, [3]_\theta \, \xi^2 - 2a_2 \, [4] \, \xi^4. \end{aligned} \tag{1.117}$$

Using this we can derive the recurrence relation for the coefficients a_n^+

$$a_{n+1} = \frac{2\,[2n]_{\theta+1+2\theta-\epsilon_+}}{[2n+2]_\theta \, [2n+1]_\theta} a_n. \tag{1.118}$$

By requiring that the series be terminated, we find the energy levels

$$(\epsilon_+)_N = 2\,[2N]_\theta + 1 + 2\theta, \qquad\qquad N = 0, 1, 2..... \tag{1.119}$$

Therefore, the energy levels read:

$$E_N^+ = \frac{\omega}{2}\Big(2\,[2N]_\theta + 1 + 2\theta\Big). \tag{1.120}$$

Then, we arrive at the polynomial solution whose recurrences relation reads:

$$a_{n+1} = \left(\frac{2\left([2n]_\theta - [2N]_\theta\right)}{[2n+2]_\theta \, [2n+1]_\theta} \right) a_n. \tag{1.121}$$

Let us denote the function y corresponding to N by H_N^+. Then, H_N^+ function can be given by (See Appendix A):

$$\begin{aligned} H_0^+(x) &= 1, \\ H_1^+(x) &= 1 - \frac{2}{[1]_\theta} x^2, \\ H_2^+(x) &= 1 - \frac{2\,[4]_\theta}{[2]_\theta!} x^2 + \frac{2^2\,[4]_\theta\,([4]_\theta - [2]_\theta)}{[4]_\theta!} x^4. \end{aligned} \tag{1.122}$$

1.7.2 Odd solution

For the odd solution, we assume the series expansion

$$y = \sum_{n=0}^{\infty} b_n \xi^{2n+1}. \tag{1.123}$$

By substituting equation (1.123) into equation (1.114), we obtain the recurrence relation for the coefficients b_n^-

$$b_{n+1} = \frac{2\,[2n+1]_\theta + 1 - 2\theta - \epsilon_-}{[2n+3]_\theta\,[2n+2]_\theta} b_n. \tag{1.124}$$

Requiring that the series have to be terminated, we find the energy levels

$$(\epsilon_-)_N = 2\,[2N+1]_\theta + 1 - 2\theta, \tag{1.125}$$

thus, using $\epsilon = \frac{2E}{\omega}$ the odd energy levels read

$$E_N^- = \frac{\omega}{2}\left[2\,[2N+1]_\theta + 1 - 2\theta\right]. \tag{1.126}$$

Subsequently, the polynomial solution receives the recurrence relation

$$b_{n+1} = \frac{2\,[2n+1]_\theta - [2N+1]_\theta}{[2n+3]_\theta\,[2n+2]_\theta}. \tag{1.127}$$

Let us denote the function y corresponding to N by H_N^-. The H_N^- function is given by

$$H_0^-(x) = x, \tag{1.128}$$

$$H_1^-(x) = x - \frac{2\left([3]_\theta - [1]_\theta\right)}{[3]_\theta!}x^3, \tag{1.129}$$

$$H_2^-(x) = x - \frac{2\,[5]_\theta - [1]_\theta}{[3]_\theta!}x^3 + \frac{2^2\left([5]_\theta - [3]_\theta\right)\left([5]_\theta - [1]_\theta\right)}{[5]_\theta!}x^5 \tag{1.130}$$

Consequently, the even and odd wave functions of the harmonic oscillator with Dunkl derivatives are given by:

$$\psi_M(\xi) = e^{-\frac{\xi}{2}}H_M^\theta(\xi), \qquad M = 0, 1, 2, 3....., \tag{1.131}$$

such as

$$H_M^\theta(\xi) = \begin{cases} H_{\frac{M}{2}}, & \text{for M even,} \\ \\ H_{\frac{M-1}{2}}, & \text{for M odd} \end{cases}. \tag{1.132}$$

The total energy spectrum for the harmonic oscillator with Dunkl derivations is given by:

$$E_M = \frac{\omega}{2}\left([M]_\theta + [M+1]_\theta\right). \tag{1.133}$$

1.7.3 Operator method

Now, let us move on to the operator method for solving the harmonic oscillator problem. We define the creation and annihilation operators in our model as

$$\hat{a}^\dagger = \sqrt{\frac{m\omega}{2}}\left(\hat{x} - \frac{1}{m\omega}\hat{\mathcal{D}}_x\right), \qquad \hat{a} = \sqrt{\frac{m\omega}{2}}\left(\hat{x} + \frac{1}{m\omega}\hat{\mathcal{D}}_x\right). \tag{1.134}$$

The Hamiltonian of the system is given by

$$\hat{H} = \frac{\omega}{2}\left(\hat{a}\hat{a}^{\dagger} + \hat{a}^{\dagger}\hat{a}\right). \tag{1.135}$$

In order to determine the system switching relationship, we use

$$[\hat{x}, \hat{x}] = \left[\hat{D}_x, \hat{D}_x\right] = 0. \tag{1.136}$$

Therefore, it is easy to show that

$$\left[\hat{a}, \hat{a}^{\dagger}\right] = 1 + 2\theta\hat{R}. \tag{1.137}$$

We define the occupation number operator as

$$\hat{N} = \hat{a}^{\dagger}\hat{a}. \tag{1.138}$$

This operator satisfies the following commutation relations

$$\left[\hat{N}, \hat{a}^{\dagger}\right] = \hat{a}^{\dagger}, \qquad \left[\hat{N}, \hat{a}\right] = -\hat{a}. \tag{1.139}$$

In the Dunkl formalism, we have

$$[N]_{\theta} = \hat{a}^{\dagger}\hat{a}, \qquad [N+1]_{\theta} = \hat{a}\hat{a}^{\dagger}. \tag{1.140}$$

Using these relations and introducing the Fock space representation where $\hat{N}|n\rangle = n|n\rangle$, we can determine the energy levels

$$E_n = \frac{\omega}{2}\left([n]_{\theta} + [n+1]_{\theta}\right). \tag{1.141}$$

Remarkably, the direct and operator methods yield the same energy spectrum for the harmonic oscillator with Dunkl derivations.

To summarize, the solutions to the harmonic oscillator problem with Dunkl derivations can be obtained through the direct method using polynomial series expansions, or through the operator method using creation and annihilation operators. Both methods lead to the same energy spectrum given by equation (1.133) or equation (1.141). The wave functions can be expressed in terms of the polynomial functions $H_M^{\theta}(\xi)$ for even and odd states.

Chapter 2

Statistics of the Dunkl – Boson ideal systems

In this chapter, we investigate the statistical properties of ideal Dunkl-Boson systems. We propose a novel methodology that leverages symmetry and reflection operators to analyze the thermodynamic behavior of an ideal Bose gas within the framework of Dunkl formalism. Furthermore, we systematically compare the results obtained in this framework with those of the conventional ideal Bose gas, highlighting key differences and their significant physical implications.

A central aspect of our approach is the use of symmetry and reflection operators to extend the conventional state space into Dunkl formalism, defined through the following operator:

$$\hat{\mathcal{D}}_x = \frac{\partial}{\partial x} + \frac{\theta}{x}\left(1 - \hat{R}_x\right), \tag{2.1}$$

where $\hat{R}_x$ is the reflection operator, formally expressed as $\hat{R}_x = (-1)^{x\frac{d}{dx}}$. This transformation allows us to systematically explore the thermodynamic properties of Dunkl-Boson systems and compare these findings with the corresponding properties of conventional Bosons. Through this comparison, we aim to elucidate the fundamental differences between these two types of systems and identify the physical consequences of Dunkl operators.

We begin by exploring the theoretical foundation of the transformation from the conventional state space to Dunkl space. The mathematical tools underlying this transformation are introduced and discussed, illustrating how they enable the deformation of standard space to accommodate the formalism governing Dunkl-Boson systems. This framework allows for the discovery of new thermodynamic characteristics and properties of Bose gases within this modified space.

Subsequently, we examine the thermodynamic properties of an ideal Bose gas in Dunkl space. We derive analytical expressions for thermodynamic quantities such as internal energy, entropy, heat capacity, and the partition function. These results are compared with those of the ideal Bose gas in conventional space, emphasizing the critical distinctions that emerge from the Dunkl formalism.

Lastly, we extend our formalism to the study of black bodies, which are idealized objects that absorb and emit electromagnetic radiation perfectly. We derive expressions for the thermodynamic quantities of black bodies in Dunkl space and analyze the impact of Dunkl algebra on the characteristics of thermal radiation.

2.1 The model

Our study focuses on examining the consequences of introducing a Hamiltonian in terms of creation and annihilation operators derived from a correspondence between these operators and the coordinate and its derivative, respectively. This approach parallels the standard case where we follow the representation of the annulation and cretion operators [86]:

$$\begin{cases} \hat{a} = 1/2\left(\hat{x} + i\hat{p}\right), \\ \\ \hat{a}^{\dagger} = 1/2\left(\hat{x} - i\hat{p}\right) \end{cases} . \tag{2.2}$$

Here, we used the canonical commutation relation $[\hat{x}, \hat{p}] = i$, for prove that

$$\left[\hat{a}, \hat{a}^{\dagger}\right] = 1. \tag{2.3}$$

In this thesis, we focus on the representation

$$a^\dagger \longleftrightarrow x, \qquad\qquad a \longleftrightarrow \frac{\partial}{\partial x}, \tag{2.4}$$

which satisfies the same commutation relation: $[a, a^\dagger] = 1$.

By employing the Dunkl differential-difference operator, we establish the correspondence between the operators $\bar{\phi}_i$, ϕ_i, and the coordinate x_i, as well as its associated derivative $\mathcal{D}x_i$. This correspondence is given by:

$$\bar{\phi}_i \longleftrightarrow x_i = a_i^\dagger, \qquad \text{and} \qquad \phi_i \longleftrightarrow \mathcal{D}_{x_i} = a_i + \frac{\theta}{a_i^\dagger}(1 - R_x), \tag{2.5}$$

where the commutation relations are modified as:

$$[\phi_i, \bar{\phi}_j] = \delta_{ij}(1 + 2\theta R_i). \tag{2.6}$$

The transformed operators exhibit the following behavior when acting on number states $|n_i\rangle = |n_1, n_2, n_3, \ldots\rangle$:

$$\bar{\phi}_i|n_i\rangle = \sqrt{n_i + 1}|n_i + 1\rangle, \tag{2.7}$$

$$\phi_i|n_i\rangle = \left[\sqrt{n_i} + \frac{\theta}{\sqrt{n_i}}(1 - (-1)^{n_i})\right]|n_i\rangle. \tag{2.8}$$

The particle number operator emerges through the relation:

$$\hat{\mathcal{N}}_i = \bar{\phi}_i\phi_i \tag{2.9}$$

This leads to the eigenvalue relation:

$$\hat{\mathcal{N}}_i|n_i\rangle = [n_i + \theta(1 - (-1)^{n_i})]\,|n_i\rangle. \tag{2.10}$$

For states with even occupation numbers:

$$\hat{\mathcal{N}}_i|n_i\rangle = n_i|n_i\rangle \tag{2.11}$$

While states with odd occupation numbers yield:

$$\hat{\mathcal{N}}_i|n_i\rangle = (n_i + 2\theta)|n_i\rangle \tag{2.12}$$

A key physical consequence emerges: the spectrum of $\mathcal{N}_i$ divides into two distinct subspaces. States with even particle numbers maintain conventional behavior, whereas those with odd occupancy exhibit modified eigenvalues due to the Wigner parameter's influence.

By introducing the operators:

$$\begin{cases} \mathcal{J}_1^i = \frac{1}{2}\bar{\phi}_i\bar{\phi}_i, \\ \mathcal{J}_0^i = \frac{1}{4}(\bar{\phi}_i\phi_i + \phi_i\bar{\phi}i), \\ \mathcal{J}_{-1}^i = \frac{1}{2}\phi_i\phi_i, \end{cases} \tag{2.13}$$

we obtain a representation of the $\mathfrak{su}(1,1)$ algebra:

$$[\mathcal{J}_n^i, \mathcal{J}_m^i] = (m-n)\mathcal{J}_{n+m}^i. \tag{2.14}$$

2.2 Ideal Bose gas within the Dunkl algebra

In this section, we present the mathematical framework and thermodynamic properties of the ideal Bose gas within the context of Dunkl algebra. We begin by deriving the partition function and its constituent elements, followed by a detailed analysis of the average particle number and the condensed fraction. Furthermore, we investigate the transition temperature and its dependence on the Wigner parameter, highlighting the modifications introduced by the Dunkl algebra formalism and their implications for the system's thermodynamic behavior.

2.2.1 Partition function

The partition function is a fundamental quantity in statistical mechanics, providing insight into the thermodynamic behavior of a system. In the grand canonical ensemble, the

partition function for the Dunkl-Boson system is formulated as a sum over all possible occupation numbers, weighted by their respective energies. Through manipulation of this expression, it can be reformulated in terms of two distinct functions representing the contributions from odd and even parity. The odd parity contribution incorporates an exponential factor with alternating signs, whereas the even parity contribution reduces to a simple geometric series. These components can be further simplified using standard mathematical identities, resulting in explicit expressions for the partition function in terms of the Wigner parameter and the system's energy levels.
The total energy operator within the grand canonical formalism is expressed through:

$$\mathcal{H} = \sum_i \mathcal{N}_i(\epsilon_i - \mu), \tag{2.15}$$

where ϵ_i represents the energy of state i, and $\mathcal{N}_i = \bar{\phi}_i\phi_i$ corresponds to the number operator associated with that state.

In the grand canonical ensemble, the genaral form of the partition function is given by

$$\mathcal{Z}^D = \sum_{\mathcal{N}_1,\mathcal{N}_2,\mathcal{N}_3,\cdots} e^{-\beta\sum_i \mathcal{N}_i(\epsilon_i-\mu)}, \tag{2.16}$$

which can be written as

$$\mathcal{Z}^D = \prod_i \sum_{\mathcal{N}_i} \left\{e^{-\beta(\epsilon_i-\mu)}\right\}^{\mathcal{N}_i} = \prod_i \xi_i, \tag{2.17}$$

where

$$\xi_i = \sum_{\mathcal{N}_i} e^{-\beta\mathcal{N}_i(\epsilon_i-\mu)}. \tag{2.18}$$

We now can subdivide equation (2.18) into two functions according to the parity

$$\xi_i \equiv \xi_i^{\mathbf{odd}} + \xi_i^{\mathbf{even}}. \tag{2.19}$$

where

- For the odd parity:

$$\begin{aligned}\xi_i^{\mathbf{odd}} &= e^{-\beta(1+2\theta)(\epsilon_i-\mu)} + e^{-\beta(3+2\theta)(\epsilon_i-\mu)} + e^{-\beta(5+2\theta)(\epsilon_i-\mu)} + \cdots \\ &= e^{-2\beta\theta(\epsilon_i-\mu)} \left[e^{-\beta(\epsilon_i-\mu)} + e^{-3\beta(\epsilon_i-\mu)} + e^{-5\beta(\epsilon_i-\mu)} \cdots\right].\end{aligned} \tag{2.20}$$

  Using the relation

$$\sum_n U^{2n+1} = \frac{U}{1-U^2}, \tag{2.21}$$

  we obtain

$$\xi_i^{\mathbf{odd}} = \frac{e^{-\beta(1+2\theta)(\epsilon_i-\mu)}}{1-e^{-2\beta(\epsilon_i-\mu)}}. \tag{2.22}$$

- For the even parity:

$$\begin{aligned}\xi_i^{\mathbf{even}} &= 1 + e^{-2\beta(\epsilon_i-\mu)} + e^{-4\beta(\epsilon_i-\mu)} + \cdots \\ &= \frac{1}{1-e^{-2\beta(\epsilon_i-\mu)}},\end{aligned} \tag{2.23}$$

  where we have used the following relation

$$\sum_n U^{2n} = \frac{1}{1-U^2}. \tag{2.24}$$

Subsequently, we write the Dunkl partition function as

$$\mathcal{Z}^D = \prod_{i=1} \frac{1 + e^{-\beta(1+2\theta)(\varepsilon_i - \mu)}}{1 - e^{-2\beta(\varepsilon_i - \mu)}}. \tag{2.25}$$

As θ vanishes, the expression simplifies to the canonical form for ideal bosonic systems:

$$\mathcal{Z} = \prod_{i=1} \frac{1}{1 - ze^{-\beta\varepsilon_i}}. \tag{2.26}$$

Here, $z = e^{\beta\mu}$ represents the fugacity.

2.2.2 The average number of particules

Calculating system-wide particle counts requires applying fundamental statistical mechanics principles. By examining how the partition function's logarithm varies with chemical potential, we can extract the quantum statistics of our system. This analysis naturally separates into two distinct regimes: particles occupying the lowest energy configuration, and those distributed across higher energy states. For macroscopic systems, the summation over excited states transforms into a continuous integral, leading to an elegant mathematical formulation involving the Wigner coefficient, thermodynamic activity, and special mathematical functions.

Starting from the partition function presented in equation (2.25), we derive the particle distribution through standard thermodynamic relations:

$$N^D = \frac{1}{\beta} \frac{\partial}{\partial \mu} \log \mathcal{Z}^D|_{T,V}. \tag{2.27}$$

By substituting equation (2.25) into equation (2.27), the total number of particles can be expressed as

$$N^D = N_0^D + N_e^D, \tag{2.28}$$

where

$$N_0^D = \frac{2}{z^{-2}-1} + \frac{(1+2\theta)}{z^{-(1+2\theta)}+1}, \tag{2.29}$$

represents the quantity of particles inhabiting the system's lowest energy level, while

$$N_e^D = \sum_{i\neq 0}\left(\frac{2}{e^{2\beta\varepsilon_i}z^{-2}-1} + \frac{(1+2\theta)}{e^{\beta(1+2\theta)\varepsilon_i}z^{-(1+2\theta)}+1}\right), \tag{2.30}$$

characterizes the population of energetically elevated levels. Specifically, the distribution of particles with no momentum and without wigner parameter is given by

$$N_0 = \frac{z}{1-z}, \tag{2.31}$$

this form mirrors the standard Bose-Einstein result, constraining the thermodynamic fugacity to $0 < z < 1$. In the thermodynamic limit, where both the volume V and the number of particles N tend to infinity while maintaining a constant particle density:

$$V \to \infty, \quad N \to \infty, \quad \text{with} \quad \frac{N}{V} = \text{constant}, \tag{2.32}$$

we employ the following transformation valid in three-dimensional space:

$$\sum_{i=1}^{+\infty} \to \frac{2\pi V}{h^3}(2m)^{3/2}\int_0^{+\infty}\sqrt{\varepsilon}d\varepsilon, \tag{2.33}$$

This allows us to recast equation (2.30) as

$$\frac{N_e^D}{V} = \frac{2\pi}{h^3}(2m)^{3/2}\int\sqrt{\varepsilon}d\varepsilon\left(\frac{2}{e^{2\beta\varepsilon}z^{-2}-1} + \frac{(1+2\theta)}{e^{\beta(1+2\theta)\varepsilon}z^{-(1+2\theta)}+1}\right), \tag{2.34}$$

where h is the Planck constant, m is the particle mass, and V is the volume of the system. By using the Bose function (polylogarithm)

$$g_s(z) = \frac{1}{\Gamma(s)}\int_0^{+\infty}\frac{x^{s-1}}{e^x z^{-1}-1}dx. \tag{2.35}$$

After performing the necessary mathematical calculations, we obtain the following expression for the number of particles in excited states:

$$\frac{N_e^D}{V} = \frac{1}{\lambda^3\sqrt{2}}\left[g_{3/2}\left(z^2\right) - \sqrt{\frac{2}{1+2\theta}}g_{3/2}\left(-z^{1+2\theta}\right)\right]. \tag{2.36}$$

Here, $\lambda = \left(\frac{2\pi\hbar^2\beta}{m}\right)^{1/2}$ is the de Broglie thermal wavelength. Consequently, we can express the system-wide particle count as follows:

$$N^D = \frac{2}{z^{-2}-1} + \frac{(1+2\theta)}{z^{-(1+2\theta)}+1} + \frac{V}{\lambda^3\sqrt{2}}\left[g_{3/2}\left(z^2\right) - \sqrt{\frac{2}{1+2\theta}}g_{3/2}\left(-z^{1+2\theta}\right)\right]. \tag{2.37}$$

Exploiting a characteristic relation of the polylogarithmic function, namely:

$$g_s(z) + g_s(-z) = 2^{1-s}g_s(z^2), \tag{2.38}$$

we rewrite equation (2.37) as

$$\frac{N^D}{V} = \frac{N_0^D}{V} + \frac{1}{\lambda^3}g_{3/2}\left(z,\theta\right), \tag{2.39}$$

where

$$g_{3/2}\left(z,\theta\right) = g_{3/2}(z) + g_{3/2}(-z) - \frac{1}{\sqrt{1+2\theta}}g_{3/2}\left(-z^{1+2\theta}\right), \tag{2.40}$$

is the generalized Dunkl-Bose function. An examination of equation (2.36) reveals that N_e^D adopts non-real values when $1+2\theta < 0$. This unphysical result necessitates a stringent limitation on the Wigner coefficient: $\theta > -1/2$. As a consequence, the Dunkl framework's applicability to ideal bosonic systems is confined to this interval.

Under these constraints, Figure 2.1 illustrates the functional dependence of $g_{3/2}\left(z,\theta\right)$ on z across different values of the Wigner parameter.

Figure 2.1 The variation of $g_{3/2}(z,\theta)$ via z for different values of θ

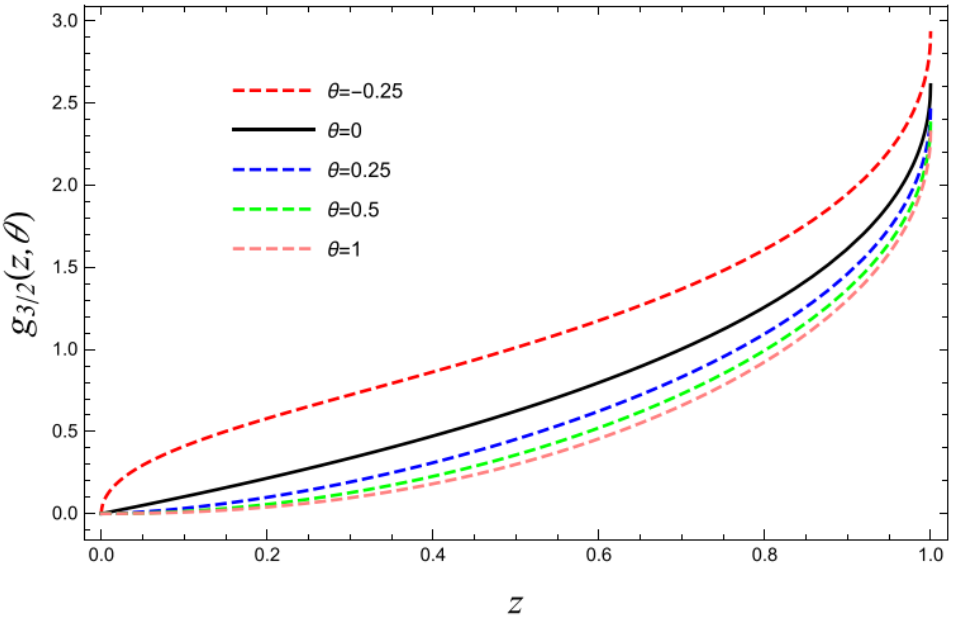

We observe that the function takes greater values when the Wigner parameter takes negative values, and smaller values when it takes positive values. We also note that, in the limit of $\theta \longrightarrow 0$, equation (2.39) reduces to the standard result:

$$\frac{N}{V} = \frac{N_0}{V} + \frac{1}{\lambda^3} g_{3/2}(z)\,, \tag{2.41}$$

2.2.3 Transition temperature and condensed fraction

The transition temperature marks the onset of BEC, where a macroscopic number of particles occupy the lowest energy state. We explore two methods to determine the transition temperature within the Dunkl algebra formalism. The first method involves setting the occupation number of the ground state to zero and deriving an equation that relates the actual total particle number to the transition temperature. This equation reveals how the Wigner parameter modifies the critical temperature of condensation.

The second method involves examining the specific heat of the system and identifying the temperature at which it reaches its maximum value. However, in this chapter, we focus on the first method. We get

$$N^D = \frac{V}{\lambda_c^3} g_{3/2}(1) \left[1 + \frac{g_{3/2}(-1)}{g_{3/2}(1)} \left(1 - \frac{1}{\sqrt{1+2\theta}}\right)\right] \equiv N, \tag{2.42}$$

with N denoting the system's complete particle count. From this relation, we can deduce the critical temperature in Dunkl's algebra as:

$$T_c^D = \frac{2\pi\hbar^2}{mk_B} \left(\frac{N}{V g_{3/2}(1)}\right)^{2/3} \left[1 + \frac{g_{3/2}(-1)}{g_{3/2}(1)} \left(1 - \frac{1}{\sqrt{1+2\theta}}\right)\right]^{-2/3}, \tag{2.43}$$

this expression reveals the substantial dependence of the transition point on the Wigner coefficient. The conventional condensation temperature emerges exclusively when θ approaches zero, yielding

$$T_c^0 = \frac{2\pi\hbar^2}{mk_B} \left(\frac{N}{V g_{3/2}(1)}\right)^{2/3}. \tag{2.44}$$

To analyze the effect of the Dunkl formalism, we express the Dunkl-condensation temperature in terms of the ordinary one as:

$$\frac{T_c^D}{T_c^0} = \left[1 + \frac{g_{3/2}(-1)}{g_{3/2}(1)} \left(1 - \frac{1}{\sqrt{1+2\theta}}\right)\right]^{-2/3}. \tag{2.45}$$

This effect is better visualized by plotting the temperature ratio versus the Wigner parameter as given in Fig. 2.2.

We observe that the transition temperature is smaller than T_c^0 when $-1/2 < \theta < 0$. On the other hand, when θ takes on positive values, T_c^D becomes greater than T_c^0.

Finally, below the transition temperature, one may use equations (2.39) and (2.42) to derive the ground state population $\frac{N_0^D}{N}$

Figure 2.2 Critical temperature ratio versus the Wigner parameter.

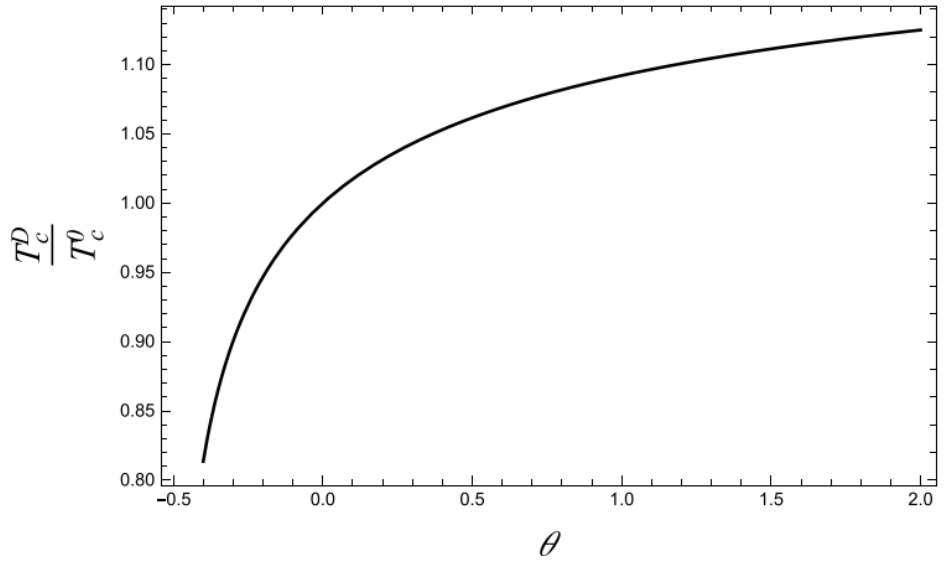

$$\frac{N_0^D}{N} = 1 - \left(\frac{T}{T_c^D}\right)^{3/2}, \tag{2.46}$$

which can be rewritten as

$$\frac{N_0^D}{N} = 1 - \left(\frac{T}{T_c^0}\right)^{3/2} \left[\frac{g_{3/2}(-1)}{g_{3/2}(1)}\left(1 - \frac{1}{\sqrt{1+2\theta}}\right) + 1\right]. \tag{2.47}$$

In Fig. 2.3, we plot the ground state population $\frac{N_0^D}{N}$ as a function of T/T_c^0 for various deformation values of θ.

2.3 Generalization of the Dunkl-Bose-Einstein gas in any dimension

We will now look at how the Dunkl-Bose-Einstein gas works when we consider different numbers of dimensions. Let's start with the basics: when a boson (a type of particle) moves freely with mass m, its energy is:

$$\varepsilon = \frac{1}{2m}(p_1^2 + p_2^2 + \cdots + p_d^2) \tag{2.47}$$

Figure 2.3 Ground state population versus the temperature ratio $\frac{T}{T_c^0}$ for varying θ.

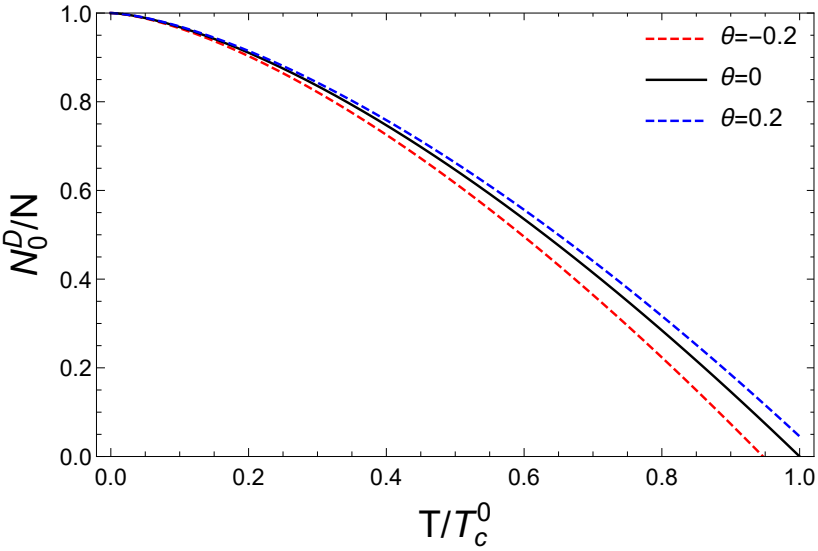

Here, $p_1, p_2, \cdots$ represent the momentum, m is the masse and d is the dimensionality.

In the phase space, the energy density of states for a free massive particle in a d-dimensional system with volume V is calculated by the standard method

$$\rho(\varepsilon)^{(d)} = \frac{V}{\Gamma(\frac{d}{2})}\left(\frac{2\pi m}{h^2}\right)^{d/2} \varepsilon^{\frac{d}{2}-1} = C\varepsilon^{\frac{d}{2}-1}, \tag{2.47}$$

where h is Planck's constant, C is just a shorter way to write all the constants together and The $\Gamma(n)$ is Gamma function.

To help visualize this, we've created a graph showing how this density of states looks in one, two, and three dimensions. You can see this in Figure 2.4.
Note that when $\varepsilon \longrightarrow 0$, $\rho^{(2)}$ remains constant, and $\rho^{(1)}$ diverges in the same limit. However, for $d > 3$, we have:

$$\lim_{\varepsilon \longrightarrow 0} \rho^{(d>3)}(\varepsilon) = 0. \tag{2.48}$$

This difference in the asymptotic behaviors of $\rho^d\,(\varepsilon \longrightarrow 0)$ implies that a finite BEC critical temperature T_c exists only in a three-dimensional system. Nonetheless, for a system

Figure 2.4 The normalized energy density of states for uniform 3D, 2D and 1D systems

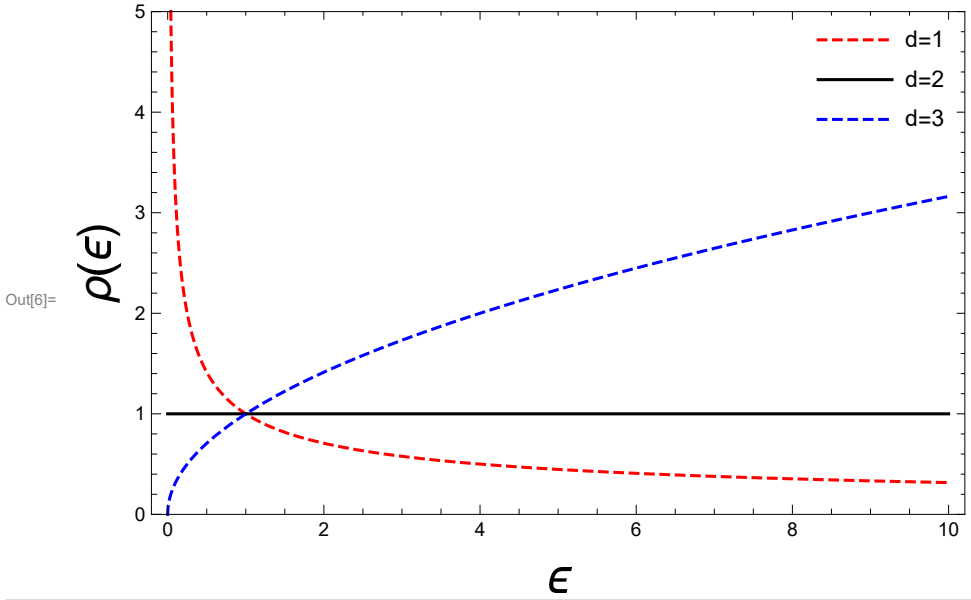

of finite size, a non-zero BEC critical temperature exists independently of dimensionality expect $d = 1$ and $d = 2$.

2.3.1 Mathematical analysis

In this section, we analyze an ideal Dunkl-Bose gas in arbitrary dimensions. Transitioning to the thermodynamic limit, where the system's volume ($V \longrightarrow \infty$) and the number of particles ($\mathcal{N} \longrightarrow \infty$) become large with a constant density ($\frac{\mathcal{N}}{V} \longrightarrow$ Cst), we employ the conversion relation

$$\sum_{i=1}^{\infty} \longrightarrow \int_0^{\infty} \rho(\varepsilon). \tag{2.49}$$

Utilizing equation (2.49), the summation (2.27) becomes

$$\mathcal{N} = \mathcal{N}_0^D + 2\int \frac{\rho\left(\varepsilon\right)}{e^{2\beta\varepsilon}e^{-2}-1}d\varepsilon + (1+2\theta)\int \frac{\rho\left(\varepsilon\right)}{e^{\beta(1+2\theta)\varepsilon}e^{1+2\theta}+1}d\varepsilon. \tag{2.50}$$

Substituting the density of states from equation (2.3), we obtain

$$\mathcal{N} = \mathcal{N}^D + \frac{V}{\lambda_{th}^{d/2}} \left[2^{1-d/2} g_{d/2}(z^2) - (1+2\theta)^{1-d/2}\, g_{d/2}\left(-z^{1+2\theta}\right) \right], \tag{2.51}$$

where

$$g_s(z) = \frac{1}{\Gamma(s)} \int \frac{x^{s-1}}{e^x z^{-1} - 1} dx, \tag{2.52}$$

is the Bose-Einstein function and

$$\lambda_{th} = \sqrt{\frac{2\pi m K T}{h^2}} \tag{2.53}$$

is the de Broglie thermal wavelength. Using the property of the Polylog function

$$2^{1-s} g_s(z^2) = g_s(z) + g_s(-z), \tag{2.54}$$

we can express

$$n = n_0^D + \frac{g_{d/2}\,(z,\theta)}{\lambda_{th}^{d/2}}, \tag{2.55}$$

where $n = \mathcal{N}/V$ is the particle density, and

$$g_{d/2}\,(z,\theta) = g_{d/2}(z) + g_{d/2}(-z) - (1+2\theta)^{1-d/2}\, g_{d/2}\left(-z^{1+2\theta}\right), \tag{2.56}$$

represents the corrected Dunkl-Bose-Einstein function. It is evident that in the limit $\theta \longrightarrow 0$, the Dunkl particle density reduces to the Bose particle density, i.e.,

$$n = n_0 + \frac{g_{d/2}(z)}{\lambda_{th}^{d/2}}, \tag{2.57}$$

Similar to the ordinary case, the BEC of a trapped Dunkl-boson system with a finite number of particles should not have an evident critical temperature. However, we can determine an effective Dunkl-critical temperature through two methods

- By setting the chemical potential to zero and assuming all particles are in the excited states.
- By identifying the temperature at which the specific heat of the system reaches its maximum value.

Here, we prefer the first method for its simplicity. After straightforward manipulations, the particle density becomes

$$n = \frac{1}{\lambda_c^{d/2}} \left[g_{d/2}(1) + g_{d/2}(-1) - (1+2\theta)^{1-d/2} g_{d/2}(-1) \right]. \tag{2.58}$$

Further manipulations yield the Dunkl-critical temperature as a function of the Bose-critical temperature as

$$T_c^D = T_c^B \left[1 + \frac{g_{d/2}(-1)}{\zeta(d/2)} \left(1 - (1+2\theta)^{d/2-1} \right) \right]^{-2/d}, \tag{2.59}$$

where $\zeta(s)$ is the Riemann-Zeta and

$$T_c^B = \frac{h^2}{2\pi m K} \left(\frac{n}{\zeta(d/2)} \right)^{2/d}, \tag{2.60}$$

is the Bose-critical temperature. The central problem examines the feasibility of achieving Bose-Einstein condensation within Dunk algebra under conditions of infinite dimensionality. When $d \to \infty$, (2.59) becomes

$$\lim_{d\to\infty} T_c^D = \frac{h^2}{2\pi m K}. \tag{2.61}$$

which implies it is impossible there is a possible to find a Dunkl-BEC in an infinite dimension.

Next, we derive the ground state population using the two equations

$$\begin{cases} \mathcal{N} &= \frac{V}{\lambda(T_c^D)} g_{d/2}(1,\theta) \\ \mathcal{N} &= \mathcal{N}_0^D + \frac{V}{\lambda(T)} g_{d/2}(1,\theta) \end{cases}. \tag{2.62}$$

Eliminating $V g_{d/2}(1,\theta)$ between the last systems, we obtain

$$\frac{\mathcal{N}_0^D}{\mathcal{N}} = 1 - \left(\frac{T}{T_c^D}\right)^{d/2}. \tag{2.63}$$

Expressing this in terms of the BEC temperature, we find

$$\frac{\mathcal{N}_0^D}{\mathcal{N}} = 1 - \left[1 + \frac{g_{d/2}(-1)}{\zeta(d/2)}\left(1 - (1+2\theta)^{d/2-1}\right)\right]^{-d/2}\left(\frac{T}{T_c^B}\right)^{d/2}. \tag{2.64}$$

2.3.2 Numerical results and discussion

We now present our results graphically, beginning with the behavior of the generalized Dunkl-Bose functions. In Figs. 2.5, 2.6 and 2.7, the function $g_{d/2}(z,\theta)$ is plotted against the fugacity for various values of the Wigner parameter and different dimensions. When $\theta = 0$, we recover the ordinary Bose function; as θ increases, the function g decreases. Notably, larger d corresponds to smaller values of g, while a negative Wigner coefficient leads to a higher value of g.

Figure 2.5 Variation of $g_{d/2}(z,\theta)$ with z for different d and $\theta = 0$.

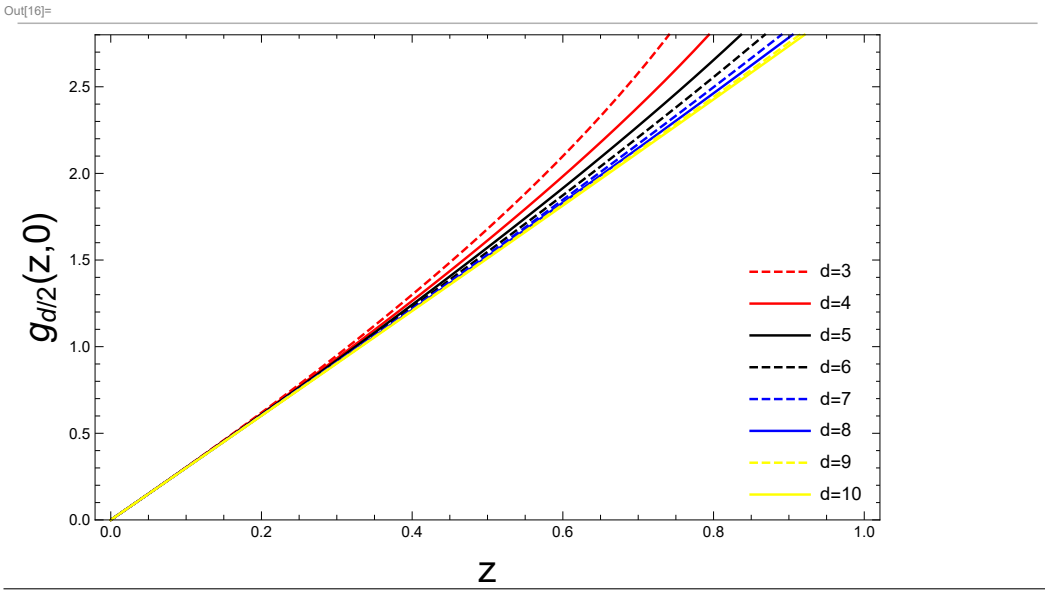

Figure 2.6 Variation of $g_{d/2}(z,\theta)$ with z for different d $\theta = 0.2$.

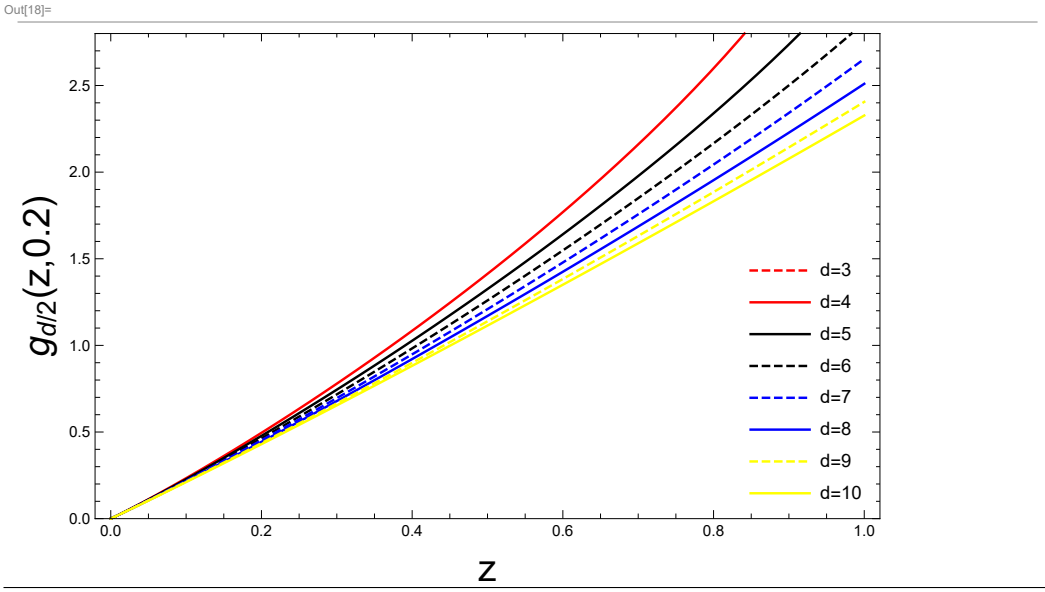

Figure 2.7 Variation of $g_{d/2}(z,\theta)$ with z for different d and $\theta = -0.2$.

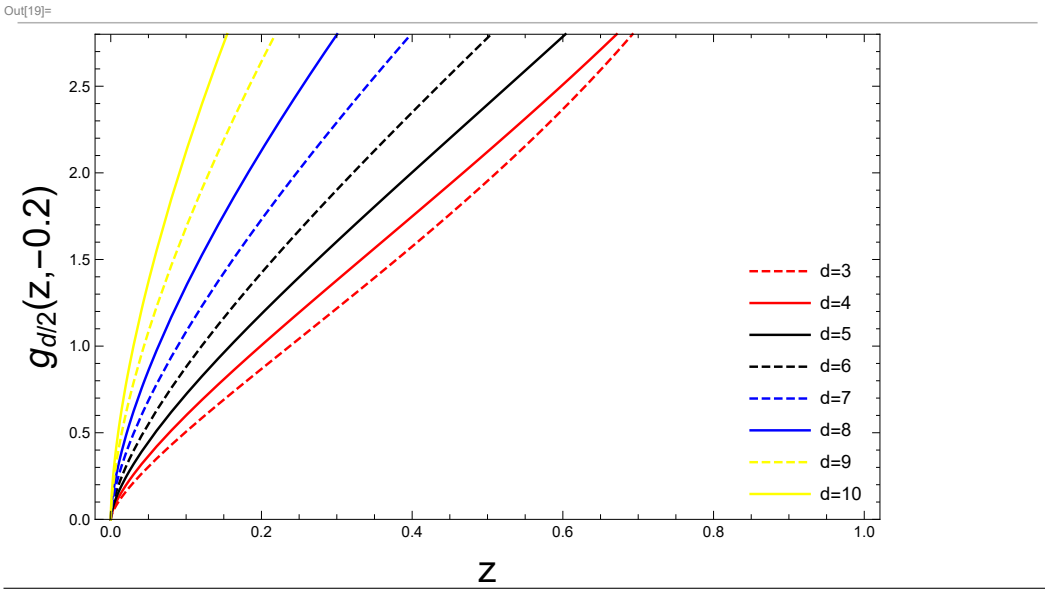

Next, in Fig. 2.8, we illustrate the change in condensation temperature ratio with respect to the Wigner parameter for different dimensionalities.

The rate increases monotonically with the Wigner parameter, exhibiting higher values in low dimensions for $\theta < 0$ and in high dimensions for positive θ. To complement our graphical analysis, we provide numerical results in three tables for the critical temperature

Figure 2.8 Critical temperature ratio versus the Wigner parameter for different dimensionallty

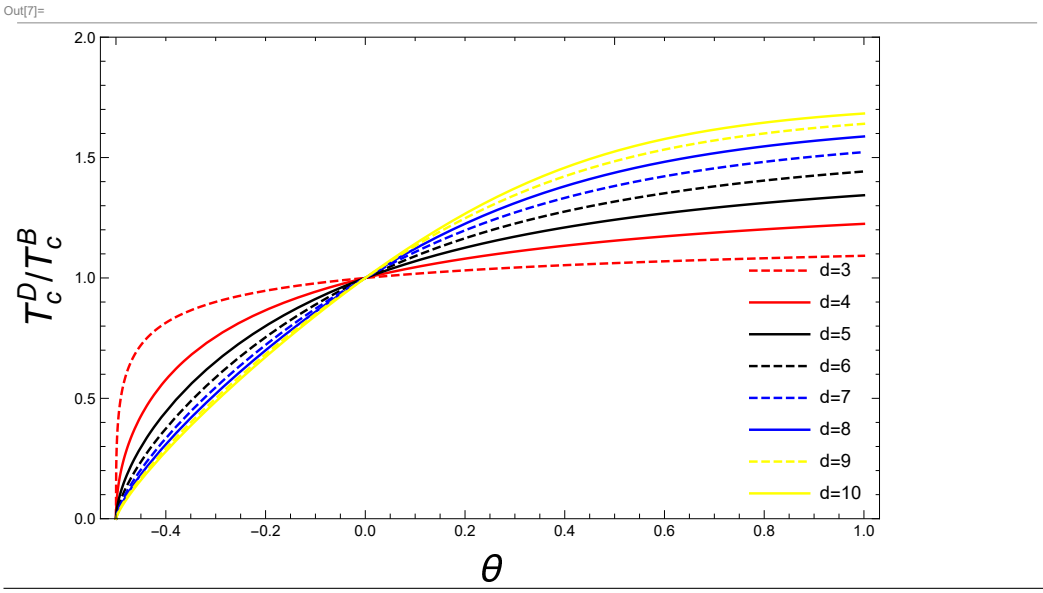

in the Dunkl algebra. The first one, Table 2.1, represents the critical temperature for a null Wigner coefficient, which is the standard case [72].

The remaining two tables, Tables 2.2 and 2.3, show case the results for varying Wigner coefficients.

Finally, we demonstrate the condensate fraction $\frac{\mathcal{N}_0^D}{N}$ versus normalized temperature $\frac{T}{T_c^B}$ for different values of the Wigner parameter and various dimensions in Figs. 2.9, 2.10 and 2.11.

Dimensionality d	Wigner parameter θ	Condensation temperature T_c^D (Kelvin)
3	0	3.13269
4	0	8.76365×10^{-4}
5	0	5.83222×10^{-6}
6	0	1.99971×10^{-7}
7	0	1.77437×10^{-8}
8	0	2.86711×10^{-9}
9	0	6.92417×10^{-10}
10	0	2.21788×10^{-10}

Table 2.1: Critical temperatures for null Wigner coefficient.

Figure 2.9 Ground state population (for $\theta = 0$)vs. temperature ratio T/T_c^B for different dimensionalities

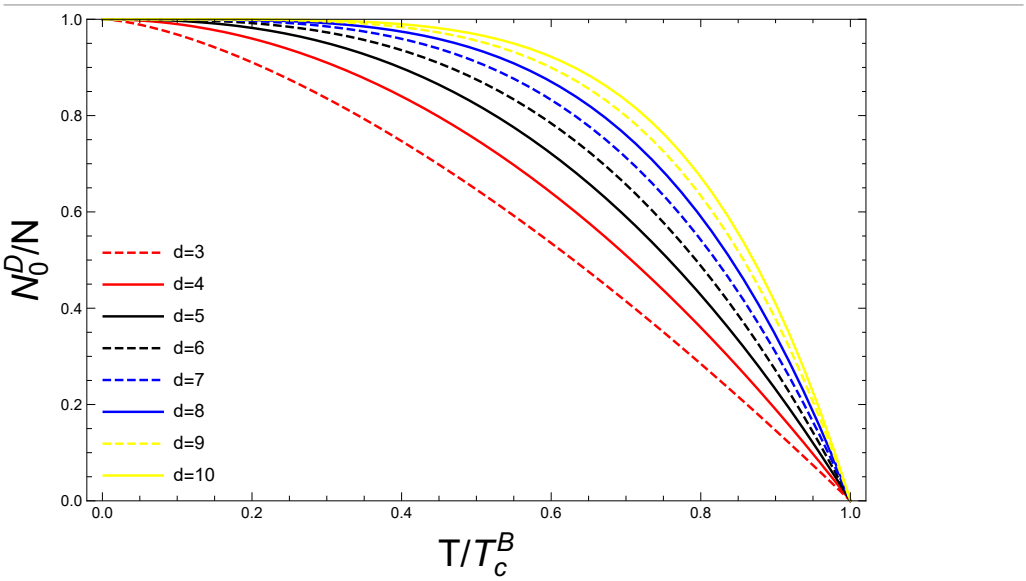

Dimensionality d	Wigner parameter θ	Condensation temperature T_c^D (Kelvin)
3	-0.49	1.58518
4	-0.49	1.73546×10^{-4}
5	-0.49	6.63698×10^{-7}
6	-0.49	1.62161×10^{-8}
7	-0.49	1.14718×10^{-9}
8	-0.49	1.57658×10^{-10}
9	-0.49	3.37192×10^{-11}
10	-0.49	9.8258×10^{-12}

Table 2.2: Critical temperatures for negative Wigner coefficient.

Figure 2.10 Ground state population (for $\theta = 0.2$)vs. temperature ratio T/T_c^B for different dimensionalities

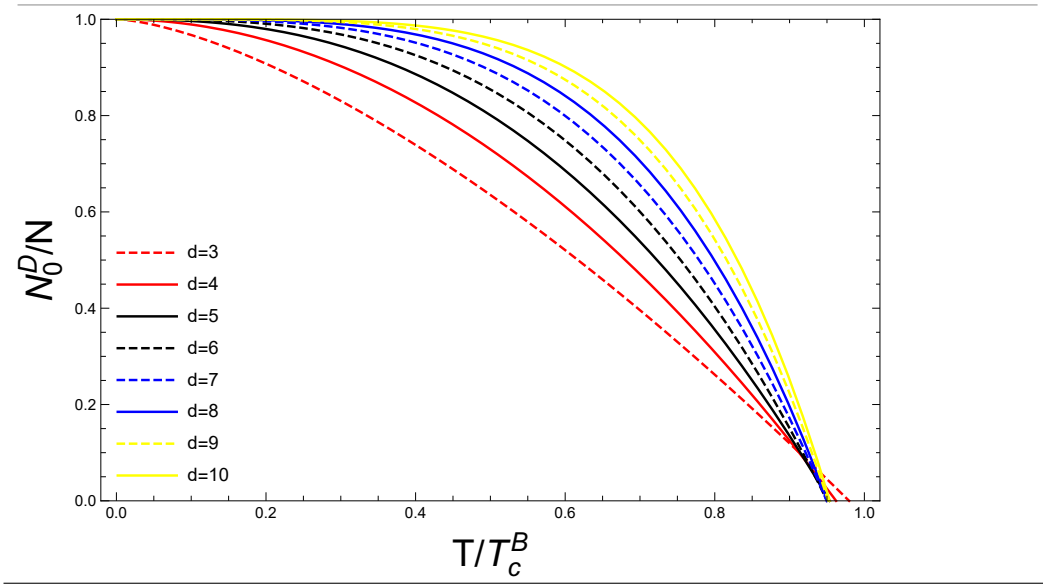

Dimensionality d	Wigner parameter θ	Condensation temperature T_c^D (Kelvin)
3	0.5	3.32572
4	0.5	1.01194×10^{-3}
5	0.5	7.24157×10^{-6}
6	0.5	2.63415×10^{-7}
7	0.5	2.45211×10^{-8}
8	0.5	4.12066×10^{-9}
9	0.5	1.02794×10^{-9}
10	0.5	3.38309×10^{-10}

Table 2.3: Critical temperatures for positive Wigner coefficient.

Figure 2.11 Ground state population (for $\theta = -0.2$)vs. temperature ratio T/T_c^B for different dimensionalities

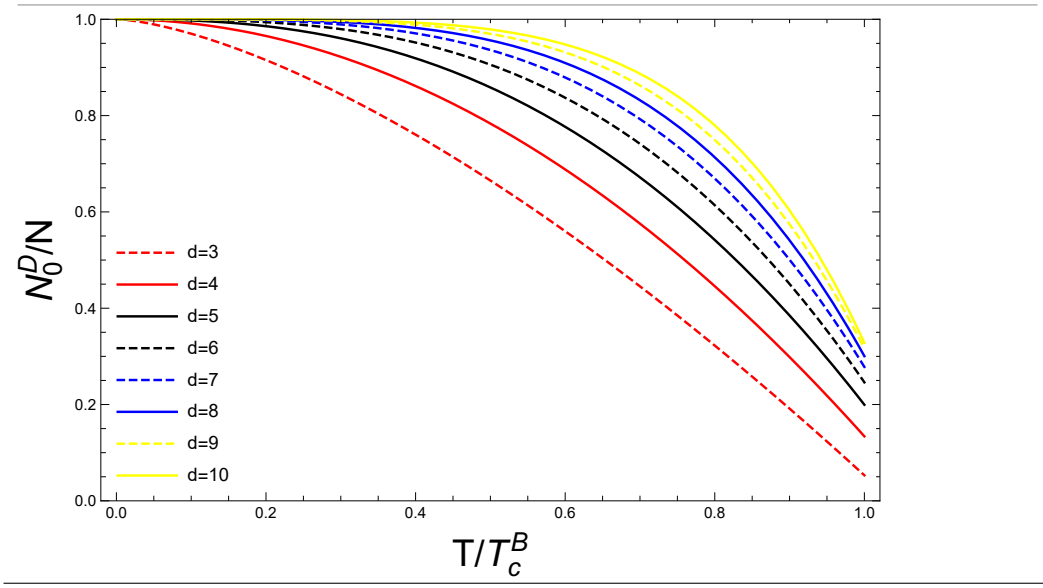

2.4 Application: blackbody radiation

Within this section, we delve into the blackbody radiation phenomenon using the Dunkl formalism approach. Our exploration commences by formulating the mean photon energy state occupation number, N_ε, with a specific focus on the case where $\mu = 0$.

$$N_\varepsilon^D = \frac{2}{e^{2\beta\varepsilon} z^{-2} - 1} + \frac{(1+2\theta)}{e^{\beta(1+2\theta)\varepsilon} z^{-(1+2\theta)} + 1}. \tag{2.65}$$

Postulating the energetic quantum representation $\varepsilon = \hbar\omega$, with ω characterizing electromagnetic oscillatory dynamics, we instantiate the photonic population enumeration across the spectral bandwidth differential ω to $\omega + d\omega$ through the subsequent mathematical articulation:

$$dN_\varepsilon^D = \frac{V}{\pi^2 c^3} \frac{\omega^2 d\omega}{e^{2\beta\hbar\omega} - 1} + \frac{V(1+2\theta)}{2\pi^2 c^3} \frac{\omega^2 d\omega}{e^{\beta(1+2\theta)\hbar\omega} + 1}. \tag{2.66}$$

Consequently, the spectral energy distribution for the considered radiation manifests as:

$$\frac{dE^D}{V} = \frac{\hbar}{2\pi^2 c^3} \left[\frac{2\omega^3}{e^{\frac{2\hbar\omega}{KT}} - 1} + \frac{(1+2\theta)\omega^3}{e^{\frac{(1+2\theta)\hbar\omega}{KT}} + 1} \right] d\omega. \tag{2.67}$$

This equation is the generalized Planck radiation law in the framework of Dunkl statistics. Based on equation (2.67), we can derive two limit cases, namely:

- The high energy limit (base frequency) i.e., ($\hbar\omega \ll K_B T$). In this case, we can estimate the energy density as

$$\frac{dE^D}{d\omega} = \frac{V}{\pi^2 c^3} \frac{\omega^2}{\beta}. \tag{2.68}$$

  This expression is classical and is invariant under the effect of Dunkl's algebra.

- The low energy limit (high frequency) i.e., ($\hbar\omega \gg K_B T$). In this case the energy density becomes:

$$\frac{dE^D}{d\omega} = \frac{V}{2\pi^2 c^3}\left[2e^{-2\beta\hbar\omega} + (1+2\theta)\, e^{-\beta(1+2\theta)\hbar\omega}\right]\omega^3. \tag{2.69}$$

Proceeding with comprehensive frequency-domain integration of equation (2.67), we derive the generalized cavity radiation energy functional:

$$\frac{E^D}{V} = \frac{\sigma}{2c}T^4\left[1 + \frac{7}{(1+2\theta)^3}\right], \tag{2.70}$$

Wherein $\sigma = \frac{K^4\pi^2}{60c^2\hbar^3}$ represents the fundamental Stefan-Boltzmann parametrization. The emergent quantum modification to classical radiation energetics manifests through the secondary component of equation (2.70). Critically, when the deformation parameter θ vanishes, the generalized energy representation collapses to its archetypal thermodynamic manifestation:

$$\frac{E}{V} = \frac{4\sigma}{c}T^4. \tag{2.71}$$

To show how the Dunkl model works in practice, we plot the quantum-adjusted energy flow in the cavity, $\frac{E^D}{V}$, as it changes with temperature. We show different curves for various deformation parameters in Figure 2.12.

We observe that the radiated energy goes up as temperature rises, just like in the normal case. Also, when temperature stays the same, the energy output drops as the adjustment factor gets bigger.

2.4.1 Thermodynamic quantites

We will now examine the thermal properties of our blackbody system. Specifically, we will analyze its available energy using the Dunkl correction mathematical approach. “‘

Figure 2.12 Dunkl-corrected energy radiation per unit volume versus the temperature for different values of θ.

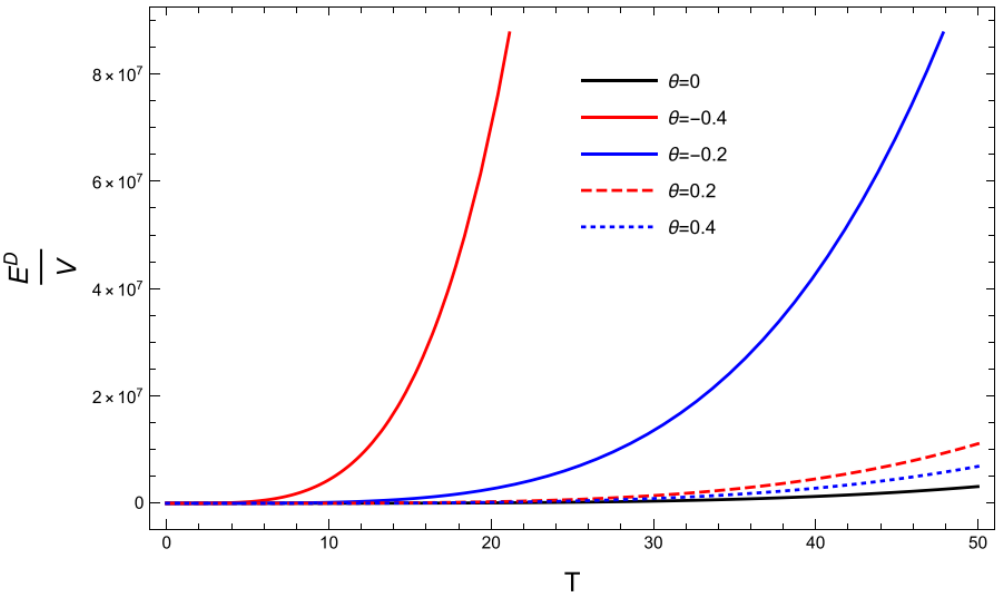

$$F^D = -T \int \frac{E^D}{T^2} dT. \tag{2.72}$$

After substituting equation (2.70) into equation (2.72), we arrive at:

$$\frac{F^D}{V} = -\frac{\sigma}{6c} T^4 \left[1 + \frac{7}{(1+2\theta)^3} \right]. \tag{2.73}$$

As we let our mathematical correction approach zero, we recover the standard formula: $F = -\frac{4V}{3c}\sigma T^4$. In the following figure, we present how the available energy varies with temperature.

Our results show that the Dunkl-Helmholtz free energy always steadily decreases as temperature rises. Additionally, when temperature T remains constant, the free energy becomes larger as the deformation parameter θ increases.

The entropy with Dunkl corrections $S = -\left(\frac{\partial F}{\partial T}\right)$ is another important quantity to study. We calculate it to be

Figure 2.13 Dunkl Helmholtz free energy per unit volume versus temperature for different values of θ.

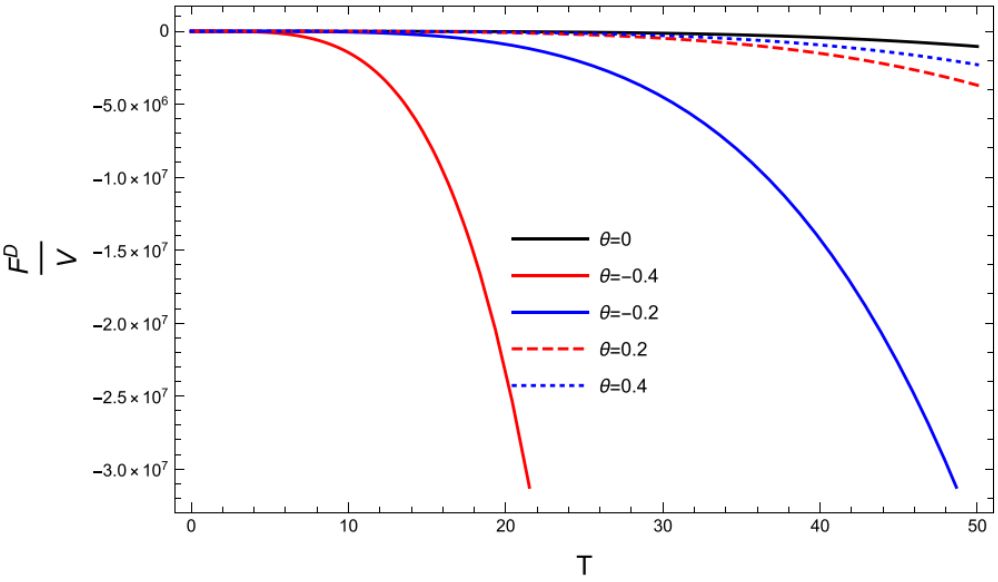

$$\frac{S^D}{V} = \frac{2}{3c}\sigma T^3 \left[1 + \frac{7}{(1+2\theta)^3}\right], \tag{2.74}$$

This demonstrates that when we combine equations (2.73) and (2.70), the thermodynamic quantities follow the usual relationship

$$F^D = E^D - TS^D. \tag{2.75}$$

The relationship between temperature and entropy (including Dunkl corrections) is shown in Figure 2.14.

When temperatures are low, we cannot see any changes caused by using the Dunkl method. However, at high temperatures, these changes become very noticeable. Also, when θ gets extremely large, we find a point where the values stop increasing and return to the usual T^3 relationship, but with a different multiplier.

After this, we will examine how the Dunkl method changes the specific heat capacity when volume stays the same. This is calculated by

Figure 2.14 The Dunkl entropy per unit volume as a function of temperature for different values of θ.

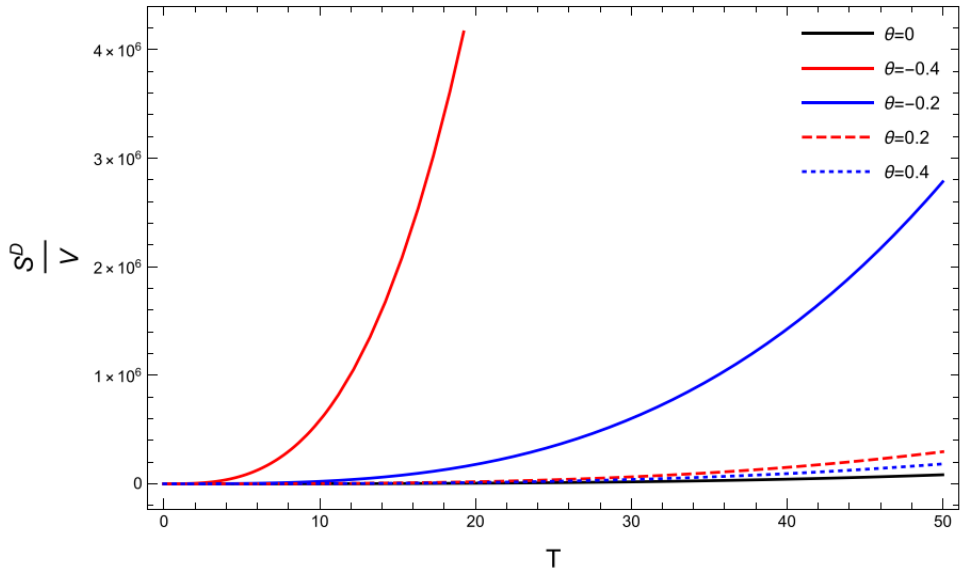

$$C_V^D = -\left(\frac{\partial E^D}{\partial T}\right)_V = \frac{2V}{c}\sigma T^4\left[1+\frac{7}{(1+2\theta)^3}\right]. \tag{2.76}$$

When θ approaches zero, equation (2.76) produces the expected traditional result. We show how the specific heat (modified by the Dunkl method) changes with temperature in Figure 2.15.

We can see that the modified specific heat function gets larger as the temperature rises. This increase happens more quickly when the Wigner parameter is negative.

Now, let's determine how the pressure function changes when we apply the Dunkl method:

$$P = -\left(\frac{\partial F}{\partial V}\right)_T. \tag{2.77}$$

When we put equation (2.73) into equation (2.77), we get

$$P^D = \frac{\sigma}{6c}T^4\left[1+\frac{7}{(1+2\theta)^3}\right]. \tag{2.78}$$

Figure 2.15 Dunkl specific heat per unit volume as a function of temperature for different values of θ.

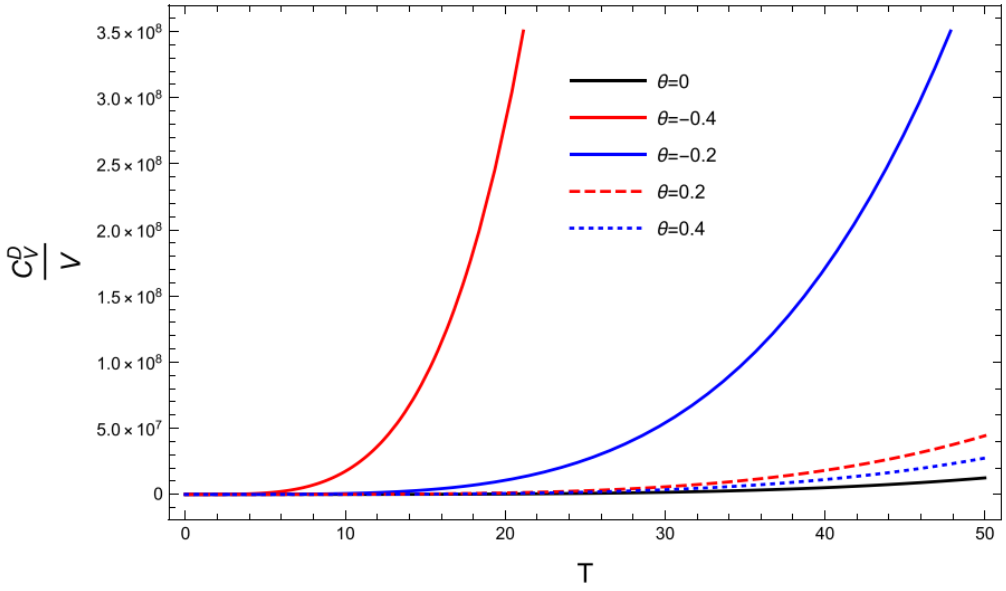

This gives us the equation of state (EOS) written as

$$P^D V = \frac{E^D}{3}, \tag{2.79}$$

This shows that the equation of state (EOS) remains unchanged when we use the Dunkl method.

This result reveals an important physical insight: while the Dunkl formalism modifies various thermodynamic quantities (such as entropy and specific heat), the fundamental equation of state preserves its original form. The invariance of the EOS indicates that the basic relationship between pressure, volume, and temperature remains robust under Dunkl modifications. Such preservation of fundamental relationships often points to deeper physical principles in the system being studied.

Chapter 3

Traps effect On Dunkl-Bose–Einstein condensation

In recent years, there has been growing interest in the study of BEC in the presence of external potentials, such as harmonic traps. These traps provide confinement that can significantly influence the properties of the condensate, leading to intriguing phenomena, including the formation of quantized vortices and shell structures.

This chapter investigates BEC of an ideal gas using the Dunkl formalism, offering a novel perspective on the subject. The analysis covers this quantum phenomenon across various systems, beginning with a three-dimensional harmonic oscillator and extending to more complex configurations, such as quasi-two-dimensional and one- to two-dimensional power-law traps.

We begin by focusing on the three-dimensional harmonic oscillator and explore the thermodynamic properties of a trapped bosonic gas. By incorporating the Dunkl statistics, we calculate various thermodynamic quantities including the average particle number and internal energy. The subsequent section broadens the scope by examining the impact of the confinement of the gas in a quasi-two-dimensional harmonic trap. At the conclusion of each section, we compare the results with those obtained using ordinary statistics to elucidate the effects of Dunkl statistics on the behavior of the trapped Bose gas.

The study of BEC in traps within the framework of Dunkl statistics provides a unique perspective on the interplay between confinement and statistical effects. It offers insights into how the Wigner parameter influences the condensate formation, density distribution, and thermodynamic properties of the trapped gas. The results obtained in this chapter contribute to a deeper understanding of the behavior of bosonic systems and provide a basis for exploring other exotic statistical systems in the context of BEC.

3.1 Ideal Dunkl−Bose gas trapped in a three-dimensional harmonic oscillator potential

Consider a system containing N neutral atoms behaving as a Bose gas, which is confined within a three-dimensional harmonic trap

$$V(x,y,z) = \frac{m\omega_1^2}{2}x^2 + \frac{m\omega_2^2}{2}y^2 + \frac{m\omega_3^2}{2}z^2, \tag{3.1}$$

in which m represents the atomic mass and ω_i denotes the frequencies of the trap. The total energy here equals the addition of each particle's individual energy [7]

$$E_{n_1,n_2,n_3} = \hbar\left(\omega_1 n_1 + \omega_2 n_2 + \omega_3 n_3\right) + E_0, \tag{3.2}$$

with n_i taking values $0, 1, 2, ...$ when $i = 0, 1, 2....$ The ground-state energy is

$$E_0 = \frac{\hbar}{2}\left(\omega_1 + \omega_2 + \omega_3\right). \tag{3.3}$$

Within the Dunkl approach, the grand canonical ensemble provides expressions for the quantities of atoms in both the lowest state and higher energy levels, which we present as follows [73]:

$$N = N_0^D + N_e^D, \tag{3.4}$$

where

$$N_0^D = \frac{2}{z^{-2}-1} + \frac{(1+2\theta)}{z^{-(1+2\theta)}+1}, \tag{3.5}$$

$$N_e^D = \sum_{i\neq 0}\left(\frac{2}{e^{2\beta E_i} z^{-2}-1} + \frac{(1+2\theta)}{e^{\beta(1+2\theta)E_i} z^{-(1+2\theta)}+1}\right). \tag{3.6}$$

In these expressions, β equals $(k_B T)^{-1}$ where k_B stands for Boltzmann's constant, while $z = e^{\beta(\mu - E_0)}$ defines the system's fugacity. The Dunkl framework in three dimensions typically contains three different Wigner parameters, but we take them all equal to θ to make calculations easier. We also set the lowest energy level to zero and write μ instead of $\mu - E_0$ to simplify our mathematical formulation.

Computing the summation shown in equation (3.6) directly is challenging. To solve this problem, we can replace the sum with a weighted integration:

$$\sum \to \int \rho(E) dE. \tag{3.7}$$

Here, Grossmann and Holthaus postulated that the density of states $\rho(E)$ was approximately given by Refs. [7, 8]

$$\rho(E) = \frac{1}{2}\frac{E^2}{(\hbar\Omega)^3} + \gamma\frac{E}{(\hbar\Omega)^2}, \tag{3.8}$$

where $\Omega = (\omega_1\omega_2\omega_3)^{1/3}$ gives the mean frequency of the confining trap, and γ represents a factor determined by numerical calculations based on the individual trap frequencies $(\omega_1, \omega_2, \omega_3)$.

The study [7] determined that γ equals 3/2 for a symmetric oscillator. This replacement holds true when dealing with many particles and small energy level differences. Through basic mathematical steps, we derive an expression for all particles:

$$N = N_0^D + 2\int_0^\infty \frac{\rho\left(E\right)dE}{e^{2\beta E}z^{-2}-1} + (1+2\theta)\int_0^\infty \frac{\rho\left(E\right)dE}{e^{\beta(1+2\theta)E}z^{-(1+2\theta)}+1}, \tag{3.9}$$

which, after integration, becomes

$$\begin{aligned} N &= N_0^D + \frac{1}{4}\left(\frac{k_BT}{\hbar\Omega}\right)^3\left\{g_3(z^2) - \frac{4}{(1+2\theta)^2}g_3\left(-z^{1+2\theta}\right)\right\} \\ &+ \frac{\gamma}{2}\left(\frac{k_BT}{\hbar\Omega}\right)^2\left\{g_2(z^2) - \frac{2}{(1+2\theta)}g_2\left(-z^{1+2\theta}\right)\right\}. \end{aligned} \tag{3.9}$$

In this equation, $g_s(z)$ represents the Polylogarithm (or Bose) function, expressed as:

$$g_s(z) = \frac{1}{\Gamma(s)}\int_0^\infty \frac{x^{s-1}}{e^x z^{-1}-1}dx. \tag{3.10}$$

By using the property,

$$g_s(z) + g_s(-z) = 2^{1-s}g_s(z^2), \tag{3.11}$$

we can rewrite equation (3.2) as:

$$N = N_0^D + \left(\frac{k_BT}{\hbar\Omega}\right)^3 g_3\left(z,\theta\right) + \gamma\left(\frac{k_BT}{\hbar\Omega}\right)^2 g_2\left(z,\theta\right), \tag{3.12}$$

where we define a new function

$$g_s\left(z,\theta\right) = g_s(z) + g_s(-z) - \frac{1}{(1+2\theta)^{s-1}}g_s\left(-z^{1+2\theta}\right), \tag{3.13}$$

This is called the Dunkl-Bose function. When θ approaches zero, the Dunkl-Bose function becomes the standard Bose function, and equation (3.12) becomes identical to equation (4) found in reference [7]. Before we study the Dunkl-BEC temperature, we want to show

Figure 3.1 The Dunkl-Bose function, $g_3(1,\theta)$, versus the Wigner parameter.

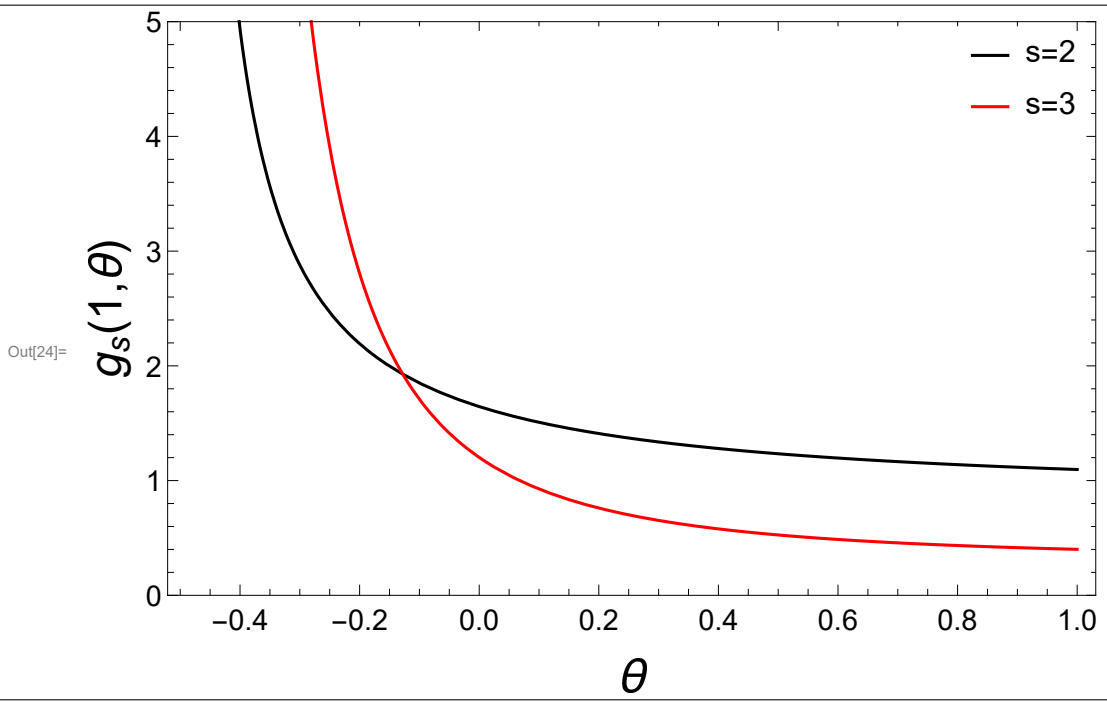

how the Dunkl-Bose function behaves. For this purpose, we show in Figure 3.1 how the Dunkl-Bose function changes with the Wigner parameter when $s = 2$ and $s = 3$.
We can see that the Dunkl-Bose function gets smaller as the Wigner parameter gets larger. We then show in Figure 3.2 how the Dunkl-Bose function with $s = 3$ changes with z for three different values of the Wigner parameter.

Figure 3.2 The Dunkl-Bose function, $g_3(z,\theta)$, versus z for different Wigner parameters.

Out[23]=

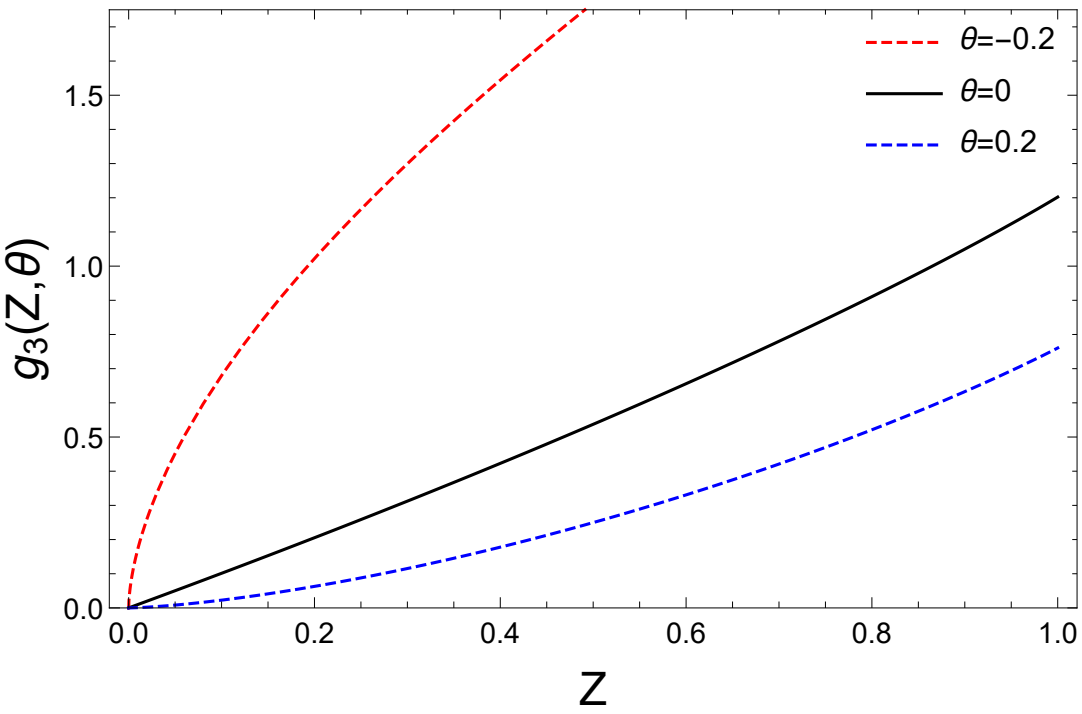

We can see that the Dunkl-Bose function always increases. When the Wigner parameter is positive, the Dunkl-Bose function has lower values than the regular Bose function. When $\theta < 0$, this pattern switches, and the Dunkl-Bose function becomes larger than the regular Bose function. These patterns are basic features of these functions and stay the same no matter what value of s we use.

3.1.1 Condensation temperature

Let's examine the condensation temperature. We know that when the temperature drops to the condensation temperature, T_c, the particles move into the lowest energy state of the trap. At the point where condensation begins, the system has almost no particles in the ground state ($N_0^D \simeq 0$) and z is nearly 1. Using these conditions, we can write the Dunkl-BEC temperature, T_c^D, as (See Appendix B):

$$T_c^D \simeq \frac{\hbar\Omega}{k_B}\left[\frac{N}{g_3(1,\theta)}\right]^{1/3}\left\{1-\frac{\gamma}{3}\left[\frac{g_2(1,\theta)}{g_3(1,\theta)^{2/3}}\right]\frac{1}{N^{1/3}}\right\}. \tag{3.14}$$

It is important to note the Dunkl-critical temperature depends on several factors: the total number of particles N, the the individual frequencies of the oscillator ω_i, the coefficient γ, also on the Wigner parameter. When θ approaches zero, we get back the standard Bose condensation temperature T_c^B that was shown in [7]:

$$T_c^B \simeq \frac{\hbar\Omega}{k_B}\left[\frac{N}{g_3(1)}\right]^{1/3}\left\{1-\frac{\gamma}{3}\left[\frac{g_2(1)}{g_3(1)^{2/3}}\right]\frac{1}{N^{1/3}}\right\}. \tag{3.15}$$

Next, we match equations (3.14) and (3.15) to construct a relationship between the Dunkl and conventional temperatures. We find the ratio:

$$\frac{T_c^D}{T_c^B} = \left[\frac{\zeta(3)}{g_3(1,\theta)}\right]^{\frac{1}{3}} \frac{1-\frac{\gamma}{3N^{1/3}}\frac{g_2(1,\theta)}{g_3(1,\theta)^{2/3}}}{1-\frac{\gamma}{18N^{1/3}}\frac{\pi^2}{\zeta(3)^{2/3}}}, \tag{3.16}$$

where $\zeta(n)$ is the Riemann-Zeta function. When the number of particles is very large ($N \to \infty$), we can ignore the second term in equation (3.14). In this case, we can approximate the Dunkl-BEC temperature as T_0^D:

$$T_0^D = \frac{\hbar\Omega}{k_B}\left[\frac{N}{g_3(1,\theta)}\right]^{\frac{1}{3}}, \tag{3.17}$$

which reduces to the ordinary case for $\theta = 0$ [7]:

$$T_0^B = \frac{\hbar\Omega}{k_B}\left[\frac{N}{\zeta(3)}\right]^{\frac{1}{3}}. \tag{3.18}$$

By comparing equation (3.17) with equation (3.18), we get the condensation temperature ratio:

$$\frac{T_0^D}{T_0^B} = \left[\frac{\zeta(3)}{g_3(1,\theta)}\right]^{\frac{1}{3}}. \tag{3.19}$$

We now show how the ratio of condensation temperatures changes with the Wigner parameter in Figure 3.3.

Figure 3.3 The variation of $\frac{T_0^D}{T_0^B}$ versus θ.

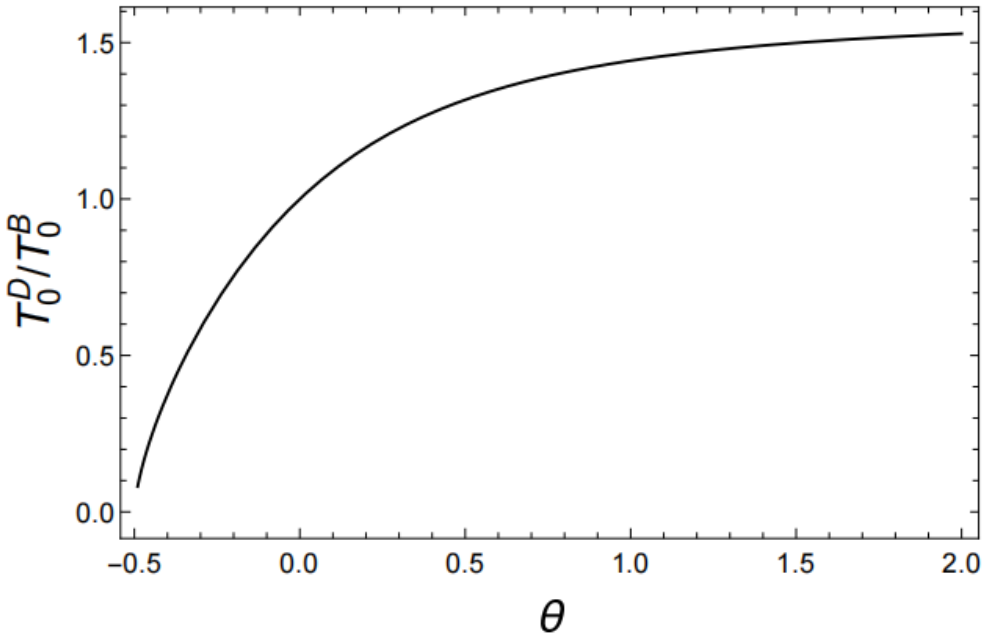

We observe that this ratio increases as the Wigner parameter increases. When the Wigner parameter is negative, the ratio stays below one. We also find that the ratio reaches a maximum value of 1.794 when the Wigner parameter becomes very large.

Using equation (3.18) in equation (3.12), we can calculate how the number of particles in the Dunkl ground state changes with temperature, giving us:

$$\frac{N_0^D}{N} = 1 - \frac{g_3(1,\theta)}{\zeta(3)}\left(\frac{T}{T_0^B}\right)^3 - \gamma\frac{g_2(1,\theta)}{\zeta^{2/3}(3)}\frac{1}{N^{1/3}}\left(\frac{T}{T_0^B}\right)^2. \tag{3.20}$$

In Figure 3.4, we show how this ratio changes with the condensation temperature ratio for a system containing two thousand particles.

Figure 3.4 The population of the Dunkl ground state ratio versus normalized temperature for different Wigner parameters.

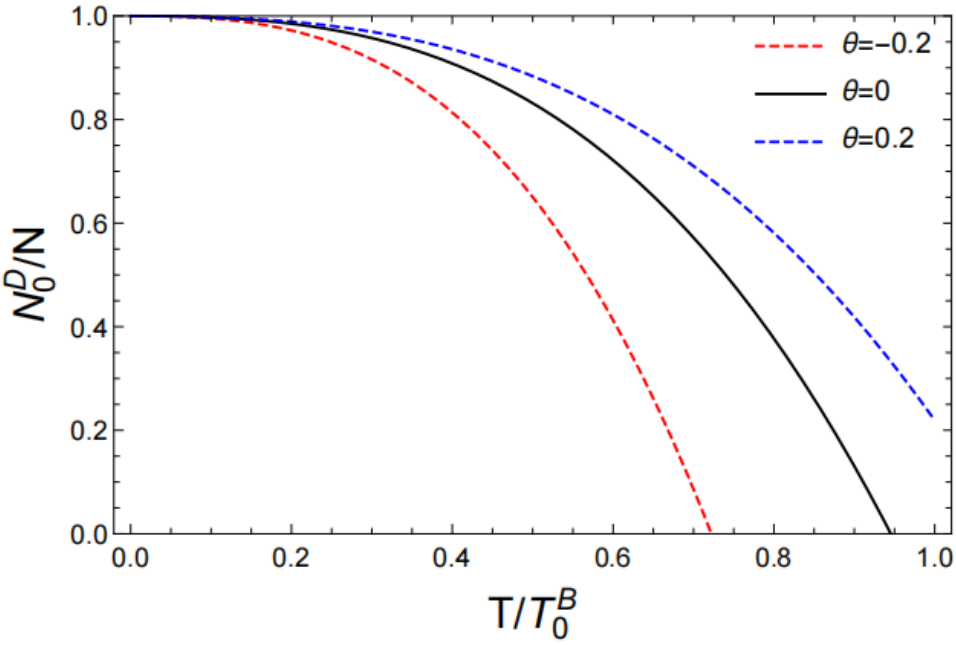

We note that when the Wigner parameter is positive, fewer particles occupy the ground state in the standard approach compared to the Dunkl approach. This means that for $\theta > 0$, the Dunkl-Bosonic system condenses more easily than the standard Bosonic system. However, when the Wigner parameter is negative, fewer particles occupy the ground state in the Dunkl approach than in the standard approach.

3.1.2 Thermodynamics of the system

Now we will examine the thermal properties of an ideal Bose gas trapped in a harmonic potential using Dunkl statistics. We begin by calculating the internal energy, U, using this equation:

$$U = \sum_i N_i E_i. \tag{3.21}$$

We now convert the summation into an integral:

$$U^D = 2\int_0^\infty \frac{E\rho\left(E\right)dE}{e^{2\beta E}z^{-2}-1} + (1+2\theta)\int_0^\infty \frac{E\rho\left(E\right)dE}{e^{\beta(1+2\theta)E}z^{-(1+2\theta)}+1}. \tag{3.22}$$

Equation (3.22) yields the following result after substituting equation (3.8) into equation (3.22):

$$\frac{U^D}{\hbar\Omega} = 3\left(\frac{k_BT}{\hbar\Omega}\right)^4 g_4(z,\theta) + 2\gamma\left(\frac{k_BT}{\hbar\Omega}\right)^3 g_3(z,\theta). \tag{3.23}$$

Next, to calculate the heat capacity, we must consider two different temperature ranges. When temperature is below T_c^D, we can use $z = 1$. However, when temperature exceeds T_c^D, we cannot do this because z becomes a complicated function of temperature. We use the standard formula:

$$C = \partial U/\partial T, \tag{3.24}$$

we find the general form of the Dunkl heat capacity for temperatures below T_c^D:

$$\frac{C_{\leq}^D}{Nk_B} = 12\frac{g_4(1,\theta)}{\zeta(3)}\left(\frac{T}{T_0^B}\right)^3 + \frac{6\gamma}{N^{1/3}}\frac{g_3(1,\theta)}{\zeta^{2/3}(3)}\left(\frac{T}{T_0^B}\right)^2, \tag{3.25}$$

In Figure 3.5, we show how the Dunkl heat capacity $C_{\leq}^D/KN$ changes with temperature $\frac{T}{T_0^B}$ for several different values of the Wigner parameter.

Figure 3.5 Heat capacity function versus $\frac{T}{T_0^B}$ of a very large number of bosons in the Dunkl formalism.

Out[26]=

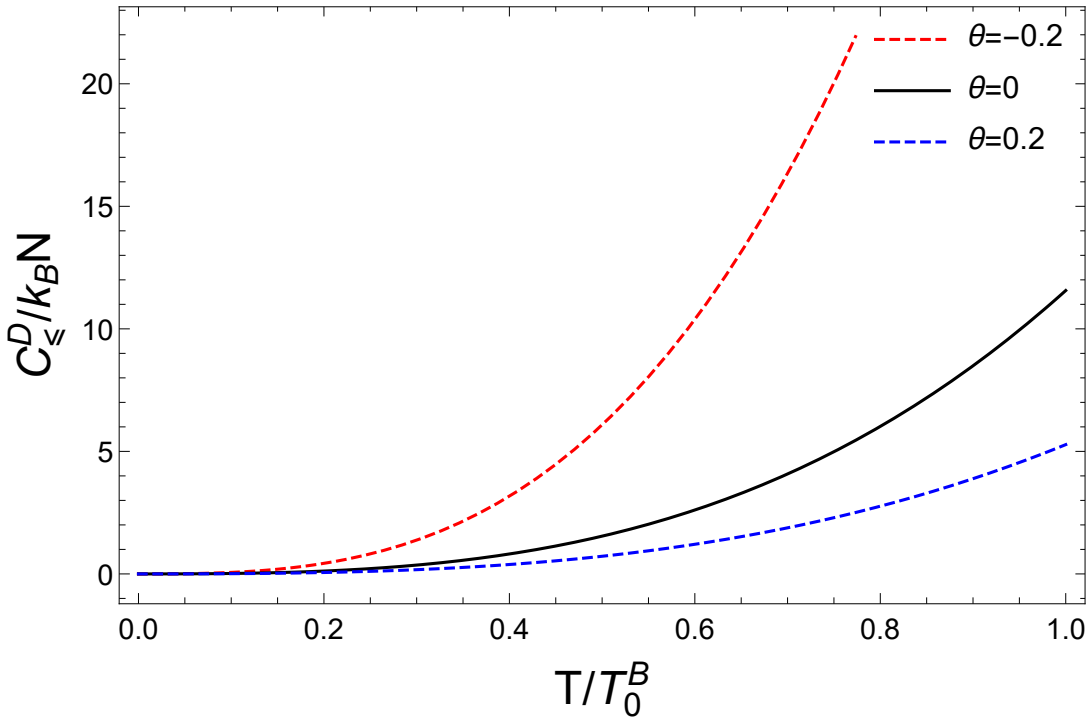

The heat capacity steadily increases with $\frac{T}{T_0^B}$. When θ and N remain constant, $C_{\leq}^{D}/k_B N$ reaches its peak near $T \simeq T_0^B$. When the Wigner parameter is less than zero, the Dunkl heat capacity grows larger than the conventional heat capacity. Conversely, when the Wigner parameter is positive, the conventional heat capacity exceeds the Dunkl heat capacity. On the other hand, for $T > T_c^D$, we obtain after some mathematical manipulation

$$\begin{aligned}\frac{C_{>}^{D}}{Nk_B} &= \frac{3}{2}\frac{g_4(z,\theta)}{\zeta(3)}\left(\frac{T}{T_0^B}\right)^3 + \frac{3\gamma}{2N^{1/3}}\frac{g_3(z,\theta)}{\zeta^{2/3}(3)}\left(\frac{T}{T_0^B}\right)^2 \\ &+ \left[\frac{3}{4}\left(\frac{T}{T_0^B}\right)^4\frac{g_3(z,\theta)}{\zeta(3)} + \frac{\gamma}{N^{1/3}}\frac{g_2(z,\theta)}{\zeta^{2/3}(3)}\left(\frac{T}{T_0^B}\right)^3\right]\frac{T_0^B}{z}\frac{dz}{dT}. \end{aligned} \tag{3.25}$$

Here, we employed the relation

$$\frac{dg_s(z^n)}{dz} = \frac{n}{z}g_{s-1}(z^n). \tag{3.26}$$

We can determine $\frac{1}{z}\frac{dz}{dT}$ using the principle that N remains unchanged. Setting $\frac{dN}{dT} = 0$,

we derive:

$$\frac{T_0^B}{z}\frac{dz}{dT} = -3\frac{T_0^B}{T}.\frac{g_3(z,\theta)}{g_2(z,\theta)}\frac{1+\frac{2\gamma}{3}\frac{\zeta^{1/3}(3)}{N^{1/3}}\frac{g_2(z,\theta)}{g_3(z,\theta)}\frac{T_0^B}{T}}{1+\gamma\frac{\zeta^{1/3}(3)}{N^{1/3}}\frac{g_1(z,\theta)}{g_2(z,\theta)}\frac{T_0^B}{T}}, \tag{3.27}$$

so the Dunkl-specific heat capacity becomes:

$$\begin{aligned}\frac{C_>^D}{Nk_B} &= \frac{3}{2}\frac{g_4(z,\theta)}{\zeta(3)}\left(\frac{T}{T_0^B}\right)^3 + \frac{3\gamma}{2N^{1/3}}\frac{g_3(z,\theta)}{\zeta^{2/3}(3)}\left(\frac{T}{T_0^B}\right)^2 \\ &- 3\frac{g_3(z,\theta)}{g_2(z,\theta)}\left[\frac{3}{4}\left(\frac{T}{T_0^B}\right)^3\frac{g_3(z,\theta)}{\zeta(3)} + \frac{\gamma}{N^{1/3}}\frac{g_2(z,\theta)}{\zeta^{2/3}(3)}\left(\frac{T}{T_0^B}\right)^2\right]\frac{\frac{T}{T_0^B}+\frac{2\gamma}{3}\frac{\zeta^{1/3}(3)}{N^{1/3}}\frac{g_2(z,\theta)}{g_3(z,\theta)}}{\frac{T}{T_0^B}+\gamma\frac{\zeta^{1/3}(3)}{N^{1/3}}\frac{g_1(z,\theta)}{g_2(z,\theta)}}.\end{aligned} \tag{3.28}$$

This expression simplifies significantly in the large N limit, yielding:

$$\frac{C_>^D}{Nk_B} = 12\frac{g_4(z,\theta)}{g_3(z,\theta)} - 9\frac{g_3(z,\theta)}{g_2(z,\theta)}. \tag{3.28}$$

Our equations for $C_<^D$ and $C_>^D$ extend the findings of [7] by including non-zero values of θ. The relationship between Dunkl heat capacity and scaled temperature T/T_c^D for several Wigner parameters is shown in Fig.3.6.

The Dunkl heat capacity displays a λ-shaped curve around the transition point for any chosen value of the Wigner parameter. Here, a λ-shaped profile means the heat capacity curve appears similar to the Greek letter λ, characterized by:

- A sharp rise as temperature approaches the critical temperature from below
- A peak at the transition temperature
- A rapid decrease after passing the critical temperature

This characteristic shape indicates a second-order phase transition in the system. The size of the discontinuous jump represents the difference between the heat capacity values just above and below the critical temperature T_c^D. This jump is significant because:

Figure 3.6 Heat capacity vs. T/T_c^D in the large N limit. The dashed horizontal line is the classical limit for $\theta = 0$

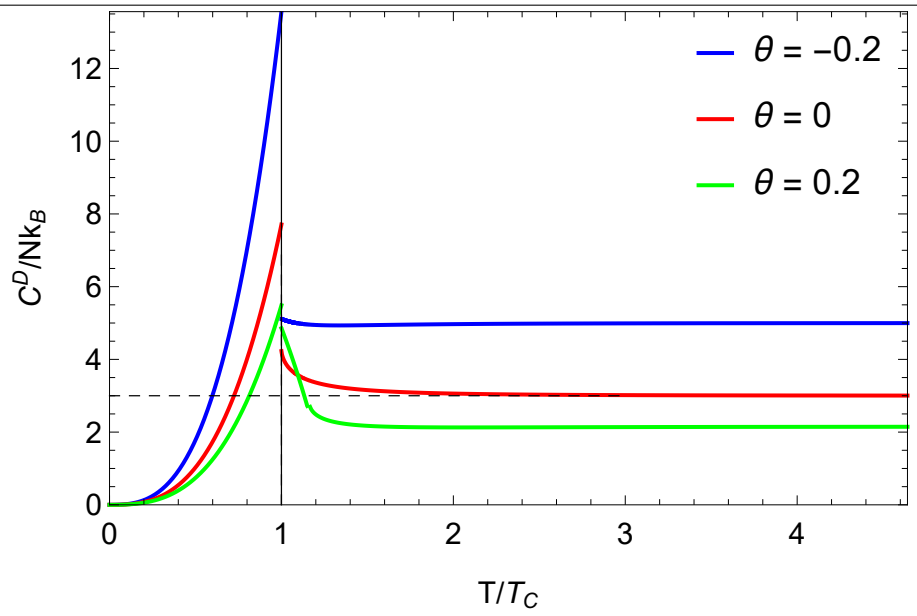

- It quantifies the strength of the phase transition
- It depends on the value of the Wigner parameter θ
- It marks the point where the system transitions from a condensed to a non-condensed phase

The presence of this λ-shaped discontinuity is a universal feature in Bose-Einstein condensation, appearing in both conventional and Dunkl-modified systems. The main difference introduced by the Dunkl formalism is that the magnitude of this jump can be modified by adjusting the Wigner parameter θ, providing an additional degree of control over the phase transition properties of the system.

The discontinuity at this transition can be expressed as

$$\frac{C_{>}^{D} - C_{<}^{D}}{Nk_B} = 9\frac{g_3(1,\theta)}{g_2(1,\theta)} \tag{3.29}$$

reduces to the known value $9\zeta(3)/\zeta(2) \simeq 6.577$ for $\theta = 0$, but differs significantly for a nonzero Wigner parameter. Moreover, the classical (high temperature) limit reads:

$$\left.\frac{C_{>}^{D}}{Nk_B}\right|_{T>>T_c} \simeq \frac{3}{1+2\theta}, \tag{3.30}$$

and we observe, as shown in the figure, that for $\theta < 0$ (resp. $\theta > 0$), the heat capacity is greater (resp. lower) than the standard $\theta = 0$ limit.

The key point here is that one may use these behaviors to estimate an upper bound (or a range) for θ when experimental results do not fully align with the theoretical predictions. In particular, one can analyze the data for slopes near the critical temperature and at high temperatures to better fit experimental observations.

3.2 Dunkl-Bose Gas trapped in quasi-harmonic potential in two-dimension

We consider N particles of an ideal Bose gas trapped in a quasi two-dimensional harmonic oscillator potential, This trap is characterized by frequencies ω_1 and ω_2. The single-particle energies are given by

$$E_n = \hbar\left(\omega_1 n_1 + \omega_2 n_2\right) + E_0, \tag{3.31}$$

where $\hbar$ is the Plank constant, $n_i = 0, 1, 2, 3....(i = 1, 2, 3)$ denotes quantum numbers, and

$$E_0 = \frac{\hbar}{2}\left(\omega_1 + \omega_2\right), \tag{3.32}$$

is the zero-point energy.

To evaluate this sum explicitly, one usually assumes that the level spacing becomes smaller and smaller as $N \longrightarrow \infty$, so that the sum (3.6) can be replaced by an integral weighted by a proper density of states, $\rho(E)$. Hence, we use the conversion relation $\sum_{i\neq 0} \rightarrow \int \rho\left(E\right) d\varepsilon$, to transform equation (3.6) into

$$N_e^D = \int \left(2\frac{\rho(E)}{e^{2\beta E_i} z^{-2} - 1} + (1+2\theta)\frac{\rho(E)}{e^{\beta(1+2\theta)E_i} z^{-(1+2\theta)} + 1} \right) dE. \tag{3.33}$$

We now parameterize the density of states as [70]

$$\rho\left(E\right) = \frac{E}{\left(\hbar\Omega\right)^2}\left[1 + \left(\frac{\bar{\omega}}{\Omega}\right)\frac{\mu}{\left(\hbar\Omega\right)}\right], \tag{3.34}$$

where $\Omega = \left(\omega_1\omega_2\right)^{1/2}$ is the geometric mean of the harmonic potential frequencies, and $\bar{\omega} = \frac{1}{2}\left(\omega_1 + \omega_2\right)$. The integral in equation (3.33) can be easily calculated by changing variables ($X = 2\beta E_i$, etc.). We find

$$N_e^D = \frac{1}{2}\left(\frac{KT}{\hbar\Omega}\right)^2\left[1 + \left(\frac{\bar{\omega}}{\Omega}\right)\frac{\mu}{\left(\hbar\Omega\right)}\right]\left\{g_2\left(z^2\right) - \frac{2}{1+2\theta}g_2\left(-z^{1+2\theta}\right)\right\}.$$

This notation can also be used to write:

$$N = N_0^D + \left(\frac{KT}{\hbar\Omega}\right)^2\left[1 + \left(\frac{\bar{\omega}}{\Omega}\right)\frac{\mu}{\left(\hbar\Omega\right)}\right]g_2\left(z,\theta\right), \tag{3.35}$$

such that

$$g_s\left(z,\theta\right) = g_s(z) + g(-z) - \frac{1}{\left(1+2\theta\right)^{s-1}}g_s\left(-z^{1+2\theta}\right), \qquad \text{with } s = 1, 2..., . \tag{3.36}$$

From the result in (3.35), one can also obtain the Dunkl transition temperature. By setting $N_0 \longrightarrow 0$, and $z = 1$ in equation (3.35)

$$N = (T_c^D)^2\left(\frac{K}{\hbar\Omega}\right)^2 g_2\left(1,\theta\right). \tag{3.37}$$

Hence, the Dunkl-BEC temperature T_c^D can be estimated as

$$T_c^D = \frac{\hbar\Omega}{K}\left[\frac{N}{g_2(1,\theta)}\right]^{1/2}. \tag{3.38}$$

In the limit $\theta \longrightarrow 0$, we find the Bose condensation temperature

$$T_c^D = \frac{\hbar\Omega}{K}\left[\frac{N}{\zeta(2)}\right]^{1/2}.. \tag{3.39}$$

By comparing equation (3.38) and equation (3.39) we get the condensation temperature ratio

$$\frac{T_c^D}{T_c^B} = \left[\frac{\zeta(2)}{g_2(1,\theta)}\right]^{1/2}. \tag{3.40}$$

In Fig. 3.7, we show the change in the condensation temperature ratio as a function of the Wigner parameter in two dimensions.

Figure 3.7 Critical temperature fraction as a function of the Wigner parameter for three and two dimensions

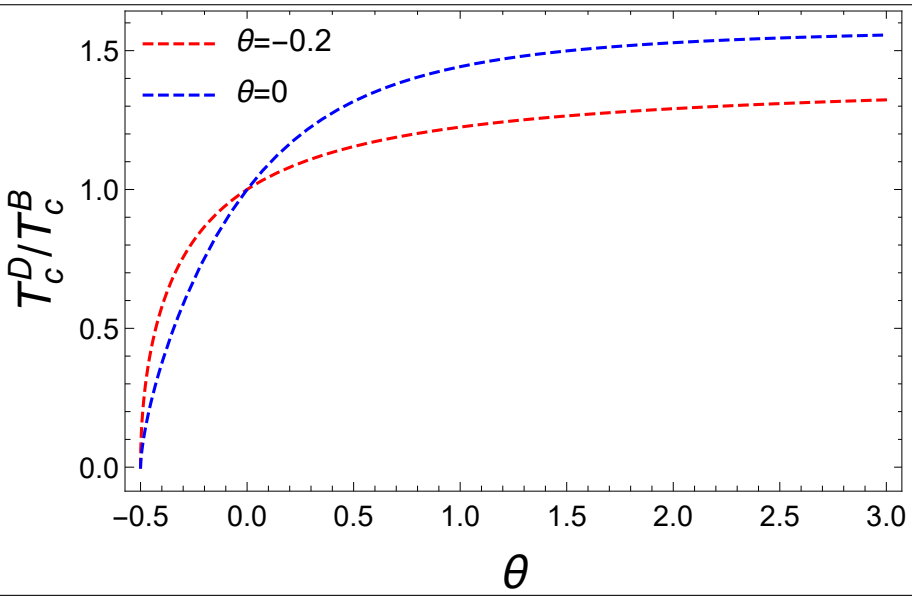

We observe that, in both dimensions, this rate increases monotonically with the increasing Wigner parameter. However, in two dimensions, the Dunkl-condensation temperature ratio is greater in the region where the Wigner parameter is negative, whereas in three dimensions, the ratio becomes larger when the Wigner parameter is positive.

Below the transition temperature the non-condensed particle number, $N - N_0^D$, where N_0^D is the Dunkl-condensate number, is still given by the right side of equation (3.2) with $z = 1$, from which we find:

$$\frac{N_0^D}{N} = 1 - \left[1 + \left(\frac{\bar{\omega}}{\Omega}\right) \frac{\mu}{(\hbar\Omega)}\right] \left(\frac{T}{T_c^D}\right)^2 . \tag{3.41}$$

Now, we derive the thermodynamic quantities of the system. First, we express the internal energy, U, according to the semi-classical formula

$$U(T) = \sum_i E_i N_i. \tag{3.42}$$

By converting the sum into an integral, we obtain the expression of the internal energy as

$$U^D = 2KT \left(\frac{KT}{\hbar\Omega}\right)^2 \left[1 + \left(\frac{\bar{\omega}}{\Omega}\right) \frac{\mu}{(\hbar\Omega)}\right] g_3(z, \theta) . \tag{3.43}$$

Now we proceed to calculate the heat capacity of the system. We start with the thermodynamic definition:

$$C = \left.\frac{dU}{dT}\right|_{N,\Omega} . \tag{3.44}$$

Within the grand canonical ensemble, the heat capacity must be determined separately in the two regimes: $T < T_c$ (condensate phase) and $T > T_c$ (gas phase). First, for the condensate phase, the functions in equation (3.36) become independent of temperature. Thus, a straightforward calculation yields:

$$\frac{C_{<}^{D}}{NK}=\frac{3}{2}\left(\frac{KT}{\hbar\Omega}\right)^{2}\left\{g_{3}(1)-\frac{4}{(1+2\theta)^{2}}g_{3}(-1)\right\}. \tag{3.45}$$

Using equations (3.36) and (3.38), the heat capacity $C_{<}^{D}$ can be written as:

$$\frac{C_{<}^{D}}{NK}=6\frac{g_{3}(1,\theta)}{g_{2}(1,\theta)}\left(\frac{T}{T_{c}^{D}}\right)^{2}. \tag{3.46}$$

In Fig. 3.8 we plot the heat capacity equation (3.46) as a function of T/T_{c}^{D} for various θ.

Figure 3.8 Heat capacity of a very large number of non interacting Bosons versus the fraction of the reduced critical temperature

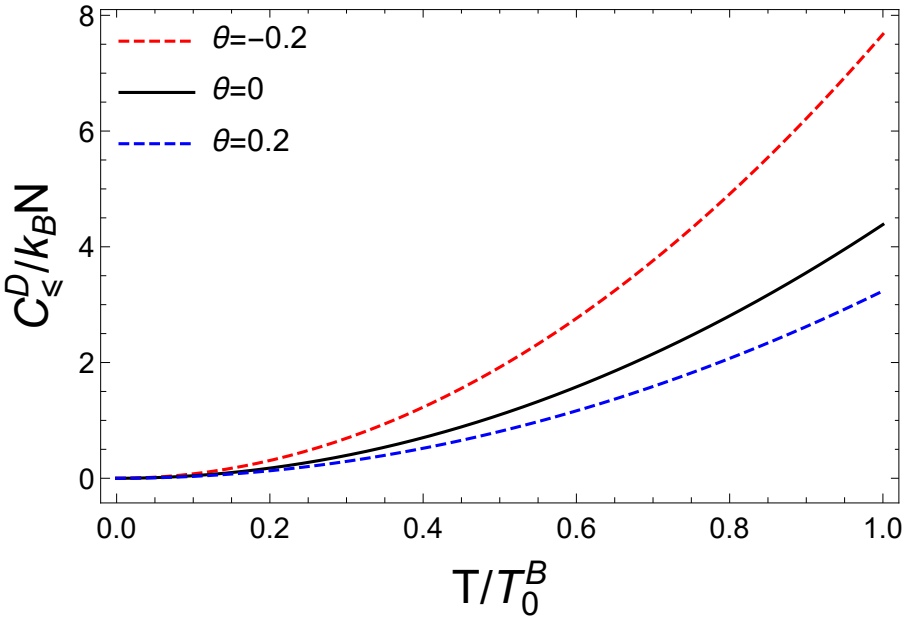

Finally, the heat capacity for the gas phase $T>T_{c}$ is more involved. Thus, it is worthwhile to utilize the polylogarithmic identity:

$$\frac{d}{dx}g_{s}\left(x^{n}\right)=\frac{n}{x}g_{s-1}\left(x^{n}\right). \tag{3.47}$$

By substituting equation (3.43) in equation (3.44), we obtain:

$$\frac{C_{>}^{D}}{NK} = \xi_{>}^{D} + \left\{ 2\frac{g_2(z,\theta)}{g_2(1,\theta)} \left[1 + \left(\frac{\bar{\omega}}{\Omega}\right) \frac{\mu}{(\hbar\Omega)} \right] \left(\frac{T}{T_c^D}\right)^3 \right\} \frac{T_c^D}{z} \frac{dz}{dT}, \tag{3.48}$$

where

$$\xi_{>}^{D} = 12\frac{g_3(z,\theta)}{g_2(1,\theta)} \left(\frac{T}{T_c^D}\right)^2 \left[1 + \left(\frac{\bar{\omega}}{\Omega}\right) \frac{\mu}{(\hbar\Omega)} \right]. \tag{3.49}$$

By using the conservation of particle number, i.e.,

$$\frac{d}{dT}N = 0. \tag{3.50}$$

in equation (3.35), we can derive the expression of the T-derivative of the fugacity z, as follows:

$$\frac{1}{z}\frac{dz}{dT} = \frac{-2}{T}.\frac{g_2(z,\theta)}{g_1(z,\theta)}. \tag{3.51}$$

Chapter 4

Condensation of ideal Dunkl-Bose Gas in power-Law Traps

We have conducted a series of studies examining ideal Bose gas systems and their condensates using the Dunkl formalism. Our research began with investigating a basic ideal Bose gas system in [73], where we showed how the Dunkl formalism affects the temperature at which condensation occurs. We then broadened our research in [74] to understand how gravity influences Dunkl-Bose-Einstein condensation (Dunkl-BEC) in both two and three dimensions. Following this, in [75], we examined Dunkl-BEC in an isotropic harmonic oscillator potential, specifically studying how the Dunkl modification changes thermal properties.

The study of Bose-Einstein condensation in low-dimensional systems gained significant momentum following Bagnato's pioneering work in 1991 [21]. His research was motivated by several key factors: First, the possibility of achieving BEC in lower dimensions offered new ways to study quantum phenomena that are difficult to observe in three dimensions. Second, low-dimensional systems presented unique opportunities to investigate the role of quantum fluctuations and collective excitations. Third, the development of sophisticated trapping techniques made it experimentally feasible to create quasi-one and quasi-two-dimensional condensates. These motivations have led to numerous theoretical

and experimental studies exploring the rich physics of low-dimensional quantum gases, making our current investigation particularly relevant to this ongoing field of research.

In this fourth study, we examine a different and important type of trapping potential: the power-law potential. Our main goal is to understand how the Dunkl formalism affects the condensate's behavior in one and two dimensions. This investigation is particularly significant as power-law potentials offer a more general framework for studying trapped Bose gases, potentially revealing new physical insights about the interplay between the trapping force and quantum statistics under the Dunkl modification.

4.1 The density of states for power-law potential

Let us begin by examining a one-dimensional system with a potential described by:

$$U(x) = U_0 \left(\frac{|x|}{L} \right)^{\eta}, \tag{4.1}$$

where $\eta < 2$. In this formula, U_0 is a fixed value, x shows the location in the system, L gives a basic length measure, and η is the number that controls how the potential changes. For this situation, we can write the density of states as

$$\rho(\epsilon) = \frac{\sqrt{2m}}{h} \int_{-l(\epsilon)}^{l(\epsilon)} \frac{1}{\sqrt{\epsilon - U(x)}} dx, \tag{4.2}$$

where $l(\epsilon) = L \left(\frac{\epsilon}{U_0} \right)^{1/\eta}$. After applying a suitable change of variable, equation (4.2) yields the following expression:

$$\rho(\epsilon) = \frac{2}{\eta} \frac{\sqrt{2m}}{h} L \frac{\epsilon^{\frac{1}{\eta} - \frac{1}{2}}}{U_0^{\frac{1}{\eta}}} F(\eta), \tag{4.3}$$

where

$$F(\eta) \quad = \int_0^1 \frac{y^{\frac{1}{\eta}-1}}{\sqrt{1-y}} dy = \frac{\sqrt{\pi}\Gamma(1/2)}{\Gamma(1/\eta+1/2)} \tag{4.4}$$

Next, let us shift our focus to a two-dimensional system. In this case, the most general potential can be expressed as:

$$U(x,y) = U_1 \left(\frac{x}{b}\right)^m + U_2 \left(\frac{y}{c}\right)^n. \tag{4.5}$$

For simplicity, we assume that the potential is isotropic, so equation (4.5) becomes:

$$U(r) = U_0 \left(\frac{r}{a}\right)^\eta. \tag{4.6}$$

In analogy to the previous case, the density of states in two dimensions can be written as:

$$\rho(\epsilon) = \frac{2\pi^2 m a^2}{h^2} \left[\frac{\epsilon}{U_0}\right]^{\frac{2}{\eta}}. \tag{4.7}$$

4.2 Dunkl-Bose Gas in One-Dimensional

Here, we study how the Bose gas behaves when using Dunkl's approach. In this framework, we can write the total number of particles, in the limit of very large systems, as:

$$N = N_0^D + \int_0^\infty d\epsilon \rho(\epsilon) \left[\frac{2}{e^{2\beta\epsilon_i} z^{-2} - 1} + \frac{1+2\theta}{e^{\beta(1+2\theta)\epsilon_i} z^{-(1+2\theta)} + 1}\right]. \tag{4.8}$$

When we put equation (4.2) into equation (4.8), we get the total number of particles as [71]

$$N = N_0^D + \frac{2}{\eta} \frac{\sqrt{2m}}{h} L \frac{F(\eta)}{U_0^{\frac{1}{\eta}}} (KT)^{\frac{1}{\eta}+\frac{1}{2}} \Gamma\left(\frac{1}{2}+\frac{1}{\eta}\right) g_{\frac{1}{2}+\frac{1}{\eta}}(z,\theta), \tag{4.9}$$

where

$$g_{\frac{1}{2}+\frac{1}{\eta}}(z,\theta) = g_{\frac{1}{2}+\frac{1}{\eta}}(z) + g_{\frac{1}{2}+\frac{1}{\eta}}(-z) - (1+2\theta)^{\frac{1}{2}-\frac{1}{\eta}}\, g_{\frac{1}{2}+\frac{1}{\eta}}\left(-z^{1+2\theta}\right), \tag{4.10}$$

is the Bose-Dunkl function in its general form. When θ approaches zero, we get back the usual results that we find in the standard case:

$$N = N_0 + \frac{2}{\eta}\frac{\sqrt{2m}}{h} L \frac{F(\eta)}{U_0^{\frac{1}{\eta}}} (KT)^{\frac{1}{\eta}+\frac{1}{2}}\, \Gamma\left(\frac{1}{2}+\frac{1}{\eta}\right) g_{\frac{1}{2}+\frac{1}{\eta}}(z). \tag{4.11}$$

Based on equation (4.9), it is possible to derive the Dunkl transition temperature. This can be achieved by setting $N_0 = 0$ and $z = 1$ in equation (4.9). Consequently, the estimated condensation temperature, denoted as T_c^D, is given by:

$$\left(KT_c^D\right) = \left[\frac{\eta}{2}\frac{Nh}{\sqrt{2m}}\frac{U_0^{\frac{1}{\eta}}}{F(\eta)}\frac{1}{\Gamma\left(\frac{1}{2}+\frac{1}{\eta}\right) g_{\frac{1}{2}+\frac{1}{\eta}}(1,\theta)}\right]^{\frac{2\eta}{\eta+2}}. \tag{4.12}$$

To compare the normal system within standard algebra with the one used in Dunkl-deformed algebra, we plot the critical temperature function (in qualitative units) in two stages. First, we show how these quantities change with η for several values of the Wigner parameter θ in Figure 4.1.

Figure 4.1 The one dimensional Dunkl critical temperature versus the potential coefficient for different values of the Wigner parameter.

Out[45]=

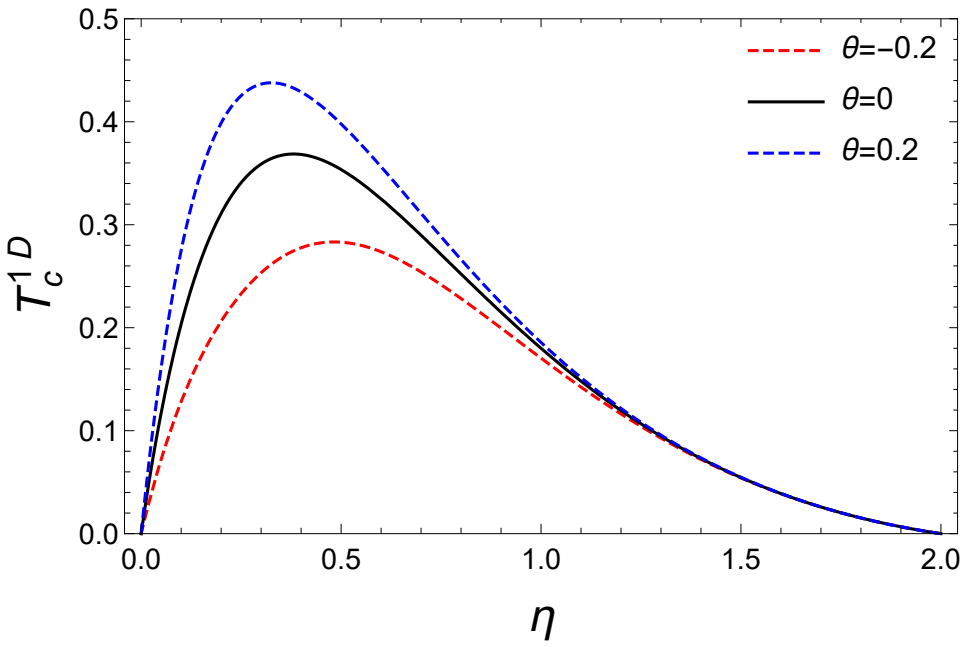

We observe that for $\eta > 1$, the deformed Dunkl algebra aligns with the standard algebra, but for $0 < \eta < 1$, Dunkl's algebra yields different critical temperature values. Specifically, when the Wigner coefficient is negative, the critical temperature is lower than the standard one, while for positive values of the Wigner coefficient, the critical temperature exceeds the standard value. It is also noteworthy that for $\eta > 2$, the system becomes complex. Fig. 4.2 shows how the transition temperature changes with varying Wigner parameter θ at several values of η

Figure 4.2 The one dimensional Dunkl critical temperature vs. the Wigner parameter θ for varying η.

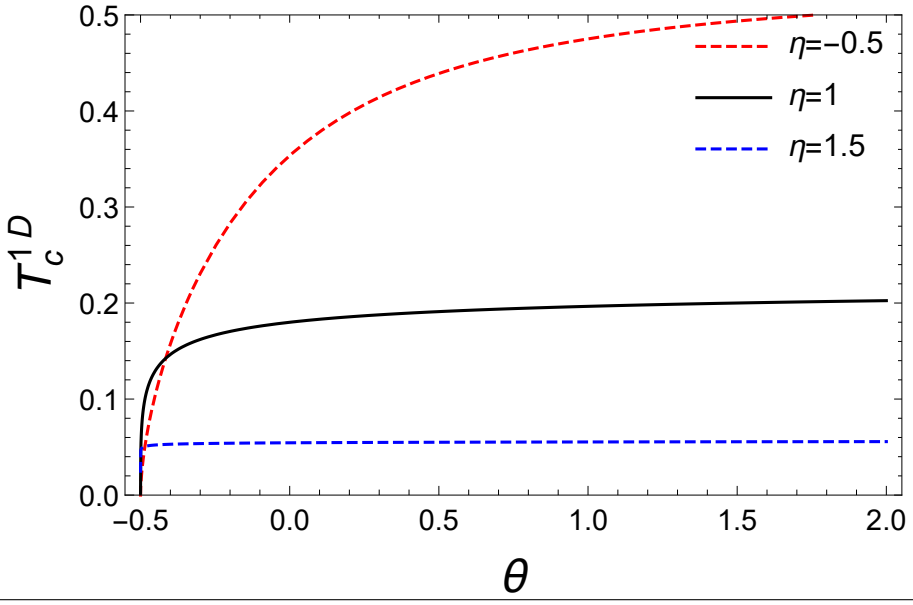

We observe that the curves reach steady states when η gets closer to 2. We then study how many particles occupy the lowest energy level at different temperatures. From equations (4.11) and (4.12), we calculate this ratio:

$$\frac{N_0^D}{N} = 1 - \left(\frac{T}{T_c^D}\right)^{\frac{1}{2}+\frac{1}{\eta}}. \tag{4.13}$$

For $T < T_c^D$, we can re-express this as:

$$\frac{N_0^D}{N} = 1 - \left\{1 + \frac{g_{\frac{1}{\eta}+\frac{1}{2}}(-1)}{g_{\frac{1}{\eta}+\frac{1}{2}}(1)}\left[1 - (1+2\theta)^{\frac{1}{2}-\frac{1}{\eta}}\right]\right\}\left(\frac{T}{T_c^B}\right)^{\frac{1}{2}+\frac{1}{\eta}}. \tag{4.14}$$

In the limit $\theta \to 0$, equation (4.14) reduces to the standard case:

$$\frac{N_0^D}{N} = 1 - \left(\frac{T}{T_c^B}\right)^{\frac{1}{2}+\frac{1}{\eta}}. \tag{4.15}$$

Fig. 4.3 and Fig. 4.4 illustrate the condensate fraction as a function of normalized temperature for $\eta = 0.5$ and $\eta = 1.5$.

Figure 4.3 The ground state population versus $\frac{T}{T_c^B}$ for different values of the Wigner parameter and for $\eta = 0.5$.

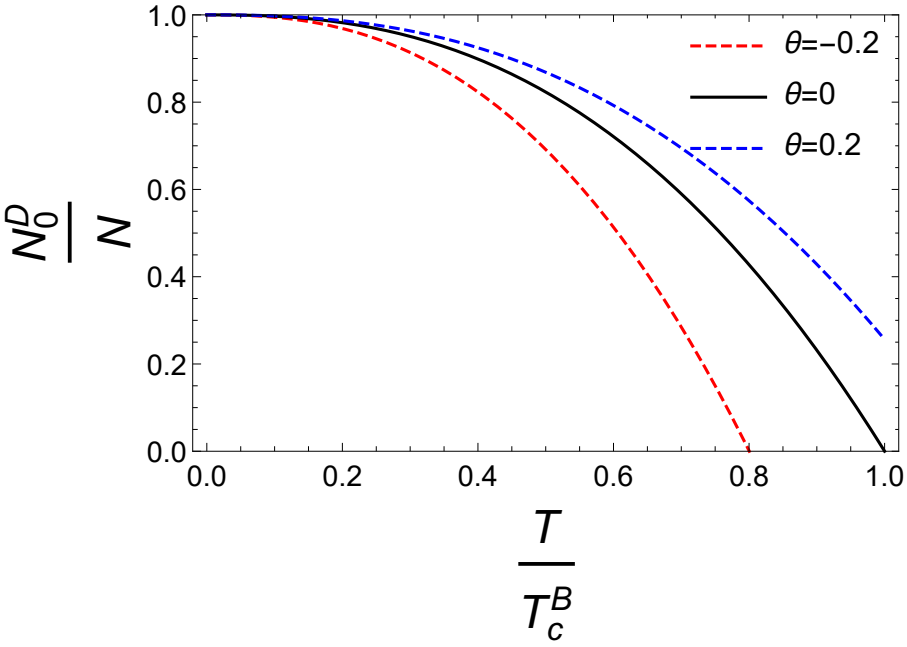

Figure 4.4 The ground state population versus $\frac{T}{T_c^B}$ for different values of the Wigner parameter and for $\eta = 1.2$.

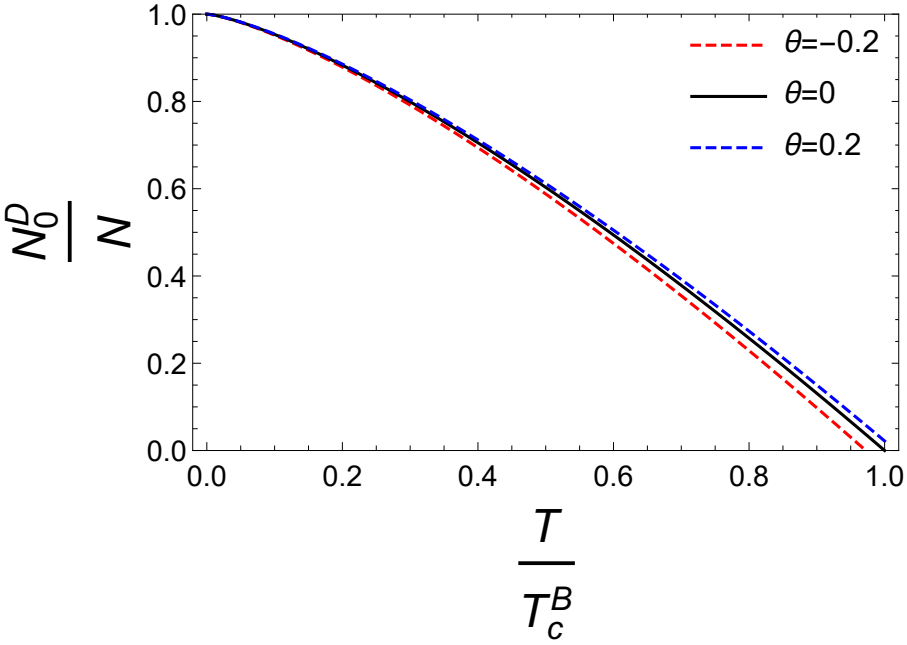

We observ that the ground state population decreases monotonically. The Wigner parameter influences this rate of decrease, either enhancing or diminishing it depending on whether the parameter is positive or negative. This effect becomes more pronounced as the temperature approaches the critical value.

The analysis now turns to the thermal behavior of a Bose gas in a power-law trap using Dunkl statistics. We start by calculating the system's energy through:

$$U^D = \sum_i \varepsilon_i N_i^D, \tag{4.16}$$

After converting the sum into an integral, the internal energy becomes:

$$U^D = \mathcal{U}\left[2^{-\left(\frac{1}{\eta}+\frac{1}{2}\right)} g_{\frac{1}{\eta}+\frac{3}{2}}(z^2) - \frac{1}{(1+2\theta)^{\frac{1}{\eta}-\frac{1}{2}}} g_{\frac{1}{\eta}+\frac{3}{2}}(-z^{1+2\theta})\right]. \tag{4.17}$$

where

$$\mathcal{U} = \frac{2\sqrt{2mL^2}F(\eta)}{\eta h U_0^{\frac{1}{\eta}}}\Gamma\left(\frac{1}{\eta}+\frac{3}{2}\right)(KT)^{\frac{1}{\eta}+\frac{3}{2}}. \tag{4.18}$$

The heat capacity in the regime $T < T_c$ is given by

$$C_<^D = \frac{2}{\eta}\frac{\sqrt{2m}}{h} L \frac{K\left(\frac{1}{\eta}+\frac{3}{2}\right)}{U_0^{\frac{1}{\eta}}} F(\eta)\Gamma\left(\frac{1}{\eta}+\frac{3}{2}\right)(KT)^{\frac{1}{\eta}+\frac{1}{2}}\, g_{\frac{1}{\eta}+\frac{3}{2}}(1,\theta). \tag{4.19}$$

In the regime $T > T_c$, using the property

$$\frac{dg_s(x^n)}{dx} = \frac{n}{x} g_{s-1}(x^n), \tag{4.20}$$

we find:

$$C_>^D = \mathcal{C}_{>1} + \mathcal{C}_{>2}\frac{1}{z}\frac{\partial z}{\partial T}, \tag{4.21}$$

where

$$\mathcal{C}_{>1} = \frac{2}{\eta}\frac{\sqrt{2m}}{h}L\frac{K\left(\frac{1}{\eta}+\frac{3}{2}\right)}{U_0^{\frac{1}{\eta}}}F(\eta)\Gamma\left(\frac{1}{\eta}+\frac{3}{2}\right)(KT)^{\frac{1}{\eta}+\frac{1}{2}}\, g_{\frac{1}{\eta}+\frac{3}{2}}(z,\theta), \tag{4.22}$$

$$\mathcal{C}_{>2} = \left[\frac{2}{\eta}\frac{\sqrt{2m}}{h}L\frac{1}{U_0^{\frac{1}{\eta}}}F(\eta)\Gamma\left(\frac{1}{\eta}+\frac{3}{2}\right)(KT)^{\frac{1}{\eta}+\frac{3}{2}}\, g_{\frac{1}{\eta}+\frac{1}{2}}(z,\theta)\right]. \tag{4.23}$$

We then used the fact:

$$\frac{df}{dT} = \frac{df}{dz}\frac{dz}{dT}. \tag{4.24}$$

To calculate the quantity $\frac{1}{z}\frac{\partial z}{\partial T}$, we assume $N_0 = 0$ and fix all the parameters, leading to:

$$N = \mathcal{C}T^{\frac{1}{\eta}+\frac{1}{2}} g_{\frac{1}{\eta}+\frac{1}{2}}(z,\theta), \tag{4.25}$$

then

$$\frac{\partial g_{\frac{1}{\eta}+\frac{1}{2}}(z,\theta)}{g_{\frac{1}{\eta}+\frac{1}{2}}(z,\theta)} = -\left(\frac{1}{\eta}+\frac{1}{2}\right).\frac{\partial T}{T}, \tag{4.26}$$

so, we can write

$$\frac{\partial g_{\frac{1}{\eta}+\frac{1}{2}}(z,\theta)}{\partial T} = -\frac{\left(\frac{1}{\eta}+\frac{1}{2}\right)}{T} g_{\frac{1}{\eta}+\frac{1}{2}}(z,\theta), \tag{4.27}$$

and

$$\frac{\partial g_{\frac{1}{\eta}+\frac{1}{2}}(z,\theta)}{\partial z} = \frac{1}{z} g_{\frac{1}{\eta}-\frac{1}{2}}(z,\theta). \tag{4.28}$$

by combining equations (1.79) and (4.28), we find

$$\frac{1}{z}\frac{\partial z}{\partial T} = -\frac{\left(\frac{1}{\eta}+\frac{1}{2}\right)}{T}\frac{g_{\frac{1}{\eta}+\frac{1}{2}}(z,\theta)}{g_{\frac{1}{\eta}-\frac{1}{2}}(z,\theta)}. \tag{4.29}$$

Finally, we write the expression of the heat capacity as:

$$C_{>}^{D} = \mathcal{C}_{>1} + \mathcal{C}_{>2}\left(-\frac{\left(\frac{1}{\eta}+\frac{1}{2}\right)}{T}\frac{g_{\frac{1}{\eta}+\frac{1}{2}}(z,\theta)}{g_{\frac{1}{\eta}-\frac{1}{2}}(z,\theta)}\right). \tag{4.30}$$

4.3 Dunkl-Bose Gas in Two-Dimensional

In this section, our focus shifts to the two-dimensional case. We will refrain from reiterating the calculation details, as they are essentially similar to those in the previous section. Therefore, the total number of particles in this case can be expressed as follows:

$$N = N_0 + \frac{2\pi^2 ma^2}{h^2}\frac{1}{U_0^{\frac{2}{\eta}}}(KT)^{\frac{2}{\eta}+1}\,\Gamma\left(\frac{2}{\eta}+1\right)g_{\frac{2}{\eta}+1}(z,\theta), \tag{4.31}$$

where

$$g_{\frac{2}{\eta}+1}(z,\theta) = g_{\frac{2}{\eta}+1}(z) + g_{\frac{2}{\eta}+1}(-z) - (1+2\theta)^{-\frac{2}{\eta}}\,g_{\frac{2}{\eta}+1}(-z^{1+2\theta}). \tag{4.32}$$

Using the same method as in the one-dimensional case ($d = 1$), we now calculate the Dunkl-critical temperature:

$$\left(KT_c^D\right) = \left[\frac{Nh^2}{2\pi^2 ma^2}U_0^{\frac{2}{\eta}}\frac{1}{\Gamma\left(\frac{2}{\eta}+1\right)g_{\frac{2}{\eta}+1}(z,\theta)}\right]^{\frac{\eta}{2+\eta}}. \tag{4.33}$$

In Fig. 4.5 and Fig. 4.6, we illustrate the Dunkl condensation (or critical) temperature in two dimensions.

Figure 4.5 The two dimensional Dunkl critical temperateur vs the potential coefficient for differnts values of the wigner parametre

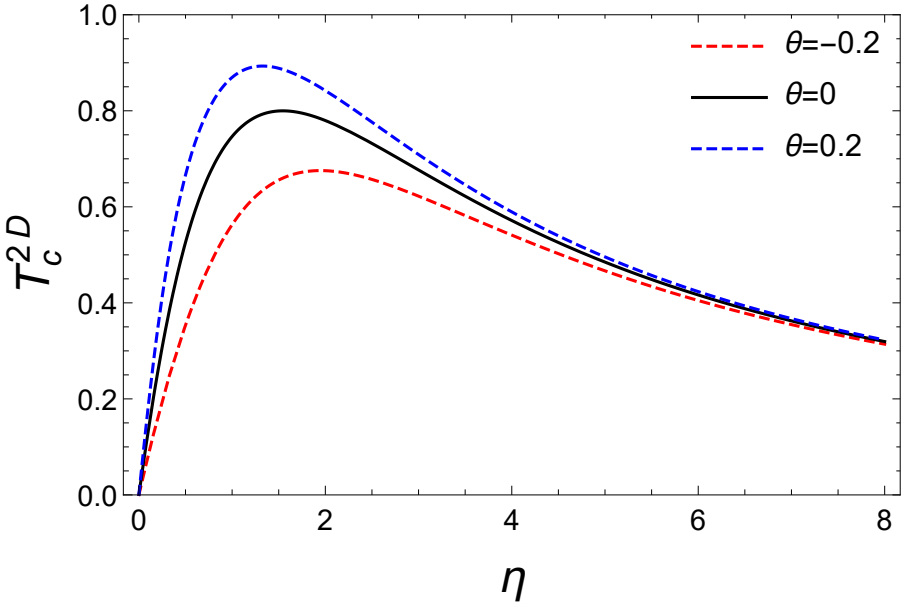

Figure 4.6 The two dimensional Dunkl critical temperateur vs the potential coefficient for differnts values of the wigner parametre

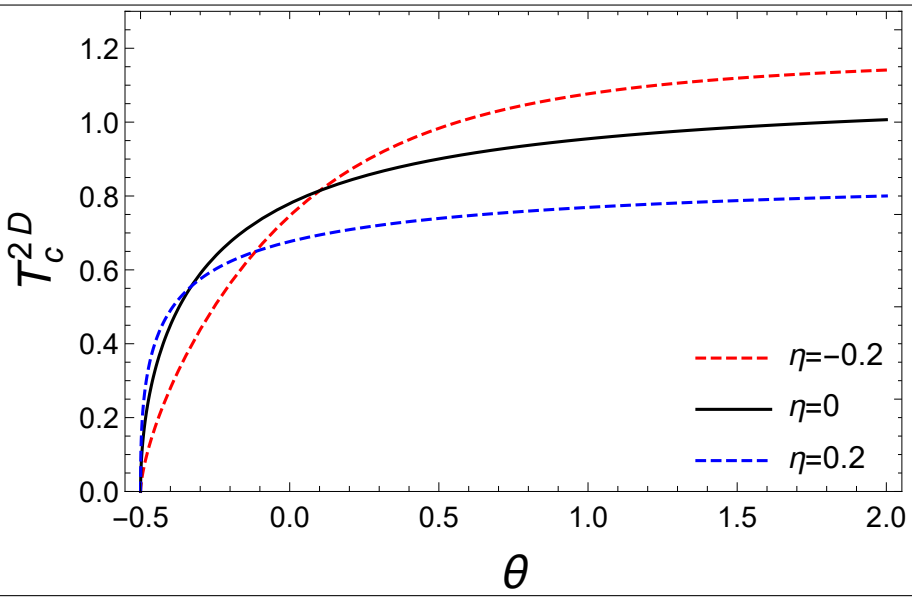

Fig. 4.5 shows how the Dunkl-BEC temperature T_c^D changes with the potential parameter at different Wigner parameter values. The patterns in two dimensions are similar to the one-dimensional case, with T_c^D reaching a maximum before rising or falling based on the

Wigner parameter value. However, the two-dimensional case differs in that Dunkl-BEC can occur for any positive, finite value of η, without restrictions. Fig. 4.6 illustrates how T_c^D varies with the Wigner parameter for three different potential parameter values. The impact of the Wigner parameter changes based on whether it is positive or negative, and its effects also depend on the chosen potential parameter values.
For temperatures below T_c^D, the fraction of particles in the lowest energy state $\frac{N_0^D}{N}$ takes the form:

$$\frac{N_0^D}{N} = 1 - \left\{ 1 + \frac{g_{\frac{2}{\eta}+1}(-1)}{g_{\frac{2}{\eta}+1}(1)} \left[1 - (1+2\theta)^{-\frac{2}{\eta}} \right] \right\} \left(\frac{T}{T_c^B} \right)^{\frac{2}{\eta}+1} . \tag{4.34}$$

When we set the Dunkl parameter to zero, the fraction of condensed particles becomes

$$\frac{N_0^D}{N} = 1 - \left(\frac{T}{T_c^B} \right)^{\frac{2}{\eta}+1} . \tag{4.35}$$

Figures 4.7 and 4.8 show how the proportion of condensed particles changes with relative temperature. We plot this for three different Wigner parameter values to demonstrate how the Dunkl framework affects the system.

Figure 4.7 : The ground state population versus $\frac{T}{T_c^B}$ for different values of the Wigner parameter and for $\eta = 1$

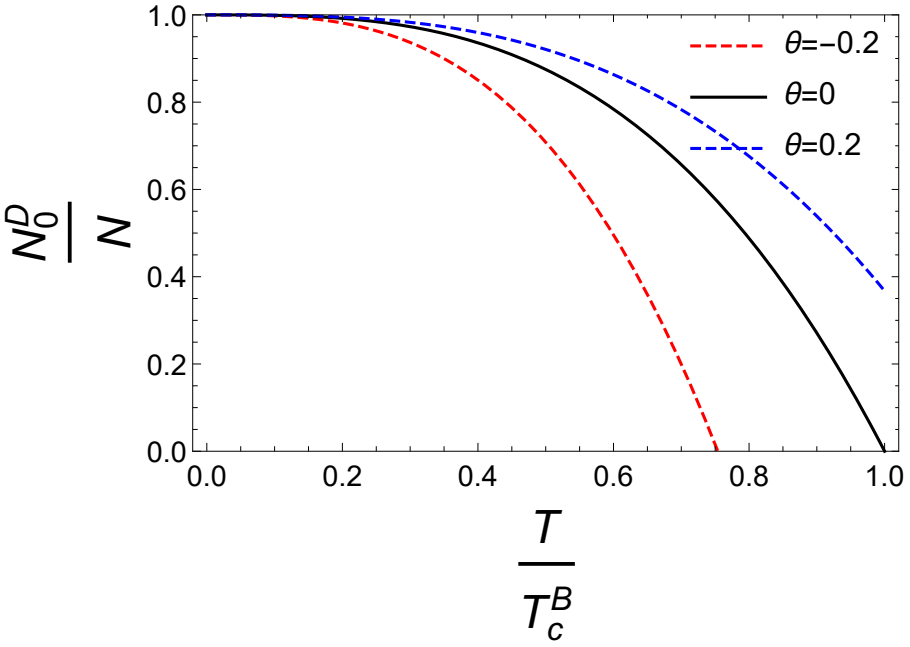

Figure 4.8 : The ground state population versus $\frac{T}{T_c^B}$ for different values of the Wigner parameter and for $\eta = 3$

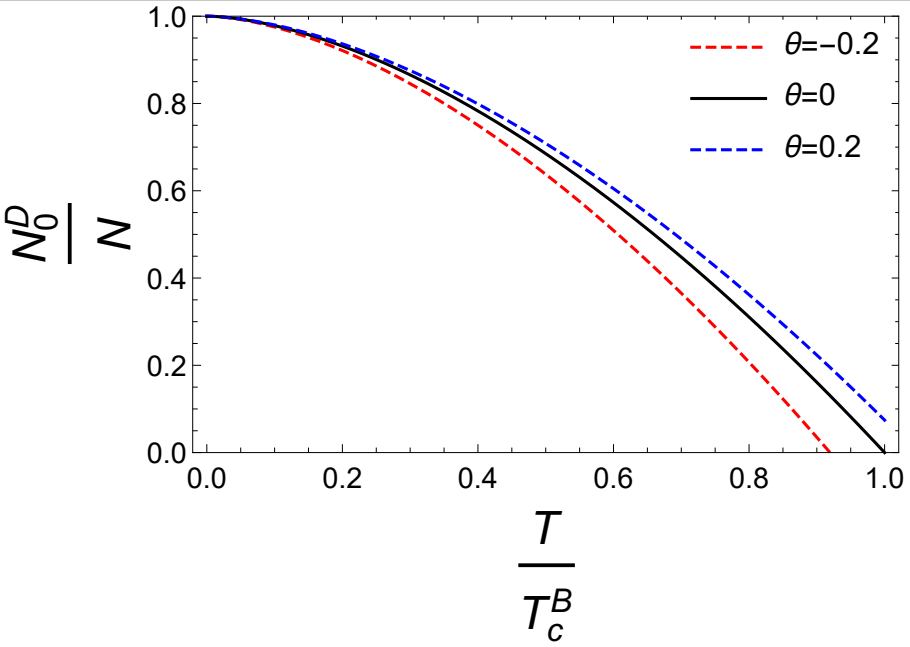

We note that the characteristic effect is the same as in the one-dimensional case.

Similar to the previous section, we finally derive the Dunkl corrected internal energy. To this end, we use equation (4.16) and convert the sum into an integral. After some algebraic manipulation, we obtain the internal energy function in the form:

$$U^D = \frac{2\pi^2 ma^2}{\eta^2 U_0^{\frac{2}{\eta}}}\Gamma\left(\frac{2}{\eta}+2\right)(KT)^{\frac{2}{\eta}+2}\left\{2^{-\left(\frac{2}{\eta}+1\right)}g_{\frac{2}{\eta}+2}(z^2) - \frac{1}{(1+2\theta)^{\frac{2}{\eta}-1}}g_{\frac{2}{\eta}+2}(-z^{1+2\theta})\right\}. \tag{4.35}$$

By using the same methodology as the section 1 we find the following results for $T < T_c$:

$$C_<^D = \frac{2\pi^2 ma^2}{\eta^2 U_0^{\frac{2}{\eta}}}\Gamma\left(\frac{2}{\eta}+2\right)K\left(\frac{2}{\eta}+2\right)(KT)^{\frac{2}{\eta}+1}\,g_{\frac{2}{\eta}+2}(1,\theta). \tag{4.36}$$

Finally

$$C_>^D = C_{>3}^D + C_{>4}^D\left(-\frac{\frac{2}{\eta}+1}{T}\frac{g_{\frac{2}{\eta}+1}(z,\theta)}{g_{\frac{2}{\eta}}(z,\theta)}\right). \tag{4.37}$$

where

$$C_{>3}^D = \frac{2\pi^2 ma^2}{\eta^2 U_0^{\frac{2}{\eta}}}\Gamma\left(\frac{2}{\eta}+2\right)K\left(\frac{2}{\eta}+2\right)(KT)^{\frac{2}{\eta}+1}\,g_{\frac{2}{\eta}+2}(z,\theta), \tag{4.38}$$

$$C_{>4}^D = 2\frac{2\pi^2 ma^2}{\eta^2 U_0^{\frac{2}{\eta}}}\Gamma\left(\frac{2}{\eta}+2\right)(KT)^{\frac{2}{\eta}+2}\,g_{\frac{2}{\eta}+1}(z,\theta). \tag{4.39}$$

In this chapter, we have studied the behavior of a Dunkl-deformed ideal Bose gas confined within a one- and two-dimensional power-law potential. Using the Dunkl formalism, we derived the critical temperature and condensate fraction. We find that the Dunkl parameters significantly modify the condensation temperature and the condensate fraction. Our results generalize the findings of [73,75] by incorporating the effects of a more general trapping potential. The differences between one- and two-dimensional systems are discussed, emphasizing how dimensionality influences the condensation phenomena. These findings open up possibilities for further exploration into the thermodynamic properties of Dunkl-deformed quantum gases.

Conclusion

In this thesis, we explored the domain of Bose gases within the framework of deformed algebra, with a specific focus on Wigner-Dunkl quantum mechanics. The study began with a foundational examination of Wigner algebra and its generalization to Wigner-Dunkl quantum mechanics. This framework extends conventional quantum mechanical structures, allowing for a broader range of applications and deeper insights into physical phenomena.

We then investigated the properties of an ideal Bose gas within the Dunkl formalism. The research presented in "Ideal Bose Gas and Blackbody Radiation in the Dunkl Formalism" highlighted how the introduction of the Dunkl operator modifies the traditional descriptions of an ideal Bose gas. These modifications affect key thermodynamic properties such as specific heat and entropy, and lead to a shift in the Bose-Einstein condensation temperature. Additionally, the study examined the spectral distribution of blackbody radiation, showing that the Dunkl operator induces deviations from the Planck distribution, potentially explaining certain anomalies observed in experimental blackbody radiation spectra.

Moreover, insights from our recent preprints further extend the application of the Dunkl formalism to more complex systems and phenomena. The first preprint delves into the statistical mechanics of a Bose gas influenced by the Dunkl operator, revealing novel statistical behaviors, such as modified particle distribution functions and shifts in the critical temperatures for phase transitions. The second preprint explores the implications of Dunkl deformation on quantum gases confined in various potential traps, illustrating significant changes in their density profiles and energy spectra. These studies underscore the robustness and versatility of the Dunkl approach, suggesting its relevance to a wide array of physical systems beyond traditional quantum gases.

The research conducted in this thesis opens several promising avenues for future ex-

ploration. The deformation of algebraic structures considered in Wigner-Dunkl quantum mechanics provides fertile ground for discovering new physical insights and for developing more advanced theoretical models. Potential directions for future studies include:

- We apply the Dunkl formalism to interacting Bose gases and investigate the resultant modifications in their phase transitions and critical behavior.
- Extending the Dunkl approach to fermionic systems and examining its implications for quantum statistics and condensed matter physics.

In conclusion, this thesis has demonstrated the power and potential of deformed algebraic structures in advancing our understanding of quantum statistical systems. By integrating the Dunkl formalism into the study of Bose gases, we have uncovered novel thermodynamic properties and established a foundation for future theoretical and experimental research. The findings presented not only contribute to the field of quantum mechanics, but also pave the way for interdisciplinary applications and deeper explorations into the fundamental nature of quantum systems.

APPENDICES

This section contains the supplementary appendices to the thesis.

A One-dimensional Dunkl-Schrödinger equation

This appendix provides comprehensive step-by-step derivations for the key equations presented in the first chapter. We focus particularly on establishing the connections between recurrence relations and hypergeometric, Bessel and H_N functions.

Let's start with the cas $n = 0$, thus we can find

$$\begin{cases} a_1^+ &= -\frac{2mE_+}{(2)(1+2\theta)}a_0^+ \\ a_2^+ &= -\frac{2mE_+}{(4)(3+2\theta)}a_1^+ = \frac{(2mE_+)^2}{(2)(1+2\theta)(4)(3+2\theta)}a_0^+ \\ a_3^+ &= -\frac{2mE_+}{(6)(5+2\theta)}a_2^+ = \frac{-(2mE_+)^3}{(2)(1+2\theta)(4)(3+2\theta)(6)(5+2\theta)}a_0^+ \end{cases}, \tag{A.0}$$

this pattern gives:

$$a_n^+ = \frac{(-1)^n(2mE_+)^n}{(2)(1+2\theta)(4)(3+2\theta)...(2n)(2n-1+2\theta)}a_0^+. \tag{A.1}$$

We can rewrite this using the Pochhammer symbol $(a)_n = a(a+1)(a+2)...(a+n-1)$:

$$a_n^+ = \frac{(-1)^n(2mE_+)^n}{2^n \cdot n! \cdot (\frac{1}{2}+\theta)_n}a_0^+. \tag{A.2}$$

The even parity solution then becomes:

$$\psi_+^{\lambda=0} = a_0^+ \sum_{n=0}^{\infty} \frac{(-1)^n(2mE_+)^n}{2^n \cdot n! \cdot (\frac{1}{2}+\theta)_n}x^{2n}. \tag{A.3}$$

Let's substitute $z = -\frac{mE_+x^2}{2}$, we can write:

$$\psi_+^{\lambda=0} = a_0^+ \sum_{n=0}^{\infty} \frac{z^n}{n! \cdot (\frac{1}{2}+\theta)_n}, \tag{A.4}$$

this is precisely the definition of the hypergeometric function ${}_0F_1$ with a single parameter $\frac{1}{2}+\theta$:

$$\psi_+^{\lambda=0} = a_0^+ \cdot {}_0F_1\left(;\frac{1}{2}+\theta;-\frac{mE_+x^2}{2}\right). \tag{A.5}$$

Taking $a_0^+ = 1$ for normalization purposes, we get

$$\psi_+^{\lambda=0} = {}_0F_1\left(;\frac{1}{2}+\theta;-\frac{mE_+x^2}{2}\right). \tag{A.6}$$

This hypergeometric function can be rewritten in terms of the Bessel function using the identity:

$$ {}_0F_1(;c;-\frac{z^2}{4}) = \Gamma(c)\left(\frac{z}{2}\right)^{1-c} J_{c-1}(z), \tag{A.7} $$

with $c = \frac{1}{2} + \nu$ and $z = \sqrt{2mE_+}x$, we obtain:

$$ \psi_+ = N_+ x^{1/2-\nu} J_{\nu-1/2}(\sqrt{2mE_+}x). \tag{A.8} $$

Where N_+ is a normalization constant.

In the next step, we will review the steps of finding equations. For $N = 0$, the recurrence relation gives $a_1 = 0$ since $[2n]_\nu - [2N]_\nu = 0$ when $n = N = 0$. This terminates the series, resulting in:

$$ {}^+_0(\xi) = a_0 = 1 \tag{A.9} $$

(normalizing with $a_0 = 1$).

For $N = 1$, we compute the first two terms:

For $n = 0$:

$$ a_1 = \frac{2([0]_\nu - [2]_\nu)}{[2]_\nu[1]_\nu} a_0 = \frac{2(0-2)}{2(1+2\nu)}(1) = -\frac{2}{[1]_\nu}. \tag{A.10} $$

For $n = 1$:

$$ a_2 = \frac{2([2]_\nu - [2]_\nu)}{[4]_\nu[3]_\nu} a_1 = 0. \tag{A.11} $$

This terminates the series, resulting in:

$$ H_1^+(\xi) = 1 - \frac{2}{[1]_\nu}\xi^2. \tag{A.12} $$

For $N = 2$, we compute the first three terms:

For $n = 0$:

$$ a_1 = \frac{2([0]_\nu - [4]_\nu)}{[2]_\nu[1]_\nu} a_0 = \frac{2(0-4)}{2(1+2\nu)}(1) = -\frac{4}{[2]_\nu[1]_\nu}. \tag{A.13} $$

For $n = 1$:

$$ a_2 = \frac{2([2]_\nu - [4]_\nu)}{[4]_\nu[3]_\nu} a_1 = \frac{2(2-4)}{4(3+2\nu)}\left(-\frac{4}{[2]_\nu[1]_\nu}\right), \tag{A.14} $$

simplifying:

$$a_2 = \frac{2(-2)}{4(3+2\nu)}\left(-\frac{4}{[2]_\nu[1]_\nu}\right) = \frac{2^2[4]_\nu([4]_\nu - [2]_\nu)}{[4]_\nu!}, \tag{A.15}$$

where we've used $[4]_\nu! = [4]_\nu[3]_\nu[2]_\nu[1]_\nu$.

For $n = 2$:

$$a_3 = \frac{2([4]_\nu - [4]_\nu)}{[6]_\nu[5]_\nu}a_2 = 0. \tag{A.16}$$

This terminates the series, resulting in Eq.(1.122):

$$H_2^+(\xi) = 1 - \frac{2[4]_\nu}{[2]_\nu!}\xi^2 + \frac{2^2[4]_\nu([4]_\nu - [2]_\nu)}{[4]_\nu!}\xi^4. \tag{A.17}$$

B Dunkl-Bose-Einstin condensation in Harmonic trap

In this appendix we will cover some mathematical details regarding critical temperature.

First, for the critical temperature we put $N_0^D = 0$ and $z = 1$ in Eq. (3.12):

$$N = \left(\frac{K_B T_c^D}{\hbar\Omega}\right)^3 g_3\left(1,\theta\right) + \gamma\left(\frac{K_B T_c^D}{\hbar\Omega}\right)^2 g_2\left(1,\theta\right), \tag{B.1}$$

$$\left(T_c^D\right)^3 \left(\frac{K_B}{\hbar\Omega}\right)^3 \left[g_3(1,\theta) + \gamma\left(\frac{\hbar\Omega}{K_B}\right)\frac{g_2(1,\theta)}{T_c^D}\right] = N, \tag{B.2}$$

$$T_c^D = \left(\frac{\hbar\Omega}{K_B}\right)\left(\frac{N}{g_3\left(1,\theta\right)}\right)^{1/3}\left[1 + \gamma\left(\frac{\hbar\Omega}{K_B}\right)\frac{g_2(1,\theta)}{g_3(1,\theta)}\frac{1}{T_c^D}\right]^{-1/3}, \tag{B.3}$$

then, we replace T_c^D by it's expression:

$$T_c^D = \left(\frac{\hbar\Omega}{K_B}\right)\left(\frac{N}{g_3\left(1,\theta\right)}\right)^{1/3}\left[1 + \gamma\frac{g_2(1,\theta)}{\left(g_3(1,\theta)\right)^{2/3]}}\right]^{-1/3}, \tag{B.4}$$

here, we use the approximation $(1+x)^{-n} = 1 - nx$, we find Eq. (3.14):

$$T_c^D = \left(\frac{\hbar\Omega}{K_B}\right)\left(\frac{N}{g_3\left(1,\theta\right)}\right)^{1/3}\left[1 - v\frac{\gamma}{3}\frac{g_2(1,\theta)}{\left(g_3(1,\theta)\right)^{2/3]}}\right]. \tag{B.5}$$

References

[1] A.Einstein, Sitzber. Kgl. Preuss. Akad. Wiss.**261** (1924).

[2] A.Einstein, Sitzber. Kgl. Preuss. Akad. Wiss.**3** (1925).

[3] S. N. Bose, Z. Phys. **26**, 178 (1924). (1996).

[4] M. H. Anderson, J. R. Ensher, M. R. Matthews, C. E. Wieman, and E. A. Cornell, Science **269**, 198 (1995).

[5] W. Ketterle, and N. J. van Druten, Phys. Rev. A **54**, 656 (1996).

[6] W. Greiner, L. Neise and H. Stocker, Thermodynamics and Statistical Mechanics (Springer Verlag, New York, 1995).

[7] S. Grossmann, M. Holthaus, Phys. Lett. A **208**, 188 (1995).

[8] S. Grossmann, M. Holthaus, Z. Naturforsch. A **50**, 921 (1995).

[9] Q. -J. Zeng, Y. -S. Luo, Y. -G. Xu, H. Luo, Physica A **398**, 116 (2014).

[10] Q. -J. Zeng, Z. Cheng, J. -H. Yuan, Physica A **391**, 563 (2012).

[11] K. Kirsten, D. J. Toms, Phys. Rev. A **54**, 4188 (1996).

[12] K. Kirsten, D. J. Toms, Phys. Lett. A **222**, 148 (1996).

[13] R. Napolitano, J. De Luca, V. S. Bagnato, and G. C. Marques, Phys. Rev. A **55**, 3954 (1997).

[14] F. Dalfovo, S. Giorgini, L. P. Pitaevskii, and S. Stringari, Rev. Mod. Phys. **71**, 463 (1999).

[15] J. R. Anglin and W. Ketterle, Nature **416**, 211 (2002).

[16] C. J. Wu, I. Mondragon-Shem, X. F. Zhou, Chin. Phys. Lett. **28**, 097102 (2011).

[17] J. T. Lewis, J. V. Pule, Commun. Math. Phys. **36**, 1 (1974).

[18] L. J. Landau, I. F. Wilde, Commun. Math. Phys. **70**, 43 (1979).

[19] M. van den Berg, J. T. Lewis, Physica A **110**, 550 (1982).

[20] V. Bagnato, D. E. Pritchard, and D. Kleppner, Phys. Rev. A **35**, 4354 (1987).

[21] V. Bagnato, D. E. Pritchard, and D. Kleppner, Phys. Rev. A **44**, 7439 (1991).

[22] H. A. Gersch, J. Chem. Phys. **27**, 928 (1957).

[23] A. Widom, Phys. Rev. **176**, 254 (1968).

[24] D. B. Baranov and V. S. Yarunin, Phys. Lett. A **285**, 34 (2001).

[25] J. I. Rivas and A. Camacho, Mod. Phys. Lett. A **26**, 481 (2011).

[26] T. G. Liu, Y. Yu, J. Zhao, X. Wang, X. Wang, and Q. H. Liu, Physica A **388**, 2383 (2009).

[27] C. F. Du, H. Li, Z. Q. Lin, and X. M. Kong, Physica B **407**, 4375 (2012).

[28] W. J. Mullin, J. Low Temp. Phys. **106**, 615 (1997).

[29] E. P. Wigner, Phys. Rev. **77**, 711 (1950).

[30] L. M. Yang, Phys. Rev. **84**, 788 (1951).

[31] C. F. Dunkl, T. Am. Math. Soc. **311**, 167 (1989).

[32] M. Rösler, Lecture Notes in Mathematics **1817**, 93 (2003).

[33] C. F. Dunkl, J. Phys. A: Math. Gen. **35**, 10391 (2002).

[34] L. Lapointe, L. Vinet, Commun. Math. Phys. **178**(2), 425 (1996).

[35] S. Kakei, J. Phys. A **29**, L619 (1996).

[36] S. M. Klishevich, M. S. Plyushchay, M. Rausch de Traubenberg, Nucl. Phys. B **616**, 419 (2001).

[37] P. A. Hortváthy, M. Plyushchay, M. Valenzuela, Ann. Phys. **325**, 1931 (2010).

[38] V. Genest, M. Ismail, L. Vinet, A. Zhedanov, J. Phys. A **46**, 145201 (2013).

[39] V. Genest, L. Vinet, A. Zhedanov, J. Phys. A **46**, 325201 (2013).

[40] V. Genest, M. Ismail, L. Vinet, A. Zhedanov, Commun. Math. Phys. **329**, 999 (2014).

[41] V. Genest, L. Vinet, A. Zhedanov, J. Phys. Conf. Ser. **512**, 012010 (2014).

[42] M. R. Ubriaco, Physica A **414**, 128 (2014).

[43] V. Genest, A. Lapointe, L. Vinet, Phys. Lett. A **379**, 923 (2015).

[44] E. J. Jan, S. Park, W. S. Chung, J. Kor. Phys. Soc. **68**, 379 (2016).

[45] M. Salazar-Ramirez, D. Ojeda-Guillén, V. D. Granados, Eur. Phys. J. Plus **132**, 39 (2017).

[46] M. Salazar-Ramirez, D. Ojeda-Guillén, R. D. Mota, V. D. Granados, Mod. Phys. Lett. A **33**, 1850112 (2018).

[47] S. Sargolzaeipor, H. Hassanabadi, W. S. Chung, Mod. Phys. Lett. A **33**, 1850146 (2018).

[48] W. S. Chung, H. Hassanabadi, Mod. Phys. Lett. A **34**, 1950190 (2019).

[49] S. Ghazouani, I. Sboui, M. A. Amdouni, M. B. El Hadj Rhouma, J. Phys. A: Math. Theor. **52**, 225202 (2019).

[50] R. D. Mota, D. Ojeda-Guillén, M. Salazar-Ramírez, V. D. Granados, Ann. Phys. **411**, 167964 (2019).

[51] W. S. Chung, H. Hassanabadi, Rev. Mex. Fis. **66**, 308 (2020).

[52] Y. Kim, W. S. Chung, H. Hassanabadi, Rev. Mex. Fis. **66**, 411 (2020).

[53] D. Ojeda-Guillén, R. D. Mota, M. Salazar-Ramírez, V. D. Granados, Mod. Phys. Lett. A **35**, 2050255 (2020).

[54] R. D. Mota, D. Ojeda-Guillén, M. Salazar-Ramírez, V. D. Granados, Mod. Phys. Lett. A **36**, 2150066 (2021).

[55] R. D. Mota, D. Ojeda-Guillén, M. Salazar-Ramírez, V. D. Granados, Mod. Phys. Lett. A **36**, 2150171 (2021).

[56] A. Merad, M. Merad, Few-Body Syst. **62**, 98 (2021).

[57] W. S. Chung, H. Hassanabadi, Mod. Phys. Lett. A **36**, 2150127 (2021).

[58] W. S. Chung, H. Hassanabadi, Eur. Phys. J. Plus. **136**, 239 (2021).

[59] H. Hassanabadi, M. de Montigny, W. S. Chung, Physica A **580**, 126154 (2021).

[60] S. H. Dong, W. H. Huang, W. S. Chung, P. Sedaghatnia, H. Hassanabadi, EPL **135**, 30006 (2021).

[61] B. Hamil, B. C. Lütfüoğlu, Few-Body Syst, **63**, 74 (2022).

[62] B. Hamil, B. C. Lütfüoğlu, Eur. Phys. J. Plus **137**, 812 (2022).

[63] P. Sedaghatnia, H. Hassanabadi, W. S. Chung, B. C. Lütfüoğlu, S. Hassanabadi, J. Kriz, arXiv:2208.12416 [quanth-ph].

[64] R. D. Mota, D. Ojeda-Guillén, Mod. Phys. Lett. A **37**(01), 2250006 (2022).

[65] S. Hassanabadi, J. Kriz, B. C. Lütfüoğlu, H. Hassanabadi, Phys. Scr. **97**, 125305 (2022).

[66] S. Hassanabadi, J. Kriz, B. C. Lütfüoğlu, H. Hassanabadi, Under review.

[67] S. Hassanabadi, P. Sedaghatnia, W. S. Chung, B. C. Lütfüoğlu, J. Kriz, H. Hassanabadi, arxiv:2209.03122 [hep-th].

[68] L. Vinet, A. Zhedanov, Rev. Math. Phys. **34**, 2250025, (2022).

[69] A. S. Hassan, A.M. El-Badry, Physica B **404** 1947 (2009).

[70] A. S. Hassan, Phys. B **405** 1040 (2010).

[71] W. S. Dai, M. Xie, Phys. Rev. A **67**, 027601 (2002).

[72] A. B. Acharyya and M. Acharyya, Acta Physica Polonica Series B **43**, 9 (2012).

[73] F. Merabtine, B. Hamil, B. C. Lütfüoğlu, A. Hocine, M. Benarous, J. Stat. Mech. **5**, 053102 (2023).

[74] B. Hamil, B. C. Lütfüoğlu, Physica A **623**, 128841 (2023).

[75] A. Hocine, B. Hamil, F. Merabtine, B. C. Lütfüoğlu, and M Benarous, Rev. Mex. Fis. **70**, 051701 (2024).

[76] A. Hocine, F. Merabtine, B. Hamil, B. C. Lütfüoğlu and M. Benarous, Ind. J. Phys. **99**, 775782 (2025)

[77] Lourek, I., Tribeche, M. Lett. A **381**, 452 (2017).

[78] A. Aliano, G. Kaniadakis, E. Miraldi. Physica B **325**, 35 (2003).

[79] K. Ourabah, M. Tribeche. Phys. Rev. E **89**, 062130 (2014)x.

[80] A. Guha, P.K. Das. Physica A **495**, 18 (2018).

[81] A. M. Gavrilik, A. P. Rebesh. Mod. Phys. Lett. B **26**, 1150030 (2012).

[82] L. F. Matin, and S. Miraboutalebi. Physica A. **520**, 10 (2015).

[83] P. Bosso. Phys. Rev. D **97** 126010 (2018).

[84] H. Goldstein. (1980). *Classical Mechanics*. Addison-Wesley.

[85] J. J. Sakurai. (1994). *Modern Quantum Mechanics*. Addison-Wesley.

[86] Claude Cohen-Tannoudji. *Mécanique quantique*. Tome 1 et 2.

[87] Guo, X.Y., et al. Chin. Phys. B **32**, 010307 (2023).

[88] P. A. M. Dirac. (1930). *The Principles of Quantum Mechanics*. Oxford University Press.